THE ROLE OF ACTIVITY AND SYNAPTIC CELL ADHESION MOLECULES OF THE NEUREXIN FAMILY IN THE REFINEMENT OF SYNAPSES BETWEEN HIPPOCAMPAL NEURONS

by

Dylan P. Quinn

Submitted in partial fulfillment of the requirements
for the degree of Doctor of Philosophy

at

Dalhousie University
Halifax, Nova Scotia
December 2017

TABLE OF CONTENTS

LIST OF FIGURES vi

ABSTRACT vii

LIST OF ABBREVIATIONS USED viii

ACKNOWLEDGMENTS x

CHAPTER 1: INTRODUCTION 1

1.1 Brain Development and Synapse Refinement 2

1.2 The Role of Activity in Neuronal Circuit Refinement 3

1.2.1 Synapse Competition and Elimination at the Neuromuscular Junction 3

1.2.2 Experience-Induced Changes in Cortical Synaptic Refinement 4

1.2.3 Neuronal Activity and Circuit Plasticity in the Hippocampus 6

1.2.4 Homeostatic Synaptic Plasticity 6

1.2.5 Activity-Independent Circuit Development 8

1.3 The Role of Synaptic Adhesion Molecules in Synapse Development and Circuit Refinement 9

1.3.1 Neurexins and Neuroligins in Synapse Formation and Structural Maintenance 10

1.3.2 Neurexins and Neuroligins in the Modulation of Synaptic Transmission 12

1.4 Rationales and Hypothesis 14

CHAPTER 2: GLOBAL AND SPARSE ACTIVITY BLOCKADE DIFFERENTIALLY REGULATE SYNAPSE REFINEMENT 16

2.1 Introduction 17

2.2 Methods 18

2.2.1 cDNA Constructs 18

2.2.2 Dissociated Hippocampal Cultures 19

2.2.3 Transfections 19

2.2.4 Image Acquisition of Synapse Turnover Assay 20

2.2.5 Image Analysis of Synapse Turnover Assay 21

2.2.6 Assessment of TeNT-LC Efficiency with Synaptophysin-pHluorin 22

2.3 Results 23

2.3.1 Characteristics of Synaptic Refinement in Rat Dissociated Hippocampal Neurons 23

2.3.2 Synapse Size Predicts Synapse Survival 24

2.3.3 Global Blockage of Ionotropic Glutamate Receptors Decreases Synapse Elimination 25

2.3.4 Synapse-Specific Silencing of Neurotransmitter Release Reduces Synapse Formation but has no Effect on Synapse Elimination 26

2.4 Discussion 27

CHAPTER 3: NEUREXIN PERTURBATION REDUCES THE STABILITY OF SYNAPTIC CONTACTS 42

3.1 Introduction 43

3.2 Methods 43

3.2.1 Generation of shRNA Nrxn Knockdown Constructs 43

3.2.2 cDNA Constructs 44

3.2.3 Immunocytochemistry and Western Blotting 45

3.2.5 Neuronal-COS7 Co-culture Assay 46

3.2.6 Assessment of Synaptic Density 47

3.2.7 Quantification of Synapse Turnover 48

3.3 Results 48

3.3.1 Molecular Tools for Disrupting the Function of all Nrxn Isoforms 48

3.3.2 Nrxn Disruption Reduces Synapse Density 50

3.3.3 Nrxn Disruption Reduces the Stability of Synaptic Contacts 51

3.4 Discussion 52

CHAPTER 4: NEUREXIN PERTURBATION RESULTS IN A REDUCTION IN READILY RELEASABLE SYNAPTIC VESICLE POOL SIZE 65

4.1 Introduction 66

4.2 Methods 67

4.2.1 Additional cDNA Constructs 67

4.2.2 Immunocytochemistry 67

4.2.3 Assessment of Active Zone Size 67

4.2.4 Synaptophysin-pHluorin Experiments 68

4.2.5 GCaMP6m Experiments 69

4.3 Results 69

4.3.1 Nrxn Disruption Reduces Active Zone Protein Content 69

4.3.3 Overexpression of a Dominant-Negative Nrxn construct Reduces Presynaptic Calcium Influx 72

4.4 Discussion 73

CHAPTER 5: NEUREXINS STABILIZE SYNAPSES INDEPENDENT OF NEURONAL ACTIVITY 82

5.1 Introduction 83

5.2 Methods 83

5.3 Results 83

5.3.1 Nrxns Stabilize Synapses Independent of Global Activity Blockade 83

5.3.2 Nrxns Stabilize Synapses Independent of Sparse Neuronal Activity 84

5.4 Discussion 85

CHAPTER 6: DICUSSION 90

6.1 The Role Neuronal Activity in Synapse Refinement 91

6.2 The Role of Synaptic Cell Adhesion in Synapse Refinement 92

6.3 SAMs and Activity-Dependent Mechanisms in Synapse Refinement: Cooperative Function or Independent Roles? 93

6.4 Conclusion 95

REFERENCES 96

APPENDIX A: NEURONAL KNOCKDOWN SCREEN 107

LIST OF FIGURES

Figure 2.1. Synapse turnover assay in rat dissociated hippocampal neurons 30

Figure 2.2. Pre- and postsynaptic specializations participated in synapse formations and eliminations 32

Figure 2.3. Synapse size predicts synapse survival 34

Figure 2.4. Ionotrophic glutamate receptor blockade reduced synapse elimination but has no effect on synapse formation 36

Figure 2.5. TeNT-LC expression inhibits neurotransmitter release 38

Figure 2.6. TeNT-LC expression has no effect on synapse elimination but significantly reduces synapse formation 40

Figure 3.1. Molecular tools for disrupting Nrxn function 55

Figure 3.2. Perturbation of Nrxn function blocks the synaptogenic effect of LRRTM2 in co-culture synapse formation assay 57

Figure 3.3. Nrxn disruption reduces synaptic density 59

Figure 3.4. Nrxn perturbation reduces the stability of synaptic contacts 61

Figure 3.5. Models for the role of Neurexin in synapse formation and maturation 63

Figure 4.1. Nrxn perturbation reduces active zone cytomatrix protein content 76

Figure 4.2. Nrxn perturbation attenuates neurotransmitter release 78

Figure 4.3. Overexpression of a dominant-negative Nrxn construct decreases presynaptic calcium influx 80

Figure 5.1. Neurexins stabilize synapses independent of global activity blockade 86

Figure 5.2. Neurexins stabilize synapses independent of sparse neuronal activity 88

ABSTRACT

Nervous system development is characterized by the selective removal of superfluous synaptic contacts and the strengthening of synapses that are useful for circuit function and behaviour. Historically, neuronal activity was thought essential for the process of synapse refinement. However, recent work shows that synapses can form and mature in the absence of neuronal activity, suggesting that other factors may also modulate synapse refinement. In this thesis, I examine the role of activity and synaptic cell adhesion molecules (SAMs) in the modulation of synapse refinement in dissociated hippocampal neurons. To test the role of activity in synapse refinement, I sparsely transfected hippocampal neurons with tetanus toxin light chain (TeNT-LC), a protease that disrupts neurotransmitter release. To examine if SAMs function in synapse refinement, I designed shRNA and mutant constructs to perturb the function of neurexins, a family of presynaptic SAMs. I then performed time-lapse imaging of fluorescently labeled synapses and record how these manipulations effect the percentage of stable, eliminated, and newly formed synapses over 24 hours. Blockade of neurotransmission with TeNT-LC expression had no effect on synapse elimination rates. Interestingly, perturbation of neurexin function at synapses decreased the stability of synaptic contacts, causing synapses to be eliminated at an enhanced rate. The effect of neurexin-perturbation on synapse stability persisted even when tested during activity blockade, showing that neurexins are able to modulate synapse refinement independent of their effect on synaptic transmission. Our findings indicate that differential SAM expression by populations of afferent neurons may be important in establishing appropriate inputs onto postsynaptic neurons through activity-independent competitive mechanisms. Disruption of this function may have profound impacts on circuit development and function and explain why mutations in neurexins are associated with autism and other neurodevelopmental disorders.

LIST OF ABBREVIATIONS USED

AMPA	α-amino-3-hydroxy-5-methyl-4-isoxazolepropionic acid
APV	(2R)-amino-5-phosphonovaleric
ASD	Autism Spectrum Disorder
BFP	Blue Fluorescent Protein
Bsn	Bassoon
CB1	Cannabinoid Receptor 1
CCD	Charge-Coupled Device
cDNA	Complementary Deoxyribonucleic Acid
CMV	Cytomegalovirus
DNQX	6,7-dinitroquinoxaline-2,3-dione
EGFP	Enhanced Green Fluorescent Protein
FCS	Fetal Calf Serum
GABA	Gamma-Aminobutyric Acid
HBS	HEPES-Buffered Saline
HEPES	4-(2-hydroxyethyl)-1-piperazineethanesulfonic Acid
Hmr	Homer1b
HRP	Horseradish Peroxidase
HSP	Homeostatic Synaptic Plasticity
IC	Intracortical
iGluR	Ionotropic Glutamate Receptor
LNS	Laminin, Neurexin, Sex-specific Globulin Domain
LTD	Long-Term Depression
LTP	Long-Term Potentiation
MEM	Minimum Essential Medium
mEPSC	Miniature Excitatory Postsynaptic Current
mIPSC	Miniature Inhibitory Postsynaptic Current
mRNA	Messenger Ribonucleic Acid
NL	Neuroligin
NGL	Netrin-G Ligand
NMDA	N-methyl-D-aspartate
NMJ	Neuromuscular Junction
Nrxn	Neurexin
NSF	N-ethylmaleimide Sensitive Fusion Protein
LAR	Leukocyte Common Antigen-Related
LRRTM	Leucine-Rich Repeat Transmembrane Protein
PBS	Phosphate-Buffered Saline
PSC	Postsynaptic Current
PN	Pyramidal Neuron
Pr	Release Probability
PSD95	Postsynaptic Density Protein 95
PV	Parvalbumin
Rac1	Ras-related C3 Botulinum Toxin Substrate 1
RIM	Rab3-associated molecule
RRP	Readily Releasable Pool

LIST OF ABBREVIATIONS USED (Cont.)

SAM	Synaptic Cell Adhesion Molecule
SNARE	SNAP (Soluble NSF Attachment Protein) Receptor
shRNA	Short-Hairpin Ribonucleic Acid
SST	Somatostatin Positive Interneuron
Syph-mCh	Synaptophysin tagged to monomeric mCherry
SypHl	Synaptophysin tagged to pHluorin
TBS	Tris-Buffered Saline
TC	Thalamocortical
TeNT-LC	Tetanus Toxin Light Chain
TTX	Tetrodotoxin

ACKNOWLEDGMENTS

I would like to express my deep gratitude to my supervisor, Dr. Stefan Krueger, whose expertise, knowledge, and passion for science, has shown me what research is all about. No matter how busy you were, you were always available to discuss science and life with kindness and honesty. I really appreciate that. You taught me how to 'do good science' and to never cut corners. Lessons I will always keep with me.

Thank you to Dr. Jim Fawcett for serving on my committee and providing scientific guidance, resources, career advice and hospitality over the years. Thank you to my committee members Dr. Vic Rafuse, Dr. Alan Fine, and Dr. Roger Croll for overseeing my work and contributing to my development as a scientist. Also, thank you all for the work and life advice you gave me during our occasional one-on-one conversations.

Annette Kolar, thank you for your friendship, knowledge, and all the help with day-to-day challenges in the lab. Thank you for showing me how to work at the bench early on. Thanks to lab mate Sydney Harris for all your hard work and image analysis over the last two years. Thanks to Yi-ling Hu for your friendship and assistance with experiments. Thanks to Ulli Hoger and Alexander Goroshkov for your intellectual input and assistance with technical issues. Alice Smith, Jennifer Graves, and Chris MacNeil, thank you for all the support with scheduling and grant applications during my time at Dalhousie.

Thanks to Michael Wigerius for your friendship and always being willing to talk openly about the challenges of science and life. The enthusiasm and passion you bring to research is inspiring. Thanks to fellow students and coworkers Pia Elustondo, Borbala Podor, Matthew MacDougall, Eric Fisher, Jeff Gagnon, Andrea Nuschke and Jean Lui, Jeremy Toma, and Ian MacDonald, for the fun times, great conversation and support over the years.

The best result of my time at graduate school was finding best friend and partner, Noelle d'Eon. You brighten my days with your warmth, kindness, intellect, and humor. Your love and support has made all the hard work that went into this thesis a whole lot easier. Thank you!

To my parents, John and Bonnie Quinn, I am extremely grateful for your love and continuous support as I struggled to find my true interest (which I now have!). Both of you take a genuine interest in my work, which means a whole lot to me.

CHAPTER 1

INTRODUCTION

1.1 Brain Development and Synapse Refinement

The enormous complexity of the vertebrate brain is largely determined during development. During this time, approximately 90 billion neurons of many different subtypes form specific connections with one another. This process generally occurs in a stereotyped fashion from individual to individual. Subtle differences that do occur likely contribute to the behavioural and cognitive differences that are observed between individuals. Wiring complexity is especially evident at neurons that receive multiple, location-specific afferent inputs from distinct classes of presynaptic neurons. For example, CA1 pyramidal neurons in the hippocampus receive entorhinal input to distal dendritic tufts, CA3 pyramidal input to proximal and basal dendrites, and inhibitory inputs to the soma (Spruston, 2008). In addition, different afferents onto the same postsynaptic cell can have drastically different functional properties, both in terms of basal synaptic strength and expression of synaptic plasticity. Insight into the developmental rules that shape neural circuits will be essential in understanding how mature circuits control behaviour and why circuits form and function abnormally in neurodevelopmental disorders.

One process that is critical to circuit development is synapse refinement, the selective elimination of superfluous synapses that were formed early in development and the functional maturation of synapses that are important to circuit function. In the human cortex, enhanced synapse formation during the first 1–2 years is followed by a prolonged period of synapse elimination that reduces synaptic density by about 50% as the mature cortex begins to take shape (Huttenlocher, 1990; Piochon et al., 2016). Three hypotheses may explain the function of superfluous synapse formation in developing nervous systems. Firstly, high synaptic densities may provide flexibility and allow circuits to be pruned in numerous ways by sensory input. Secondly, superfluous synapses may be a vestige of an earlier developmental phase that relied on hyper-connectivity. For example, spontaneous wave-like activity that occurs in the retina may require a density of connectivity that is later detrimental to circuit development. Thirdly, extra synapse

formation may be the result of the limited number of unique guidance cues that are available to specify early circuits (Riccomagno and Kolodkin, 2015).

Impairments in synapse refinement may contribute to neurodevelopmental disorders such as autism spectrum disorder (ASD; Courchesne et al., 2003; Supekar et al., 2013) a finding which is supported by analysis of ASD mouse models. For example, patDp/ + mice, which have a common ASD-associated mutation, have impaired synapse elimination in the cerebellum and show deficits in cerebellar-dependent motor learning (Piochon et al., 2014). Similarly, single-allele deletion of the ASD-associated gene, MDGA2, which modulates synaptic cell adhesion, causes aberrant circuit development, cortical hyperactivity and impaired social and cognitive function (Connor et al., 2016).

Neuronal activity is thought necessary to drive synapse elimination and maturation events in many developing neuronal circuits. Molecular cues, such as synaptic cell adhesion molecules, may also play an active role in synapse refinement considering they are essential for synapse development and associated with developmental disease. In this thesis, I test the role of neuronal activity and synaptic cell adhesion in the formation, elimination, and stabilization of synapses in developing neural networks.

1.2 The Role of Activity in Neuronal Circuit Refinement

Classic studies by Hubel and Wiesel documented the effect of sensory deprivation on visual cortex organization and laid the groundwork for subsequent studies on synaptic refinement and its relationship to neuronal activity. In the next section, I review the role played by activity in modulating synapse refinement within various neuronal systems such the neuromuscular junction (NMJ), the somatosensory cortex, and the hippocampus.

1.2.1 Synapse Competition and Elimination at the Neuromuscular Junction

Perhaps the most interesting and striking example of activity-dependent synapse refinement occurs at the NMJ. At birth, skeletal muscles are innervated by approximately

10 motor neuron axons (Ribchester and Barry, 1994; Tapia et al., 2012). In the subsequent 2 weeks, synapses and axons are removed from the postsynaptic endplate until a single motor neuron remains (Darabid et al., 2014; Tomàs et al., 2017). Time-lapse imaging experiments of dually innervated muscles revealed that axons terminals are highly dynamic during this time of synaptic competition, with both terminals showing periods of territory gain and loss (Walsh and Lichtman, 2003). Following approximately 2 days of structural plasticity, one 'loser' axon ultimately withdrawals from a synaptic area which is then taken over by a competing nerve input. (Walsh and Lichtman, 2003; Darabid et al., 2014). It is thought that differences in presynaptic release efficiency determine the outcome of this competitive process (Kopp et al., 2000; Buffelli et al., 2003). Perhaps the strongest evidence for this model comes from genetic studies in which neurotransmitter release from one of two inputs to a dually innervated target cell is selectively inhibited (Buffelli et al., 2003). By disrupting the gene for choline acetyltransferase, the enzyme essential for acetylcholine biosynthesis, Buffelli et al. showed that inactive terminals are preferentially eliminated at developing NMJs. It has also been suggested that the synchronicity of firing between competing inputs is important for competitive pruning at the NMJ (Favero et al., 2012). If two competing axons are fired in synchrony, competitive synapse elimination is diminished and the period of polyneuronal innervation is prolonged. Conversely, if asynchronous action potentials are imposed on competing axons, synapse elimination occurs as normal. It has been hypothesized that asynchrony of competing inputs is necessary for synaptic competition because it allows the efficiency of inputs to be separately sensed by the postsynaptic endplate or associated perisynaptic Schwann cells (Darabid et al., 2013). Such a temporal separation of synaptic strengths may be necessary for synapse elimination and stabilization mechanisms to be directed to the appropriate inputs (Favero et al., 2012; Darabid et al., 2014).

1.2.2 Experience-Induced Changes in Cortical Synaptic Refinement

The rodent barrel cortex is a classic model system for investigating the role of experience-induced neuronal activity in circuit refinement and structural plasticity. The

power of the barrel cortex system lies in the one-to-one mapping of whiskers on the snout to anatomically defined structures in the contralateral somatosensory cortex called barrel fields (Van der Loos and Woolsey, 1973). Neurons within each barrel field respond best to deflection of the corresponding whisker (Feldman, 2009). Somatotopic maps of the whiskers are also present in the thalamus and brainstem called 'barreloids' and 'barrelettes' respectively. Recent work has shown that columnar development in the barrel cortex relies on neurotransmission at thalamocortical afferents (Li et al., 2013). The role of experiential activity in this stereotyped developmental program can be examined by whisker trimming or plucking, which deprives the corresponding barrel field of sensory input. Trimming of a subset of whiskers causes the strengthening and expansion of spared whisker representations and the weakening and shrinkage of deprived whisker representations within the cortical map (Fox, 1992; Diamond et al., 1993; Glazewski and Fox, 1996).

Analysis of synaptic strength in animals that have undergone whisker deprivation suggests that neuronal activity and LTP and LTD mechanisms may be responsible for changes receptive field mapping (Feldman and Brecht, 2005; Feldman, 2009). For example, single whisker experience potentiates layer 4 (L4)-layer 2/3 (L2/3) synapses in the spared whisker column via an upregulation of GluR1-containing AMPA receptors (Clem and Barth, 2006), whereas EPSCs are reduced at L4-L2/3 synapses in deprived barrel fields (Allen et al., 2003). Time-lapse imaging experiments have shown that the changes in neuronal activity induced by whisker deprivation cause drastic changes in synapse turnover during development. Zuo and colleges showed that complete unilateral whisker trimming at 4-6 weeks caused a NMDAR-dependent reduction in spine elimination in the contralateral barrel cortex, without altering the formation of new spines (Zuo et al., 2005). Conversely, Trachtenberg and colleges found that trimming every other whisker into a 'chessboard' pattern caused enhanced turnover of dendritic spines (Trachtenberg et al., 2002). It will be interesting to see if future studies reveal a causative link between deprivation-induced LTP/LTD and structural plasticity in the barrel cortex.

1.2.3 Neuronal Activity and Circuit Plasticity in the Hippocampus

The hippocampus shows remarkable functional and structural plasticity during development and in adult. A recent report suggests that dendritic spines of CA1 neurons have an average lifetime of 1-2 weeks, which implies that in 3-6 weeks, synaptic connectivity patterns are completely refreshed (Attardo et al., 2015). As in the neocortex (Zuo et al., 2005), CA1 spine turnover is modulated by NMDAR blockade (Attardo et al., 2015), indicating that plasticity processes such as LTP and LTD may contribute to structural plasticity in the hippocampus. This notion is supported by experiments in hippocampal slice culture. In the CA1 region, LTP-inducing theta burst stimulation can induce spine and synapse formation (Nägerl et al., 2004; Nägerl et al., 2007) and LTP-inducing glutamate uncaging increases spine size (Matsuzaki et al., 2004) and promotes the stability of naturally occurring nascent dendritic spines (Hill and Zito, 2013). Similarly, LTD-inducing glutamate uncaging or electrical stimulation promote the shrinkage and elimination of spines (Oh et al., 2013; Nägerl et al., 2004). A recent study by Wiegert and Oertner tested the long-term structural and functional effects of optogenetically-induced LTD (oLTD) at developing CA3-CA1 synapses (Wiegert and Oertner, 2013). Presynaptic expression of channelrhodopsin2 and a synaptic marker allowed the visualization of light-activated presynaptic boutons and postsynaptic expression of GCaMP3, and CFP in CA1 dendrites allowed synapse structure and function to be recorded at single synapses. Wiegert and Oertner (2013) found that oLTD facilitated the elimination of synapses from the hippocampal circuit. Interestingly, the elimination of depressed synapses was not a random process but occurred preferentially at synapses that had a lower initial release probability (Wiegert and Oertner, 2013). These studies provide strong evidence that activity-mediated changes in synaptic strength contribute to structural plasticity and the refinement of developing circuits.

1.2.4 Homeostatic Synaptic Plasticity

Neuronal circuit development is a period of unparalleled structural and functional plasticity for developing neurons. High rates of synapse turnover and shifts in synaptic

strength likely cause large-scale alterations in synaptic input to single neurons. Compensatory mechanisms, such as homeostatic synaptic plasticity (HSP), are thought to readjust synaptic strength and neuronal excitability during periods of altered synaptic input. The first detailed analysis of HSP was performed in cultured cortical neurons (Turrigiano et al., 1998). Turrigiano and colleges (1998) found that chronic blockade of neuronal activity with Tetrodotoxin (TTX) caused an increase in mEPSC amplitude, whereas blocking GABA receptors with bicuculline enhanced neuronal activity and caused a reduction in mEPSC size. The cumulative histograms for the effects of TTX and bicuculline on mEPSC amplitude were best fit to controls using a single multiplicative factor, suggesting that activity perturbation scaled all synapses according to their initial strength. Synaptic scaling allows neurons in developing circuits to retain their relative synaptic strengths while compensating for large scale changes in synaptic input and spiking frequency (Turrigiano et al., 1998). Subsequent work has shown that HSP operates by the transcription-dependent insertion or removal of AMPA and NMDA receptors into the postsynaptic membrane (O'Brien et al., 1998; Watt et al., 2000; Wierenga et al., 2005; Ibata et al., 2008). Presynaptic calcium influx and release probability, are also altered in response to chronic activity perturbation (Zhao et al., 2011; Murthy et al., 2001), suggesting that a transsynaptic signal may coordinate pre- and postsynaptic responses (Vitureira et al., 2012).

Synapses also show structural change in response to activity perturbation. Pharmacological silencing *in vitro* and retinal lesions *in vivo* have been shown to enhance the size of presynaptic active zones and dendritic spines (Murthy et al., 2001; Keck et al., 2013). Excitatory synapse density, as assessed by mEPSC frequency, or dendritic spine density, is generally unaffected by inactivity (Turrigiano et al., 1998; Keck et al., 2013). However, mIPSC frequency, as well as spine turnover are reduced by network silencing, suggesting that circuits can actively change synapse numbers in response to activity perturbation (Okabe et al., 1999; Keck et al., 2013).

1.2.5 Activity-Independent Circuit Development

Though the aforementioned studies show that neuronal activity can direct developmental structural plasticity, numerous studies report that circuit development can proceed in the absence of neuronal activity (Molnár et al., 2002; Varoqueaux et al., 2002; Kerschensteiner et al., 2009; Lu et al., 2013; Sigler et al., 2017). Two recent studies tested the effect of abolished neurotransmission on circuit development in the hippocampal CA1 region. Lu et al. (2013) used mice lacking AMPAR subunits (GluA1, GluA2, and GluA3) and the obligatory NMDAr subunit (GluN1), to test the effect of abolished fast glutamatergic neurotransmission on CA1-pyramidal neuron (CA1-PN) morphology in hippocampal slices. In a complementary approach, Sigler et al. (2017) analyzed CA1-PN morphology in mice that were lacking presynaptic proteins essential for glutamatergic and GABAergic neurotransmitter release, Munc13-1 and Munc13-2. Although electrophysiological measures showed that neurotransmission was drastically reduced by these manipulations, morphological features such dendrite complexity, spine/synapse number and synapse ultrastructure were unaffected (Lu et al., 2013; Sigler et al., 2017). Work in the developing retina also questions the role of activity in synapse refinement. Kerschensteiner and colleges (2009) selectively blocked neurotransmitter release from ON bipolar cells by expression of TeNT-LC, a protease which cleaves vesicle-associated membrane protein 2 (VAMP2) and inhibits vesicle fusion. Using time-lapse imaging, they analyzed synapse turnover at retinal ganglion cells that receive input from single ON bipolar cells. Though synapse formation rates were decreased in TeNT-LC axons, surprisingly, neurotransmission blockade had no effect on synapse elimination. These studies provide compelling evidence that synapse formation and stabilization does not require synaptic activity. Furthermore, these results indicate that cell-intrinsic genetic programs and the action of cell surface recognition molecules such as synaptic cell adhesion molecules may play a key role in neuronal circuit development and refinement (Sigler et al., 2017). In the next section of this introduction, I discuss the role of synaptic cell adhesion molecules in the formation, elimination and functional maturation of synapses in developing circuits.

1.3 The Role of Synaptic Adhesion Molecules in Synapse Development and Circuit Refinement

As outlined above, neuronal circuit refinement is characterized by elevated rates of synapse turnover, as new synapses are auditioned for a place in the developing circuit. Appropriate synapses between neurons are strengthened and maintained whereas inappropriate synapses are weakened and eliminated. Synaptic adhesion molecules (SAMs) are transmembrane proteins that are uniquely suited to mediate this structural plasticity as they can interact with prospective partner neurons via extracellular domains and communicate this information inside the cell via intracellular domains (Rawson et al., 2017).

The role of SAMs in circuit development gained recognition following co-culture experiments in which SAMs expressed in non-neuronal cells were cultured with neurons (Scheiffele et al., 2000). Some families SAMs were able to induce the formation of 'hemisynapses', clusters of pre- or postsynaptic material within axons or dendrites that traversed SAM-expressing cells. This valuable assay has subsequently revealed numerous SAMs that induce hemisynapses such as Neuroligins, SynCAMs, Neurexins, LRRTMs, NGL-3, and LAR (Scheiffele et al., 2000; Biederer et al., 2002; Graf et al., 2004; Craig et al., 2006; Linhoff et al., 2009; Woo et al., 2009).

The *in vivo* study of SAMs in synaptogenesis has yielded interesting results. Some studies report that *in vivo* knockdown or deletion of single isoforms or complete families of CAMs reduces synapse density (Robbins et al., 2010; Williams et al., 2011; Li et al., 2015; Chen et al., 2017). Conversely, evidence also indicates that many classes of SAMs are not required for the initial stages of synaptogenesis but instead are essential for synapse function (Missler et al., 2003; Varoqueaux et al., 2006; Chubykin et al., 2007; Anderson et al., 2015). These studies suggest that by organizing synaptic transmission, individual SAMs may function in the functional maturation of synapses. Recent studies also indicate the structural and functional roles of different SAMs vary depending on the identity of the synapse that is under analysis. In the remainder of this introductory

chapter, I will discuss neurexins and neuroligins, SAMs important for the structural maintenance and function of synapses in developing circuits.

1.3.1 Neurexins and Neuroligins in Synapse Formation and Structural Maintenance

Neurexins (Nrxns) were discovered as receptors for α-latrotoxin, a component of *Latrodectus* spider venom that triggers massive neurotransmitter release (Ushkaryov et al., 1992). Nrxns are presynaptic adhesion molecules expressed from three genes in mammals (Nrxn1, Nrxn2, and Nrxn3). Each gene employs two promoters which create the longer α-Nrxn and the shorter β-Nrxn isoforms (Tabuchi and Südhof, 2002). The best studied and only conserved postsynaptic adhesion partner for Nrxns are neuroligins (NL), which constitute a family of 4 genes in rodents with NL 1-3 expressed in the mouse brain (Ichtchenko et al., 1995; Scheiffele et al., 2000). Mutations Nrxn and NL genes are associated with neurodevelopmental diseases such as ASD (Südhof, 2008), indicating a role of these SAMs in the functional development of neural circuits.

Initial evidence that Nrxns and NL induced synapse formation came from co-culture studies in which neurons are grown with non-neuronal cells that express Nrxn or NL. Scheiffele et al. (2000) showed that NL expressed at the surface on HEK293 cells induced the clustering of presynaptic proteins and recycling-competent synaptic vesicles in contacting axons (Scheiffele et al., 2000). Subsequent work showed that NL1 and NL2 selectively localize to excitatory and inhibitory synapses, respectively, and NL3 is present at both excitatory and inhibitory synapses (Song et al., 1999; Poulopoulos et al., 2009; Budreck and Scheiffele, 2007). Work by Graf and colleges (2004) showed that Nrxns expressed on the surface of COS cells causes the aggregation of postsynaptic glutamatergic and GABAergic scaffolding proteins and receptors in contacting dendrites (Graf et al., 2004). These and subsequent studies revealed that the affinity of Nrxn-NL binding is modulated by both the Nrxn isoform involved (α vs β) and the inclusion or exclusion of alternatively spliced sequences in both molecules (reviewed in Craig and Kang, 2007; Siddiqui and Craig, 2011). Nrxn-NL interactions appear to also promote synapse formation between neurons as overexpression or knockdown of NLs in cultured

hippocampal neurons leads to an increase and decrease in synaptic density, respectively (Chih et al., 2005).

These *in vitro* studies suggesting a synaptogenic role for Nrxn and NL contrast with *in vivo* work indicating a more complex function for Nrxns and NL in synapse development and function. Analysis of brainstem sections and cultured hippocampal neurons from constitutive NL1-3 KO mice showed normal excitatory and inhibitory synapse densities, suggesting that NLs do not control the initial formation of synaptic contacts (Varoqueaux et al., 2006). Similarly, isoform specific knockout of all 3 α-Nrxns or all 3 β-Nrxns caused no change in excitatory synapse density (Missler et al., 2003; Anderson et al., 2015). To circumvent possible compensatory mechanisms that may take place in constitutive KO animals, the Sudhof lab recently developed conditional KOs for Nrxns and NL, which reveal distinct, synapse specific roles for Nrxn and NL in synapse formation and function (Aoto et al., 2015; Zhang et al., 2015; Chen et al., 2017; Chanda et al., 2017). For example, Zhang et al. (2015), showed that cKO of all NLs in cerebellar Purkinje cells caused a specific reduction in density of climbing fiber synaptic input, but left the density of parallel fiber synapses onto Purkinje cells unaffected. Moreover, cKO of NLs in cerebellar Purkinje cells has no effect on inhibitory synapse numbers whereas deletion of NLs from hippocampal CA1 pyramidal cells causes a 30% reduction in inhibitory synapse density (Zhang et al., 2015; Jiang et al., 2016). Similarly, cell-type specific deletion of Nrxns from parvalbumin (PV) interneurons caused a large reduction in the density of PV-pyramidal neuron synapses in the neocortex but specific deletion of Nrxn in somatostatin (SST) interneurons had no effect on the density of SST synapses onto the same class of pyramidal neuron (Chen et al., 2017). These studies suggest that Nrxns and NLs may be dispensable for synapse formation and stability at many synapses, but play an essential role at others.

Neurexins and neuroligins also play important roles in synapse development in *Drosophila*. In *Drosophila,* knockout of Nrxn (dNrxn) or NL1 (dNL1) disrupts the localization of synaptic vesicles, active zone proteins and glutamate receptors (Li et al., 2007; Banovic et al., 2010). The presynaptic active zone protein Syd-1, is important for

clustering dNrxn at active zones (Owald et al., 2012). Consequently, Syd-1 also plays a role in clustering postsynaptic dNL1, which organizes the assembly of postsynaptic specializations (Owald et al., 2012). Recent work suggests that dNrxn may also play a role in the regulation of F-actin at presynaptic specializations (Rui et al., 2017). Rui and coworkers (2017) showed that dNrxn forms a complex with Scribble and beta-Pix, which can activate the actin regulator Rac1 and enhance actin polymerization. It will be interesting to see if future work in mammalian systems reveals a similar role for Nrxn in presynaptic actin regulation.

1.3.2 Neurexins and Neuroligins in the Modulation of Synaptic Transmission

Neurotransmission operates via calcium-induced fusion of synaptic vesicles with the presynaptic membrane and release of neurotransmitters onto precisely localized postsynaptic receptors. Knockout studies suggest that Nrxn and NL play a role in enabling neurotransmission by organizing both the presynaptic release machinery and postsynaptic receptors. At many types of synapses, Nrxn perturbation reduces the likelihood of neurotransmitter release, likely by attenuating action potential-evoked presynaptic calcium transients (Missler et al., 2003; Anderson et al., 2015; Chen et al., 2017). Missler and colleges found that knockout of all 3 α-Nrxns reduced release probability at excitatory and inhibitory synapses in the neocortex and brainstem (Missler et al., 2003). α-Nrxn triple KO mice also had reduced whole-cell calcium currents and showed evoked-PSCs that were less sensitive to calcium channel inhibitors compared to control synapses. The finding that Nrxns can modulate presynaptic function opens the possibility that transsynaptic interactions between Nrxns and its postsynaptic ligands may be utilized to mediate retrograde control of neurotransmission by postsynaptic neurons. This notion is supported by work from Anderson and collaborators who reported that elimination of all β-Nrxns led to a tonic increase in endocannabinoid synthesis in postsynaptic neurons which resulted in a reduction in presynaptic calcium transients and release probability (Anderson et al., 2015). Consistent with this finding, a modulation of the expression of NL1 has been shown to result in bidirectional changes in neurotransmitter release probability in CA1 pyramidal neurons in the hippocampus (Futai

et al., 2007). It should be noted, however, that several studies of synaptic preparations of mice with eliminated or attenuated expression of postsynaptic Nrxn ligands failed to observe alterations in neurotransmitter release (Soler-Llavina et al., 2011; Zhang et al., 2015; Chanda et al., 2017).

On the postsynaptic side, Nrxn ligands can modulate neurotransmission by stabilizing postsynaptic glutamate receptors. Thus, NL1 and NL2, are important for the organization of neurotransmitter receptors and scaffold proteins at excitatory and inhibitory synapses respectively. At excitatory synapses, NL1 recruits PSD95 and ionotropic glutamate receptors to synapses (Kornau et al., 1995; Irie et al., 1997; Heine et al., 2008; Barrow et al., 2009; Mondin et al., 2011). Accordingly, knockout of NL1 impairs AMPAR and NMDAR-mediated currents without affecting inhibitory neurotransmission (Chubykin et al., 2007; Jiang et al., 2016; Chanda et al., 2017). Moreover, other neurexin ligands may share the glutamate receptor recruiting function of NLs (Aoto et al., 2013; Aoto et al., 2015). Aoto et al. showed that hippocampal neurons devoid of Nrx3α/β have a selective reduction in AMPAR-mediated neurotransmission due to reduced retention of AMPARs at the postsynaptic membrane (Aoto et al., 2015). In a related study, Nrxn3 perturbation reduced the surface expression of the adhesion molecule LRRTM2, a postsynaptic Nrxn ligand (Aoto et al., 2013). Together these studies indicate that presynaptic Nrxn3 acts to stabilize postsynaptic AMPAR by activating LRRTM2 and possibly other ligands (Aoto et al., 2013; Aoto et al., 2015; but see Soler-Llavina et al., 2011). The role of neurexin ligands in the recruitment of neurotransmitter receptors, however, is not limited to excitatory synapses. At inhibitory synapses, NL2 interacts with collybistin and the scaffolding protein gephyrin to recruit GABA receptors to synapses (Poulopoulos et al., 2009) and deletion of NL2 causes a specific impairment in inhibitory neurotransmission (Chubykin et al., 2007; Jiang et al., 2016; Chanda et al., 2017).

In accordance with the synapse-specific effects of Nrxn and NL perturbation on synapse density, recent evidence suggests that Nrxns and NLs are essential for neurotransmission at certain types of synapses but dispensable at others. Analysis of 2

types of inhibitory neocortical synapses onto pyramidal cells revealed that pan-Nrxn KO drastically reduces release probability and presynaptic calcium transients in SST axons but has no effect on calcium handling or neurotransmitter release in from PV neurons (Chen et al., 2017). In a similar manner, deletion of all NLs from Purkinje cells causes a postsynaptic deficit in neurotransmission at excitatory climbing fiber input but has no effect on the reception of excitatory input from parallel fibers (Zhang et al., 2015). These studies highlight the complexity of Nrxn-NL interactions in synapse formation and function.

As discussed in this introduction, neuronal activity and synaptic cell adhesion play important roles in modulating circuit development. Neuronal activity is essential for shaping the development of some circuits but is seemingly dispensable in others. Synaptic cell adhesion molecules are ideally suited to modulate synapse refinement by controlling synapse structure (ie: synapse formation, elimination, or stabilization) and function (ie: neurotransmitter release and reception). In this thesis, we first test the role of global and synapse-specific activity perturbation on synapse elimination. Then we examine how the Nrxn family of cell adhesion molecules regulates synapse stability and neurotransmitter release. In a final set of experiments, we test if Nrxns stabilizes synapses by promoting functional neurotransmission or by providing structural adhesive support to synapses.

1.4 Rationales and Hypothesis

The principle hypothesis of this thesis is: *Neuronal activity and synaptic cell adhesion will modulate the stability and function of synapses in developing neural networks*. Specific hypothesis for each study in this thesis are as follows:

Hypothesis 1: Global blockade of neuronal activity will reduce synapse elimination in developing neuronal cultures whereas synapse specific blockade of activity will not.

In Chapter 2, I use time-lapse imaging of fluorescently labeled synapses in hippocampal cultures to test the effects of global or synapse-specific activity blockade on synapse stability.

Hypothesis 2: Perturbation of synaptic cell adhesion molecules of the neurexin family will destabilize synapses in developing neuronal culture.

In Chapter 3, I test this hypothesis by designing shRNA knockdown and neurexin dominant-negative constructs to perturb neurexin function. I then measure the effect of neurexin perturbation on synapse stability using fluorescent time-lapse imaging.

Hypothesis 3: Perturbation of neurexins will disrupt active zone content, calcium influx and neurotransmitter release at presynaptic boutons.

In Chapter 4, I use immunocytochemistry and genetically encoded sensors for axonal calcium and synaptic vesicle exocytosis to test the role of neurexins in presynaptic function.

Hypothesis 4: Neurexins stabilize synapses in an activity-independent manner.

In Chapter 5, I test if attenuated neurotransmission is the causative factor for synapse destabilization in response to perturbation of neurexin function by assessing if effects of knockdown of neurexin expression on synapse stability persist in the presence of global or synapse-specific activity blockade.

CHAPTER 2

GLOBAL AND SPARSE ACTIVITY BLOCKADE DIFFERENTIALLY REGULATE SYNAPSE REFINEMENT

2.1 Introduction

During development, synapses show an unparalleled level of structural plasticity as the concurrent processes of synapse formation and elimination control the refinement of neuronal connections. To allow for functional adaptation during development, circuits are first built with many unnecessary synapses that are later weakened and eliminated. The selective stabilization of suitable synapses and removal of inappropriate synapses leads to the establishment of a mature circuit.

Neuronal activity is thought to be essential for the refinement of neuronal circuits. Even before birth, neurons fire bursts of action potentials which can spread throughout neurocircuits via synaptic transmission and gap junctions (Blankenship and Feller, 2009). Neuronal activity can modulate structural synaptic plasticity within developing circuit in numerous ways. Large-scale increases or decreases in spiking frequency can induce homeostatic synaptic plasticity (HSP), whereby the size (Murthy et al., 2001) and strength (Turrigiano et al., 1998) of synapses are scaled down or up in response to prolonged increases or decreases in neuronal activity (Keck et al., 2017). Smaller groups or clusters of synapses can compete for space in developing circuits in a process called heterosynaptic plasticity whereby signalling at highly active synapses along a dendritic branch contributes to the weakening of less active neighboring synapses (Yasuda et al., 2011; Oh et al., 2015). At individual synapses, the processes of long-term potentiation and long-term depression can lead to the stabilization or elimination of synapses, respectively (Hill and Zito, 2013; Oh et al., 2013; Wiegert and Oertner, 2013). Neurotransmitter release may also play a role in synapse formation as the release of glutamate near dendrites has been shown to induce filopodia and dendritic spine formation (Richards et al., 2005; Kwon and Sabatini, 2011).

However, circuit refinement has also been shown to proceed normally in the absence of neuronal activity. For example, studies in the retina show that the elimination of synapses from ON-bipolar cells onto ON-OFF retinal ganglion cells is unaltered by activity silencing (Kerschensteiner et al., 2009). Also, blockade of activity in the

hippocampus via genetic deletion of ionotropic glutamate receptors (Lu et al., 2013) or proteins required for synaptic vesicle exocytosis (Sigler et al., 2017) has little effect on circuit development, questioning the role of activity in neuronal refinement.

In this chapter, we test the role that neuronal activity plays in the refinement of synapses in dissociated hippocampal neurons. To gain insight into multiple types of activity-modulated structural plasticity, we utilize two approaches to silence neuronal activity, global network silencing via iGluR blockade and synapse-specific silencing via sparse expression of Tetanus Neurotoxin Light Chain (TeNT-LC). Our data reveal that synapse turnover is differentially effected by global and synapse specific activity blockade and suggest that homeostatic synaptic plasticity leads to enhanced stability of synaptic contacts.

2.2 Methods

2.2.1 cDNA Constructs

To simultaneously visualize and inactivate sparse populations of presynaptic boutons we created a construct that encodes for TeNT-LC and Synaptophysin-mCherry (Syph-mCh). A TeNT-LC cDNA construct was purchased from Addgene (Plasmid #32640). Using PCR, we added AgeI and MfeI restriction sites to N- and C-termini of the TeNT-LC coding sequence using the primers 5'-AAACCGGTCGCCACCATGACCAT GATTACGCCAAGCTATTTAGG-3' (forward) and AACAATTGTTAAGCGGTA CGGTTGTACAGGTTTTC -3' (reverse), respectively. Via AgeI and MfeI, TeNT-LC was then cloned into a pE vector immediately downstream of a cytomegalovirus (CMV) promoter, which created pE-TeNT. Next, using primers 5'-AAACATGTTCTGTGGATAACCGTATTACCG-3' (forward) and 5'-AAACATGTG-CGTTAAGATACATTGATGAGTTTGG-3' (reverse), we inserted PciI sites at the N- and C-terminal ends of a CMV-Syph-mCh cassette, which was then inserted into pE-TeNT at a unique PciI site to create TeNT-LC-Syph-mCh. Synaptophysin-pHluorin (SypHl) was created by isolating the rat synaptophysin cDNA (accession no.

NM_012664) from brain total RNA by RT-PCR and ligating it into a pEGFP-C1-based expression vector. A cassette containing three copies of superecliptic pHluorin was then inserted into the synaptophysin cDNA between the codons for amino acids 184 and 185 using a PCR approach (Matz et al., 2010). The Synaptophysin-mCherry construct was generated by fusing the ORF of synaptophysin (obtained via RT-PCR) in-frame to the 5′ end of mCherry cDNA contained in a pEGFP-C1-based expression vector. Homer1B was a gift from Dr. Carlo Sala. The Homer1B sequence was PCR-amplified with primers encoding AgeI and BamHI sites and ligated into a BspEI/BamHI-cut pEGFP-C1 vector to create EGFP-Hmr1b.

2.2.2 Dissociated Hippocampal Cultures

Dissociated neuronal cultures were prepared from E18 embryonal Sprague Dawley rat hippocampi. All experiments on animals were approved by the Dalhousie University Committee on Laboratory Animals (UCLA Protocol #15–113) and performed in accordance with the approved guidelines. Following dissection, hippocampi were incubated in 0.03 % trypsin for 15 min and dissociated using a fire-polished Pasteur pipette (Matz et al., 2010). Neurons were diluted in Neurobasal medium supplemented with B27 (ThermoFisher, Waltham MA), 0.5 mM glutamine, 25 µM glutamate, and 5% fetal calf serum (FCS) and added at a density of 3-6 x 10^3 cm^{-1} to 60-mm dishes containing 5, 16-mm coverslips coated with 0.1% (wt/vol) poly-L-lysine (Peptides International). After 4 hours, the plating medium was replaced with serum-free Neurobasal supplemented with B-27 (Matz et al., 2010). Dissociated hippocampal neurons were prepared in the same manner in all subsequent chapters.

2.2.3 Transfections

For all experiments, cultures of hippocampal neurons were transfected 10–14 days after plating using a calcium-phosphate precipitation protocol. Using fire-polished forceps, coverslips were first transferred into new 60 mm dishes containing MEM and 1/100 volume B-27. For each 60-mm dish of 5 coverslips, a 300 µl precipitation mix

containing water, plasmid DNA and 0.25 M $CaCl_2$ was prepared and added in 1/10 increments to a 300 µl solution of (in mM) 274 NaCl, 10 KCl, 1.4 Na_2HPO_4, 15 D-glucose and 42 -(2-hydroxyethyl)-1-piperazineethanesulfonic acid (HEPES), pH 7.10. The plasmid DNA amounts used are noted with the description of each experiment. Following 20 minutes of incubation at room temperature, the transfection mixes were added to the neuronal cultures and incubated at 5% CO_2 and 37 ºC for 3-4 hours. Cultures were then washed with a buffer containing (in mM) 144 NaCl, 3 KCl, 3 mM $MgCl_2$, 10 mM HEPES, pH 6.70, and coverslips were transferred back into their original dishes and media. Dissociated hippocampal neurons were transfected in the same manner in all subsequent chapters.

2.2.4 Image Acquisition of Synapse Turnover Assay

To assess synapse turnover in dissociated hippocampal neurons, we fluorescently labeled pre- and postsynaptic specializations in separate populations of neurons and recorded the number of stable, newly formed and eliminated synapses that occurred over 24 hours. To image presynaptic sites, clusters of synaptic vesicles were labeled with a mCherry-tagged version of synaptophysin, a protein found in the membrane of synaptic vesicles. Postsynaptic densities were labeled with an EGFP-tagged version of the scaffolding protein Homer1b. For experiments involving iGluR blockade, Syph-mCh (20-30 µg/dish) and EGFP-Hmr (35-40 µg/dish) were transfected at 13 and 14 DIV, respectively. For experiments using TeNT-LC, either a control plasmid containing Syph-mCh (20 µg/dish) or TeNT-LC-Syph-mCh (20 µg/dish) was transfected at 13 DIV and EGFP-Hmr (30-40 µg/dish) was transfected at 14 DIV. At 16 DIV, coverslips were loaded into a circular imaging chamber and imaged with a Zeiss Observer 2.1 inverted microscope using a Photometrics Coolsnap HQ2 camera and SlideBook 6 imaging software. Experiments were performed at 36 +/- 2 °C in HBS solution containing (in mM) 110 NaCl, 5.3 KCl, 2 $CaCl_2$, 1 $MgCl_2$, 20 4-(2-hydroxyethyl)-1-piperazineethanesulfonic acid (HEPES), and 25 D-glucose adjusted to pH 7.30. Before fluorescent imaging, the rotational center of each coverslip was determined, and a 20x DIC image was acquired. Without moving the imaging chamber, immersion oil was

applied to the 63x (N.A. 1.4) objective and it was brought into the imaging path. Stacks comprising 7 images over a distance of 2.1 μm were acquired of neurons that showed Syph-mCh positive axons in contact with EGFP-Hmr positive dendrites. These are referred to Day0 (D0) images. The XY coordinates were recorded and coverslips were returned to the incubator for 24 hours. The following day, coverslips were re-loaded into the circular imaging chamber, and the chamber was rotated until the live 20x DIC image aligned with the DIC image from the previous day. Once the chamber was properly aligned, the saved coordinates were revisited, and a second image stack was acquired for each experiment (D1). Before the first imaging session, I was blinded to the experimental conditions.

2.2.5 Image Analysis of Synapse Turnover Assay

Image stacks were converted to maximum intensity projection images, background corrected, and D0 and D1 images were manually aligned using EGFP-Hmr images. Axons and dendrites which appeared unhealthy (ie: showed significant structural changes or were missing from D1 images) were excluded from analysis. Co-localizations of Syph-mCh and EGFP-Hmr that had a center-to-center distance within 0.8 μm were considered synaptic. By comparing D0 and D1 images, the number of stable, eliminated, and newly formed synapses was recorded. In a subset of experiments, we quantified the intensities of Syph-mCh and EGFP-Hmr puncta by placing segments on the images and measuring the fluorescent intensities of stable, eliminated and newly formed synapses. Synaptic regions of measurement had a size between 0.32 and 0.64 μm^2. Due to plasmid expression variability between neurons, the intensity of EGFP-Hmr/Syph-mCh puncta on each postsynaptic neuron was normalized to the average intensity of all analyzed EGFP-Hmr/Syph-mCh puncta for that neuron. All analysis was performed using IPLab software in a blinded fashion.

In figure 2.2, to calculate the percentages of stable, eliminated, and formed synapses, the counts for each were divided by the total number of analysed synapses and the results from 4 cultures were averaged. Grouping the data in this way allowed pie

graph representation and showed an overview of the rates of synapse turnover in our cultures. For figures 2.4 and 2.6 the percentage of formed synapses was calculated in the same way as described above and the percentage of eliminated synapses was calculate by dividing by the total of stable and eliminated synapses. Differences in % eliminated and % formed between Ctrl and iGluR blockade and Ctrl and TeNT-LC groups were statistically tested using Student's t-tests for independent samples.

2.2.6 Assessment of TeNT-LC Efficiency with Synaptophysin-pHluorin

To assess the silencing effect of TeNT-LC, cultures of hippocampal neurons were co-transfected with 20 µg of either a control plasmid (Syph-mCh) or TeNT-LC-Syph-mCh, along with 80 µg of Synaptophysin-pHluorin (SypHl) at 13 DIV. At 16-17 DIV Fluorescence microscopy was carried out on a Nikon TE2000 epifuorescence microscope equipped with a 60x (N.A. 1.40) objective, Smart shutter (Sutter Instruments) and Lumencor solid-state illumination. Images were acquired at 10 Hz with a Hamamatsu ORCA CCD camera and IPLab software. Experiments were performed at 36 +/- 2 °C in HBS solution (described above) supplemented with 10 µM 6,7-dinitroquinoxaline-2,3-dione (DNQX) and 50 µM (2R)-amino-5-phosphonovaleric acid (APV) to prevent recurrent excitation. Axons were selected based on Syph-mCh fluorescence, and SypHl fluorescence changes were measured in response to field stimulation employing 1-ms square current pulses yielding electrical fields of approximately 10 V/cm through platinum electrodes placed 0.5 cm apart. Image acquisition and extracellular stimulation were synchronized using a Master-8 stimulator (AMPI). Stimulus trains of 80 stimuli at 80 Hz were given to measure the readily releasable pool of synaptic vesicles. Using IPLab software, image stacks were background-subtracted and aligned. ROIs for measurement were selected on SypHl images according to a threshold-based algorithm. Synaptic regions of measurement had a size between 0.32 and 0.64 μm^2. Data were expressed as change in fluorescence (ΔF). Differences in ΔF responses between Ctrl and TeNT-LC groups statistically tested using Student's t-tests for independent samples.

2.3 Results

2.3.1 Characteristics of Synaptic Refinement in Rat Dissociated Hippocampal Neurons

Initially, we documented the characteristics of synapse refinement in untreated cultures of dissociated hippocampal neurons using time-lapse fluorescent imaging. Neurons were transfected at 13 days *in vitro* (DIV) with Synaptophysin-mCherry (Syph-mCh, Figure 2.1), to label synaptic vesicles in presynaptic specializations. At 14 DIV, a second transfection was performed to label a separate population of neurons with EGFP-Homer1b (EGFP-Hmr), a marker for the postsynaptic densities. At 16 DIV, image stacks were acquired of EGFP-Hmr expressing neurons that co-localized with Syph-mCh expressing axons (D0 images). The following day, the same fields were revisited and a second image stack was acquired (D1 images). Maximum intensity projected images were created, and the percentage of stable, eliminated, and newly formed synapses was recorded. Syph-mCh and EGFP-Hmr puncta that had a center-to-center distance of less than 0.8 μm were considered synaptic contacts. On average, 43.1 +/- 5.6% of analyzed synapses remain stable, 28.6 +/- 2.3% of synapses were eliminated, and 28.2 +/- 3.7% of synapses were newly formed over a 24-hour period (Figure 2.2B).

The structural events that underlie synapse formation and synapse elimination are currently not well understood. By fluorescently labeling both pre- and postsynaptic specializations, we have the unique opportunity to address this question. We therefore, further classified synapse eliminations and formations by the characteristics of pre- and postsynaptic structural plasticity that occurred over the two imaging sessions (Figure 2.2A-B). Synapse formations predominately involved the simultaneous appearance of pre- and postsynaptic elements in the Day1 image (55.6% of synapse formations). In a minority of instances, synapse formation occurred by the appearance of a presynaptic bouton to contact pre-existing dendritic spine (39.1%) or the formation/extension of a dendritic spine to contact a pre-existing presynaptic bouton (5.3%). For synapse eliminations, most instances involved the simultaneous disappearance of pre- and postsynaptic elements in the Day1 image (49.5% of synapse eliminations). The

remaining synapse eliminations either occurred by the disappearance of the presynaptic bouton away from a remaining dendritic spine (33.2%) or the retraction of a dendritic spine from a presynaptic bouton which remained stable in the Day1 image (17.3%). This analysis shows that in cultures of dissociated hippocampal neurons, a significant fraction of synapses is replaced in the course of 24 hours and that both pre- and postsynaptic elements contribute to synapse assembly and disassembly.

2.3.2 Synapse Size Predicts Synapse Survival

Long-term depression (LTD) in hippocampal slice cultures has been shown to cause shrinkage and the eventual elimination of dendritic spines (Zhou et al., 2004; Holtmaat et al., 2005; Bastrikova et al., 2008; Oh et al., 2013; Wiegert and Oertner, 2013; Hayama et al., 2013). Newly formed spines are also in smaller size compared to persistent spines (Knott et al., 2006; Holtmaat et al., 2006; Zito et al., 2009). To test if synapse size is predictive of synapse survival in our culture system we quantified the fluorescent intensities of Syph-mCh and EGFP-Hmr puncta over 24 hours.

Maximum intensity projections of Day0 and Day1 image stacks were auto-segmented, and the fluorescent intensity of stable, eliminated, and newly formed synapses was measured. Syph-mCh and EGFP-Hmr puncta intensities served as proxy measurement for synapses size considering that synaptic vesicle content and postsynaptic density (PSD) size are highly correlated with bouton volume and spine volume respectively (Knott et al., 2006; Arellano et al., 2007; Meyer et al., 2014). Intensity measurements for co-localized Syph-mCh and EGFP-Hmr puncta were normalized to the average intensity of all analyzed synapses for each Syph-mCh and EGFP-Hmr expressing cell. We then compared the intensities of stable and eliminated Day 0 puncta as well as stable and newly formed D1 puncta. We found that Syph-mCh and EGFP-Hmr puncta at eliminated synapses were significantly less intense compared to synapses that remained stable (Figure 2.3B). Similarly, Syph-mCh and EGFP-Hmr puncta at newly formed synapses were significantly less intense compared to stable synapses. The importance of synapse size and synapse stability became even more clear when we assigned each

synapse a proxy of size by averaging the normalized intensity values for Syph-mCh and Hmr-EGFP puncta (Figure 2.3C). Assigning these data into bins revealed that the smallest synapses were eliminated to a large degree (~50%) whereas large synapses were much more stable (Figure 2.3D). Taken together, these results indicate that in dissociated hippocampal cultures, synapse size is predictive of synapse stability.

2.3.3 Global Blockage of Ionotropic Glutamate Receptors Decreases Synapse Elimination

Neuronal activity is thought to play a major role in the regulation of synapse elimination and structural plasticity (Okabe et al., 1999; Trachtenberg et al., 2002; Yasumatsu et al., 2008; Kano and Hashimoto, 2009). Some evidence, however, also suggests that neuronal activity is not necessary for the elimination of redundant synapses in developing neuronal circuits. For example, the abolishment of glutamate release from ON bipolar cells onto ON-OFF retinal ganglion cells does not affect synapse elimination in the developing retina (Kerschensteiner et al., 2009). Also, activity blockade via the genetic deletion of all ionotropic glutamate receptors (iGluRs; Lu et al., 2013) or the deletion of proteins essential for neurotransmitter release (Sigler et al., 2017), has shown little impact on synapse density. To test if global activity modulates synapse elimination in dissociated hippocampal culture, we abolished excitatory neurotransmission by blocking NMDA and AMPA receptors and imaged synaptically connected neurons over 24 hours.

Dissociated hippocampal neurons were sequentially transfected with pre- and postsynaptic markers as described above. Following the second transfection, pharmacological blockers of NMDA receptors (APV, 50 μM) and AMPA receptors (DNQX, 20 μM) were applied to a subset of the cultures for the remainder of the experiment. Blockade of ionotropic glutamate receptors (iGluRs) significantly reduced synapse elimination rates (Ctrl = 48.1 +/- 1.7 % of synapses eliminated, iGluR Block = 40.6 +/- 1.9 % of synapses eliminated, Figure 2.4, left graph). Blockade of iGluRs did not significantly affect rates of synapse formation (Ctrl = 33.0 +/- 1.9 % of synapses formed, iGluR Block = 31.1 +/- 1.6 % of synapses formed, Figure 2.4 right graph).

These findings suggest that, while synaptic activity is not required for the formation or elimination of glutamatergic synapses, global blockade of synaptic transmission promotes the stabilization of synapses.

2.3.4 Synapse-Specific Silencing of Neurotransmitter Release Reduces Synapse Formation but has no Effect on Synapse Elimination

Blockade of glutamate receptors may promote the stability of glutamatergic synapses by preventing the induction of LTD, which has been shown to facilitate synapse elimination (Wiegert and Oertner, 2013). Alternatively, iGluR blockade could conceivably induce homeostatic alterations in postsynaptic neurons that, next to the scaling of glutamatergic synapses, may also lead to a reduction in synapse elimination in an attempt to compensate for the reduced excitatory input. To distinguish between these possibilities, we silenced neurotransmitter release at a small subset of synapses using sparse transfection of tetanus toxin light chain (TeNT-LC, Harms et al., 2005). TeNT-LC is a bacterial protease which cleaves synaptobrevin, a SNARE protein that is essential for vesicle fusion (Schiavo et al., 1992). Its sparse expression in a small subset of neurons should prevent evoked neurotransmitter release from transfected neurons without significantly affecting global activity levels in neuronal cultures. To confirm the effectiveness of TeNT-LC in blocking NT release, we used a genetically encoded sensor, synaptophysin-pHluorin (SypHl; Sankaranarayanan et al., 2000; Matz et al., 2010), to measure synaptic vesicle exocytosis at synapses that express TeNT-LC (see Figure. 2.5B for SypHl mechanism). Cultures of dissociated hippocampal neurons were co-transfected at 13 DIV with SypHl and either TeNT-LC-Syph-mCh or Syph-mCh. At 16 DIV, fields of Syph-mCh-expressing axons were selected and a high-frequency stimulus train (80 Hz for 1s) was used to compare synaptic vesicle exocytosis in TeNT-LC-expressing and control axons. As expected, TeNT-LC was very effective at inhibiting neurotransmitter release (Figure 2.5). We observed an overall reduction in synaptic vesicle exocytosis of >90% in response to 1s stimulus trains at 80 Hz (Ctrl Total ΔF = 33564 +/- 326, TeNT Total ΔF = 2564 +/- 326 per experiment, Figure 2.5C, left graph). TeNT-LC expression did not affect axon length (Ctrl = 5.99 +/- 0.48 μm, TeNT = 6.42 +/- 0.58 μm axon per 10

μm^2, Figure 2.5C, right graph). As outlined above, the expression of TeNT-LC strongly reduces synaptic vesicle exocytosis. When sparsely transfected, TeNT-LC will allow us to assess the role of NT release in synapse elimination without activating homeostatic plasticity mechanisms.

To assess the role activity blockade at a sparse subset of synapses on synapse turnover, cultures were sequentially transfected with TeNT-LC-Syph-mCh or Syph-mCh at 13 DIV and EGFP-Hmr at 14 DIV and synapses were imaged over 24 hours. In contrast to global blockade of neuronal activity, synapse-specific silencing of neurotransmission via TeNT-LC expression did not affect synapse elimination (Ctrl = 35.5 +/- 4.0 % of synapses eliminated; TeNT-LC = 33.3 +/- 3.8 % of synapse eliminated, Figure 2.6). Interestingly, synapse formation was significantly reduced by TeNT-LC expression compared to control cultures (Ctrl = 24.3 +/- 2.7 % of synapses formed; TeNT-LC = 15.5 +/- 2.5 % of synapses formed). These results suggest that abolishing neurotransmission at individual synapses has no net effect on the stability of these synapses.

2.4 Discussion

In this chapter, we document synapse refinement in fluorescently labeled dissociated hippocampal neurons. We show that both pre- and postsynaptic specializations are highly plastic during synapse refinement and that synapse size is predictive of synapse stability. Importantly, we demonstrate that neuronal activity modulates synapse turnover and highlight the differential effects of global and sparse activity blockade on the structural dynamics of synapses.

Our results show that global blockade of neuronal activity with iGluR antagonists causes an increased retention of synaptic connections. These results are consistent with previous studies in hippocampal culture (Okabe et al., 1999) and *in vivo* (Zuo et al., 2005), which show that activity blockade and sensory deprivation, respectively, increase the stability of dendritic spines. Interestingly, we find that sparse blockade of

neurotransmission with TeNT-LC expression in a subset of neurons has no effect on synapse stability. This finding is consistent with previous work in hippocampal culture showing that TeNT-LC expression does not decrease the volume of spines that oppose TeNT-LC-expressing presynaptic boutons (Lee et al., 2010). It is also in agreement with an *in vivo* study in the retina showing that TeNT-LC-mediated blockade of synaptic transmission from ON-bipolar cells affects formation, but not the elimination of ON-bipolar synapses onto ON-OFF retinal ganglion cells (Kerschensteiner et al., 2009).

A fundamental difference between global and sparse silencing of synaptic inputs is that global silencing of all synaptic input will drastically reduce spiking frequency and activate homeostatic plasticity mechanisms, whereas sparse silencing of subset of inputs will not. Global inactivity was previously shown to enhance neurotransmission (Turrigiano et al., 1998; Zhao et al., 2011), and increase synapse size (Murthy et al., 2001). Considering that we, and others, find that synapse size is predictive of synapse stability (Hill and Zito, 2013; Wiegert and Oertner, 2013), it is possible that global inactivity causes synapses to grow larger and to recruit molecules that enhance synapse stability. Therefore, enhanced synapse retention may work in parallel with enhanced synaptic strength to elevate firing rates during periods of reduced synaptic input. Alternatively, global silencing could also affect synapse turnover by preventing heterosynaptic activity. Highly active synapses have been shown to contribute to the weakening of neighboring synapses (Oh et al., 2015), a mechanism that would be abolished during chronic blockade of glutamate receptors. However, the notion that heterosynaptic competition leads to increased elimination of inactive synapses (Yasuda et al., 2011) is not supported by the findings from our experiments using TeNT-LC to silence a small subset of neurons.

Our results also show that blocking neurotransmitter release by TeNT-LC expression causes reduced synaptogenesis. Previous work has shown that neuronal activity and glutamate uncaging can facilitate the formation of dendritic spines and filopodia (Engert and Bonhoeffer, 1999; Maletic-Savatic et al., 1999; Kwon and Sabatini, 2011). Since TeNT-LC boutons have drastically reduced glutamate release, it is possible

they are less able to activate postsynaptic signaling and initiate synapse formation. Somewhat in discrepancy to this interpretation is our finding that global activity blockade using glutamate receptor antagonists did not lead to a significant reduction in synapse formation. As outlined above, iGluR blockade and sparse expression of TeNT-LC differ in their ability to induce homeostatic responses in neurons to altered global activity levels, and it is possible that this difference accounts for the discrepant effects on synapse formation. It should be noted, however, that a previous study assessing the effects of iGluR blockade on synapse turnover did find a reduction in synapse formation (Okabe et al., 1999), which makes it somewhat difficult to draw conclusions in this respect.

Figure 2.1. Synapse turnover assay in rat dissociated hippocampal neurons. (A) Experimental timeline of transfections and imaging sessions. (B) Example overview images of presynaptic vesicles labeled with Syph-mCh (red) and postsynaptic dendritic spines labeled with EGFP-Hmr (green). Images are taken on 2 consecutive days (D0 and D1) and the percentage of stable, eliminated and newly formed synapses is calculated for each postsynaptic neuron. Scale bar = 10 μm

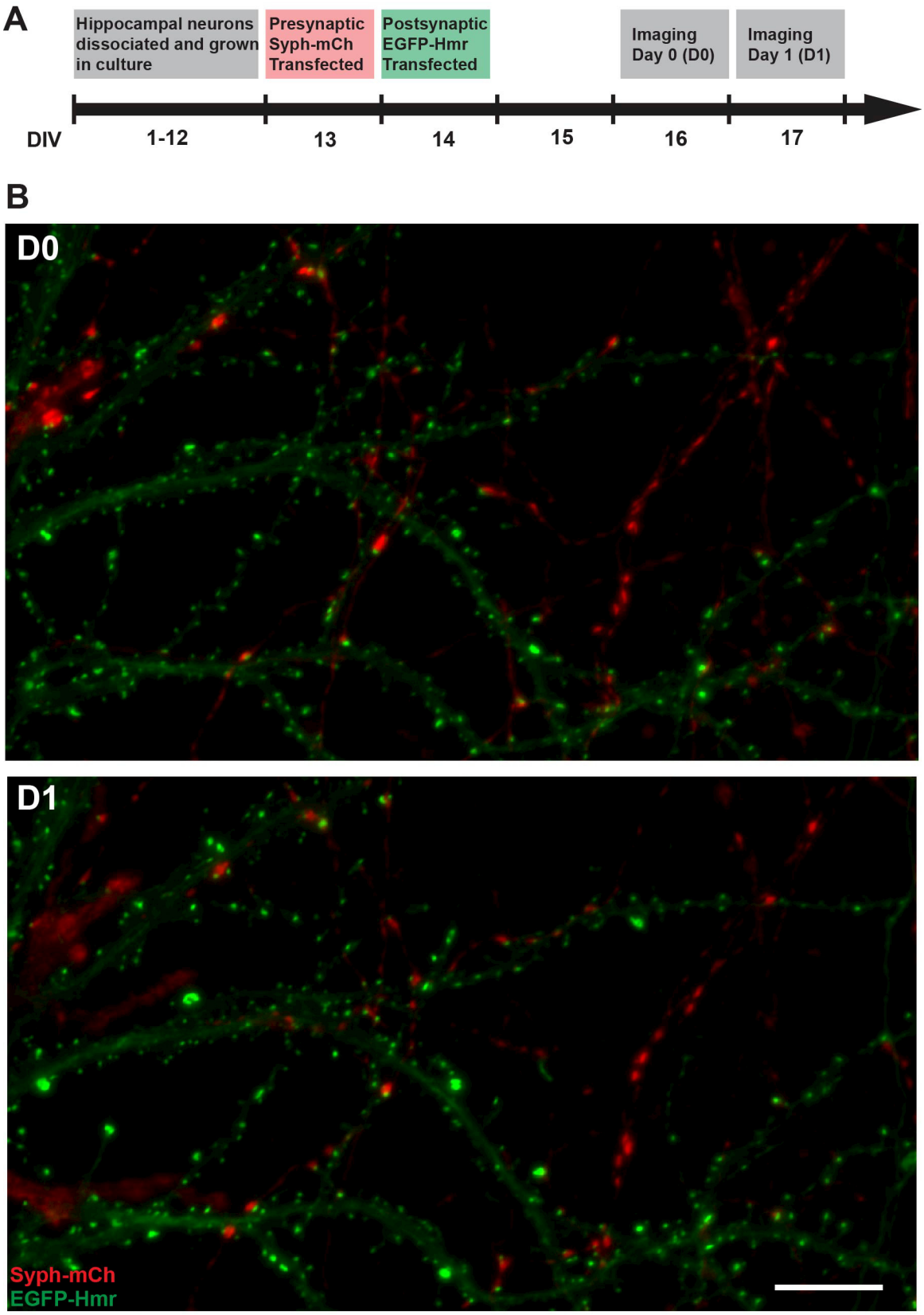
A
Hippocampal neurons dissociated and grown in culture
Presynaptic Syph-mCh Transfected
Postsynaptic EGFP-Hmr Transfected
Imaging Day 0 (D0)
Imaging Day 1 (D1)
DIV
1-12
13
14
15
16
17
B
D0
D1
Syph-mCh
EGFP-Hmr

Figure 2.2. Pre- and postsynaptic specializations participated in synapse formations and eliminations. (A) Example images of stable synapses (filled arrowheads), as well as different types of pre- and postsynaptic structural plasticity that contribute to synapse elimination (open arrowheads) and formation (asterisks). (B) Average percentages of stable (gray), eliminated (red) and formed synapses (green, n = 55 neurons over 4 cultures). Shades of green and red indicate different types of pre- and postsynaptic structural plasticity involved with synapse gain and loss (n = 427 synapses over 4 cultures, Pre = Presynaptic Syph-mCh labeled axon, Post = Postsynaptic EGFP-Hmr labeled dendritic spine). Scale bar = 1 μm.

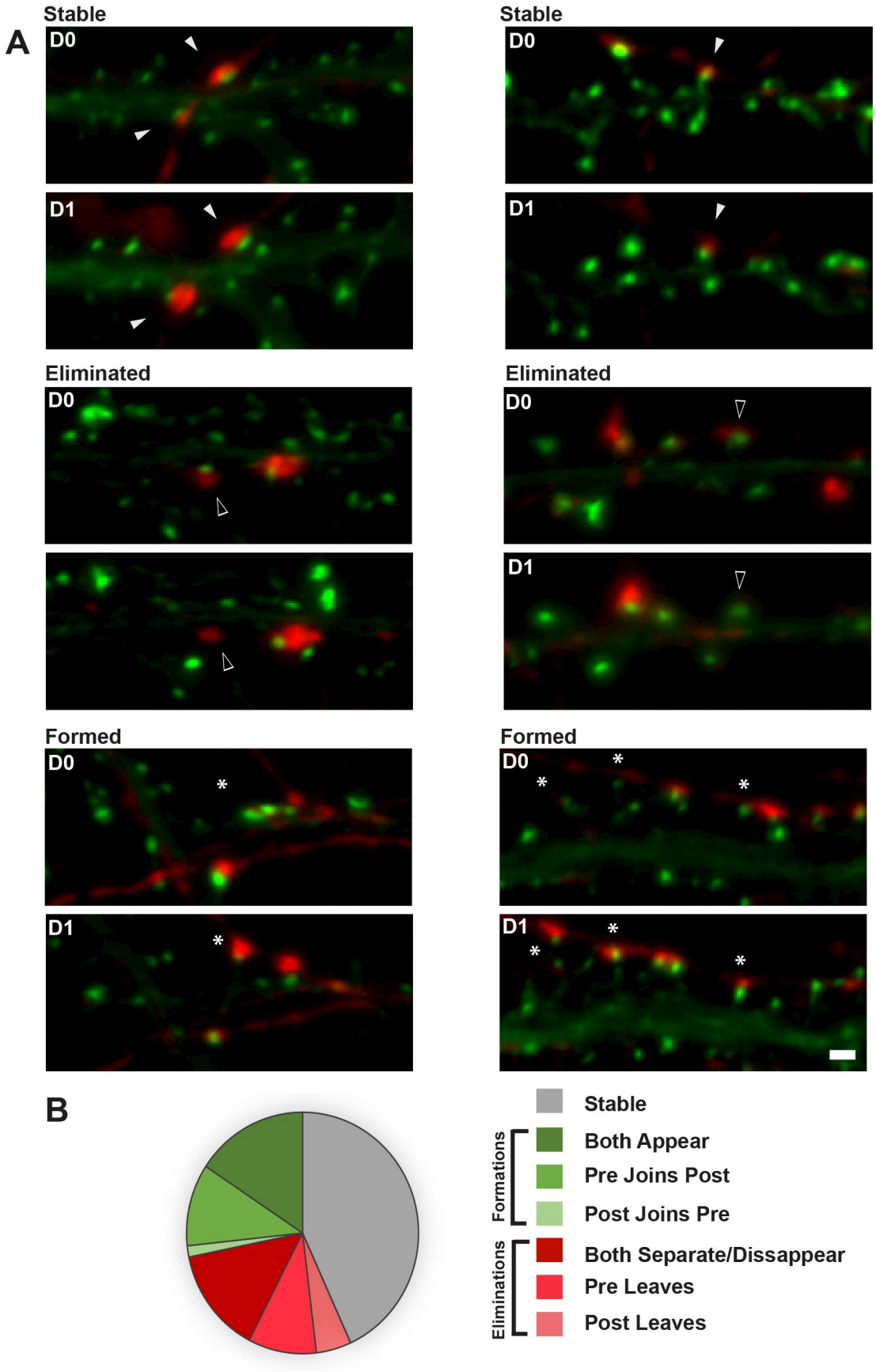
A
Stable
D0
D1
Stable
D0
D1
Eliminated
D0
D1
Eliminated
D0
D1
Formed
D0
D1
Formed
D0
D1
B
Stable
Formations
Both Appear
Pre Joins Post
Post Joins Pre
Eliminations
Both Separate/Dissappear
Pre Leaves
Post Leaves

Figure 2.3. Synapse size predicts synapse survival. (A) Example micrographs of large stable synapses (filled arrowheads), a small eliminated synapse (open arrowheads) and a small formed synapse (asterisks). (B) Normalized Syph-mCh and EGFP-Hmr puncta intensities of eliminated and newly formed synapses were significantly lower than stable synapses (Syph-mCh_{Norm}, *$p < 0.05$, left graph; EGFP-Hmr_{Norm}, ***$p < 0.001$, right graph, Mann–Whitney test). (C) The intensities of Syph-mCh_{Norm} and EGFP-Hmr_{Norm} where averaged to form a single measure for each synapse. With this measure, eliminated and newly formed synapses were again found to be significantly less intense than stable synapses (***$p < 0.001$, left graph, Mann–Whitney test). (D) Binning of data from (C) again shows that smaller synapses are often eliminated and large synapses are often retained. Numbers above bars show sum of the number of stable and eliminated synapses analyzed for each bin. B-C, n = 320 stable synapses, 163 eliminated synapses and 134 formed synapses. Data are shown as mean +/- SEM. Scale bar = 1 μm.

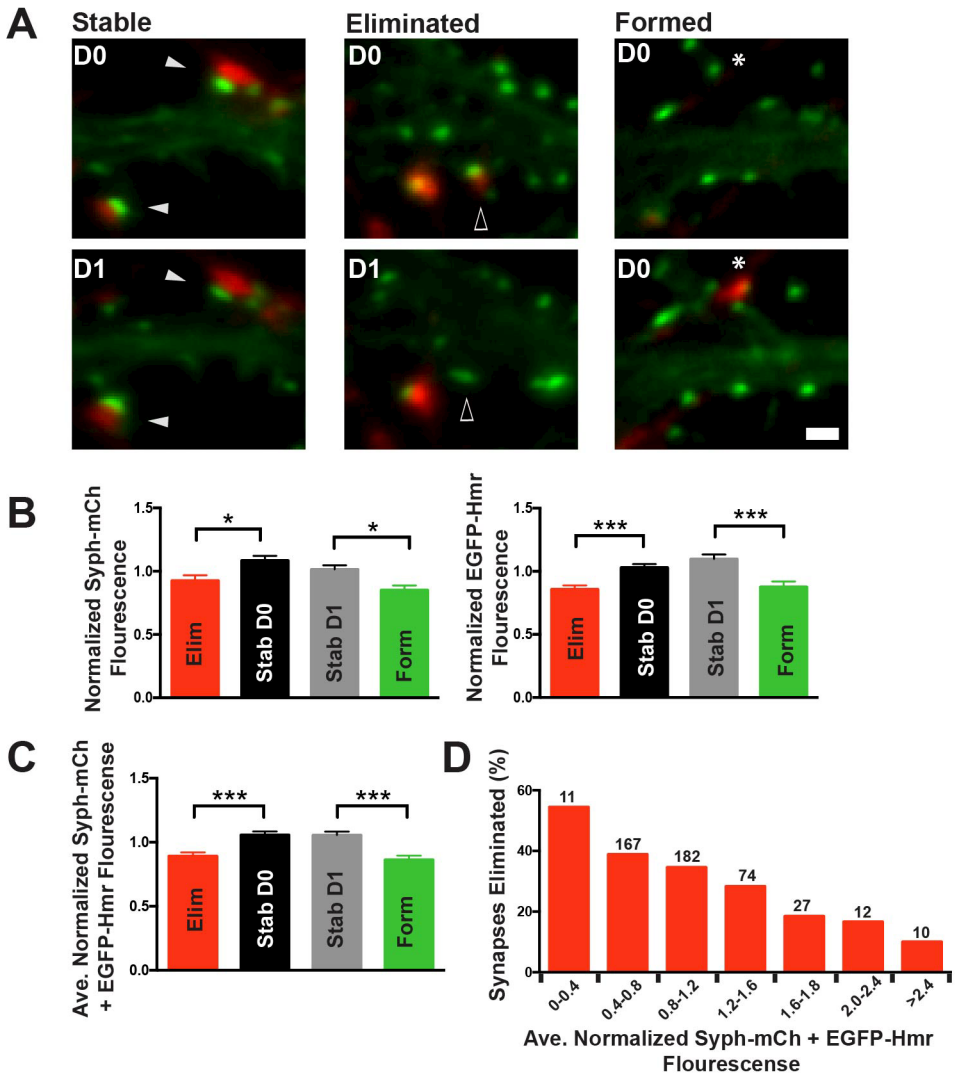
A
Stable
Eliminated
Formed
D0
D1
B
Normalized Syph-mCh Flourescence
Normalized EGFP-Hmr Flourescence
Elim
Stab D0
Stab D1
Form
C
Ave. Normalized Syph-mCh + EGFP-Hmr Flourescense
D
Synapses Eliminated (%)
11
167
182
74
27
12
10
0-0.4
0.4-0.8
0.8-1.2
1.2-1.6
1.6-1.8
2.0-2.4
>2.4
Ave. Normalized Syph-mCh + EGFP-Hmr Flourescense

Figure 2.4. Ionotrophic glutamate receptor blockade reduced synapse elimination but has no effect on synapse formation. (Eliminations: **$p < 0.01$, Student's T-test, left graph, Formations: $p = 0.46$, Student's T-test, right graph). Ctrl n = 37 neurons; iGluR Block n = 31 neurons over 2 cultures. Data are shown as mean +/- SEM.

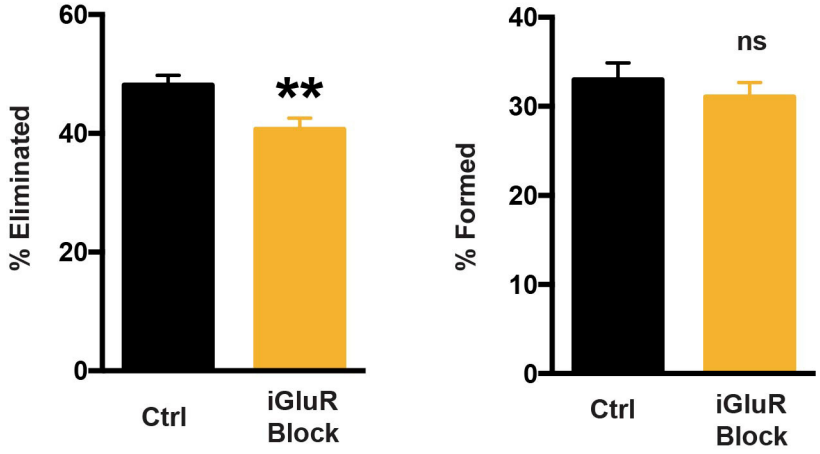
60
40
20
0
% Eliminated
**
Ctrl
iGluR
Block
40
30
20
10
0
% Formed
ns
Ctrl
iGluR
Block

Figure 2.5. TeNT-LC expression inhibits neurotransmitter release. (A) Micrographs of axons co-transfected with SypHl and either Syph-mCh (Ctrl) or TeNT-LC-Syph. Upper panel shows Syph-mCh puncta used to select fields for SypHl imaging. Lower panel shows SypHl ΔF during a high frequency stimulation of 80 Hz, 1s. (B) Mechanism of SypHl. At rest, SypHl fluorescence is low due to the acidic environment of the synaptic vesicle lumen (pH 5). Upon stimulation, pHluorin is translocated to the extracellular milieu (pH 7) and an increase in fluorescence is recorded. (C) TeNT-LC dramatically reduces the summed intensity of synaptic SypHl ΔF measurements per experiment compared to controls (***$p < 0.001$, Student's T-test, left graph). TeNT-LC expression does not affect the length of transfected axons ($p = 0.48$, Student's T-test, right graph). Ctrl n = 29 experiments; TeNT-LC n = 24 over 2 cultures. Scale bar = 1 μm. Data are shown as mean +/- SEM.

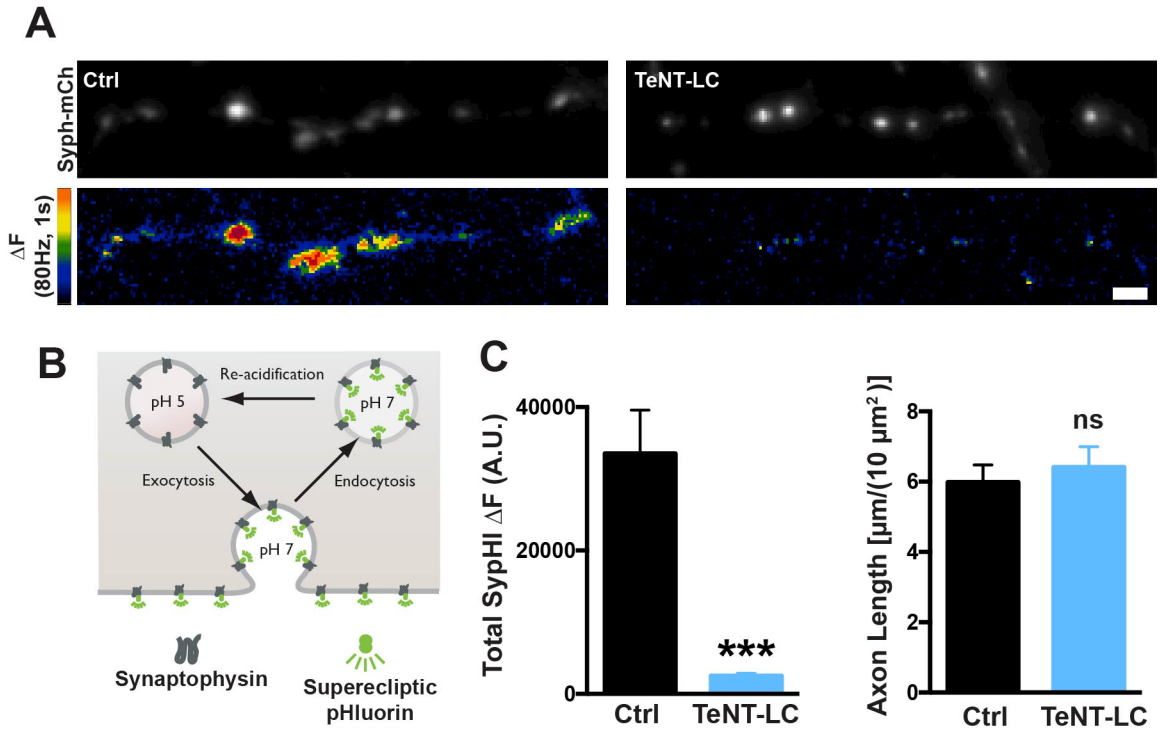
A
Ctrl
TeNT-LC
Syph-mCh
ΔF (80Hz, 1s)
B
Re-acidification
pH 5
pH 7
Exocytosis
Endocytosis
pH 7
Synaptophysin
Supereclipticpl Huorin
C
Total SypHI ΔF (A.U.)
40000
20000
0
***
Ctrl
TeNT-LC
Axon Length [μm/(10 μm²)]
8
6
4
2
0
ns
Ctrl
TeNT-LC

Figure 2.6. TeNT-LC expression has no effect on synapse elimination but significantly reduces synapse formation. (Eliminations: $p = 0.69$, Student's T-test, left graph, Formations: $*p < 0.05$, Student's T-test, right graph). Ctrl n = 18 neurons; iGluR Block n = 16 neurons over 2 cultures. Data are shown as mean +/- SEM.

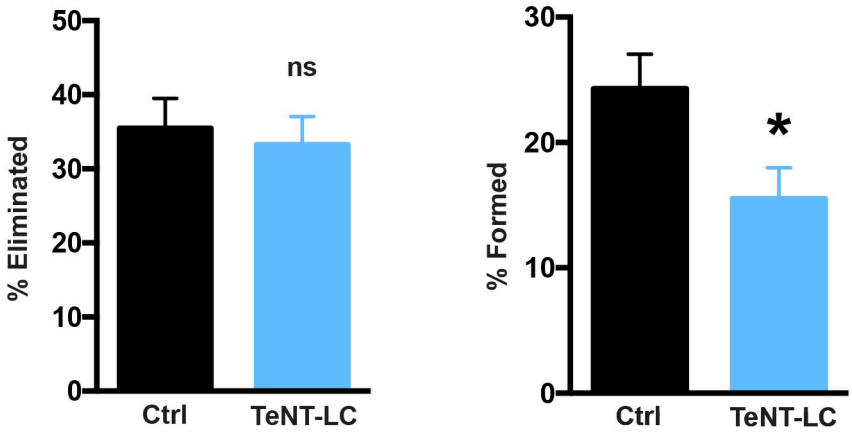
% Eliminated
50
40
30
20
10
0
ns
Ctrl
TeNT-LC
% Formed
30
20
10
0
*
Ctrl
TeNT-LC

CHAPTER 3

NEUREXIN PERTURBATION REDUCES THE STABILITY OF SYNAPTIC CONTACTS

Co-Authorship Statement

Portions of this chapter have been published in Quinn et al., 2017; Scientific Reports, 7, Article number: 42920. We, the authors hold the copyright for this publication.

DPQ performed the majority of data acquisition and analysis. DPQ and SRK designed the experiments and wrote the manuscript. SRK was the principal investigator and supervised the work.

3.1 Introduction

During neuronal circuit refinement, certain synapses are stabilized and persist longer in the circuit, whereas other synapses are eliminated. Neuronal activity has long been considered an essential modulator of the synapse elimination and stabilization events that shape developing circuits. Recent work challenges this notion by showing that neuronal morphology and density of glutamatergic synapses are unaffected in the absence of synaptic transmission (Lu et al., 2013; Sigler et al., 2017). Consistent with these studies, we have shown in Chapter 2 that neither global blockade of glutamate receptors nor sparse inactivation of neurotransmitter release with TeNT-LC abolish the elimination of glutamatergic synapses between developing hippocampal neurons. Together, these results suggest that synaptic activity is not required for synapse elimination and indicate that additional factors likely mediate the stabilization of appropriate synapses and the elimination of inappropriate during circuit refinement.

Cell adhesion proteins provide trans-synaptic contacts and are well suited to modulate synapse refinement. Mutations in genes encoding synaptic adhesion proteins have been linked to neurodevelopmental disorders, further suggesting a role of these gene products in circuit development. In this chapter, we test the role of the Nrxn family of cell adhesion molecules in synapse refinement by interfering with the function of all Nrxn isoforms using two independent approaches. Our data reveal that a pan-Nrxn perturbation has profound consequences for the stabilization of synaptic contacts during synapse refinement.

3.2 Methods

3.2.1 Generation of shRNA Nrxn Knockdown Constructs

Short-hairpin RNA (shRNA) sequences were designed using software from the Whitehead Institute (http://sirna.wi.mit.edu). Selected shRNA targeted mRNA sequences are common to both α- and β-Nrxn isoforms. The efficiency of each single shRNA

sequence in knocking down exogenous neurexin was initially screened in neurons using a fluorescent assay (described in Appendix A). Effective shRNA sequences were combined into two Nrxn triple knockdown vectors (NrxnTKD1 and NrxnTKD2), each containing unique shRNA sequences for the transcripts of the three neurexin genes, and further evaluated using western blots (described below). The NrxnTKD1 construct encoded shRNAs for targets 5'-AATAGCCAAGCAACCATAATA-3', 5'-GTGTCCAAGTGATGATGAG-3', and 5'-CAGTCTCGGGAACAACACATA-3' for knockdown of Nrxn1, Nrxn2, and Nrxn3, respectively. The NrxnTKD2 construct contained shRNA sequences for the targets 5'-GGACAGATGACATCGCCATTG-3', 5'-GAACACAGATGACCTTCTG-3', and 5'-AAGTCTCGGAAACTAGTAGAA-3' for knockdown of Nrxn1, Nrxn2, and Nrxn3, respectively. shRNA sequences were driven by either U6 or H1 promoters (see Figure 3.1A).

3.2.2 cDNA Constructs

To create the mGFP-Nrxn fusion constructs used for Western blotting, cDNAs for Nrxn-1β (M96375), Nrxn-2β (M96377, with amino acids 203-232 and 368-561 spliced out), and Nrxn-3β (XM_008764732, with amino acids 202-231 spliced out and with nucleotides 968-979 from start ATG absent) were cloned in frame at the 3' end of the mGFP cDNA in a vector allowing for the expression of the construct from a CMV promoter. Nrxn-1βΔLNS was created by deleting the LNS domain of Nrxn-1β using site-directed mutagenesis with the primers 5'-GGAATACGTCGTCCCAGCGT-GTC-3' and 5'-GGAAGGCTGGTCGGTGAAGTGC-3'. This PCR removed amino acids 87-285 (UniProtKB - Q63373) and inserted a BspEI site in its place. pHluorin-Nrxn-1βΔLNS was created by inserting an AgeI, BspEI excised pHluorin cassette into the Nrxn-1βΔLNS BspEI site. Synaptophysin-EGFP and Synaptophysin-mCherry constructs were generated by fusing the ORF of synaptophysin (obtained via RT-PCR) in-frame to the 5' end of the EGFP/mCherry cDNA contained in a pEGFP-C1-based expression vector. LRRTM2-CFP was a gift from Dr. Ann Marie Craig. CMV promoters were used to drive the expression of all exogenous sensors and constructs.

3.2.3 Immunocytochemistry and Western Blotting

Dissociated neuronal cultures were fixed with mixture of 4% paraformaldehyde and 4% sucrose in phosphate-buffered saline (PBS) at room temperature for 3 min followed by methanol at 4 °C for 10 minutes. Coverslips were washed with PBS, transferred onto parafilm wax, and blocked with 1% bovine serum albumin and 0.3 % gelatin in PBS for 1 hr. Primary antibodies were diluted in blocking solution and applied for 24 hrs at room temperature. Primary antibodies include: Bassoon (Mouse monoclonal Ab, Enzo, SAP7F407, 1:400), Homer1 (Rabbit polyclonal Ab, Synaptic Systems, Lot # 160002, 1:3000), and MAP2 (Guinea Pig polyclonal Ab, Synaptic Systems, Lot # 188004, 1:400). Coverslips were then washed with PBS and blocked for 30 minutes. Fluorescently labeled secondary antibodies were diluted in blocking solution and applied for 1 hr at room temperature. Secondary antibodies include: Alexa Fluor 660 (Goat anti-mouse, 1:1200), DyLight 549 (Donkey anti-rabbit 1:400), and AMCA (Donkey anti-guinea pig, Jackson Labs, 1:400). Coverslips were washed with PBS and mounted onto slides using Aqua-Mount (Thermo Scientific). Immunohistochemistry was done in same way in subsequent chapters.

For western blotting, HEK 293 cells were transfected using polyethylenimine with1 µg mGFP-Nrxn-1β, mGFP-Nrxn-2β, or mGFP-Nrxn-3β constructs and 10 µg of either an empty knockdown plasmid, NrxnTKD1, or NrxnTKD2 per 35 mm dish. 10 µg total protein of lysed samples per lane were loaded on an 8 % SDS-PAGE gel and then transferred to nitrocellulose membranes. Samples were blocked for 1 hour at room temperature with blocking solution (5% non-fat dry milk and 0.1% Tween-20 in TBS) and then incubated with primary antibodies overnight at 4 °C. Membranes were washed three times with 0.1% Tween-20 in TBS, blocked for 30 minutes and then incubated with HRP conjugated secondary antibodies for 1 hour at room temperature. HRP signals were detected using a chemiluminescence solution (Bio-Rad, Cat. # 170-5060). Primary antibodies used were anti-GFP (Rabbit polyclonal, Synaptic Systems, Cat# 132002, dilution of 1:5000) and anti-Tubulin (Mouse monoclonal, Sigma, 6-11B-1 at a dilution of

1:10,000). Secondary antibodies included Donkey Anti-Rabbit HRP (Jackson, 711-035-152, 1:10000) and Donkey Anti-Mouse HRP (Jackson, 715-035-150, 1:10000).

3.2.4 Characterization of pHl-Nrxn-1βΔLNS

Cultures of dissociated hippocampal neurons were transfected at 10-14 DIV with the pHl-Nrxn-1βΔLNS (pHl-ΔLNS) construct. After 3 days, cells were imaged on a Zeiss Observer 2.1 inverted microscope using a 63x objective, Photometrics Coolsnap HQ2 camera and SlideBook 6 imaging software. Image stacks of pHl-ΔLNS-transfected axons were first acquired in pH 7.3 HBS buffer. Neurons were then perfused with a pH5.5 buffer (Composition in mM: 124 NaCl, 3 KCl, 10 MES, 5 D-glucose) for 5 minutes at which point a second image stack was acquired. Neurons were then re-perfused with the original pH 7.3 HBS buffer and a final image stack was acquired. Image stacks were converted to projected images according to maximum fluorescence and pHl-ΔLNS fluorescent puncta were segmented and measured using IPLab software (www.biovis.com/software.html)

3.2.5 Neuronal-COS7 Co-culture Assay

At 10 DIV, dissociated hippocampal neurons were transfected with 60 µg of either an empty KD vector, NrxnTKD1, NrxnTKD2, or Nrxn-1βΔLNS per 60 mm dish along with 25 µg Synaptophysin-mCherry (Syph-mCh) to label presynaptic specializations and serve as a measure for presynaptic clustering. Following transfection, coverslips were transferred to 12-well plates. The next day, COS7 cells were transfected using calcium phosphate precipitation with 30 µg of CFP or LRRTM2-CFP per 35 mm well. After 24 hrs of expression, COS7 cells were trypsinized, pelleted, and re-suspended in conditioned neuronal media. COS7 cells were then seeded onto neurons at a density of approximately 10,000 cells per well of 12-well plate. Co-cultures were maintained for 48 hours and then fixed and immunostained with anti-MAP2 to label neuronal dendrites. In regions were Syph-mCh expressing axons contacted transfected COS7 cells, image stacks of 2.8 µm were acquired with a Zeiss Observer 2.1 inverted microscope using a 63x objective, Photometrics Coolsnap HQ2 camera and SlideBook 6 imaging software.

Maximum intensity projection images were created and exported for analysis. Images were analyzed for the number and intensity of Syph-mCh puncta per transfected COS7 cell using IPLab software. Contacts between Syph-mCh expressing axons and MAP2 positive dendrites were excluded from analysis. Images were acquired from two independent co-cultures.

3.2.6 Assessment of Synaptic Density

To assess the effect of Nrxn disruption on synaptic density, we performed immunocytochemistry on cultures of transfected hippocampal neurons. Neurons were transfected with three cDNA plasmids: 1) 80 μg of either TKD1, TKD2, Nrxn-1βΔLNS, or control plasmid, 2) 25 μg of synaptophysin-EGFP (Syph-EGFP), a fusion protein that labels clusters of synaptic vesicles and 3) 10 μg of cytosolic EGFP, as an axonal fill stain. Three days after transfection, neurons were immunostained for Bsn, Homer1 and MAP2 to quantify synaptic density. Experimenters were blinded to the experimental conditions during image acquisition and analysis. Fluorescence images were taken on a Nikon TE2000 epifluorescence microscope equipped with a 60 X (N.A. 1.40) objective and Hamamatsu camera (Model C4742-80-12AG). To quantify the effect of Nrxn disruption on synaptic density, we identified points at which axons of transfected neurons traversed MAP2-positive dendrites. We then determined the fraction of contact points bearing co-localized Bsn and Homer1 puncta as a measure of the density of synaptic contacts made by the transfected presynaptic neuron. An intensity threshold was set for both Homer1 and Bsn and kept constant for each experiment for a given transfected neuronal culture. Axodendritic contacts with both Homer1 and Bsn puncta intensities above threshold were scored as synaptic and contacts that failed these criteria were scored non-synaptic. Averages of the percentage of synaptic axodendritic contacts in each transfected culture were compared between groups using a one-way analysis of variance (ANOVA). Fasciculated neurites were excluded from analysis. Images were acquired from at least 2 separate hippocampal cultures.

3.2.7 Quantification of Synapse Turnover

To assess the effect of Nrxn perturbation on the stability of synaptic connections, we expressed fluorescently labeled pre- and postsynaptic proteins in hippocampal neurons and quantified the number of stable, newly formed and eliminated synapses over 24 hours. 30 μg of the presynaptic marker, synaptophysin-mCherry (Syph-mCh), was co-transfected with 80 μg of either a control plasmid, NrxnTKD1, or Nrxn-1βΔLNS at 13 DIV. In a second transfection at 15 DIV, 40 μg of PSD95-EGFP was introduced to label postsynaptic densities in a separate population of neurons. Experiments with the NrxnTKD1 construct and the Nrxn-1βΔLNS construct were performed independently. Image acquisition and analysis was performed as described in Chapter 2. In figure 3.4, to calculate the percentages of stable, eliminated, and formed synapses, the counts for each were divided by the total number of analysed synapses (ie: % formed = formed synapses/ (formed + stable + eliminated synapses)). Using a Student's t-test for independent samples, the percentage of stable, newly formed, and eliminated synapses were compared between NrxnTKD1, Nrxn-1βΔLNS and the respective control groups. Images were acquired from six separate hippocampal cultures for NrxnTKD1 experiments and two separate hippocampal cultures for Nrxn-1βΔLNS experiments.

3.3 Results

3.3.1 Molecular Tools for Disrupting the Function of all Nrxn Isoforms

To disrupt the function of all α- and β-Nrxns, we took two approaches. First, we designed Nrxn shRNA constructs that targeted each of the six primary Nrxn mRNA transcripts (Figure 3.1A). shRNA constructs were designed to target mRNA sequences present in both α- and β-Nrxn transcripts so that a single shRNA should attenuate expression of both α and β isoforms for a particular Nrxn gene. The effectiveness of individual shRNAs in reducing exogenous neurexin mRNA was first screened in a fluorescent assay in neurons (Appendix A). Effective shRNAs were then combined into

two triple knockdown vectors (TKD1 and TKD2), each with unique shRNA sequences targeted towards Nrxn 1, 2, and 3 mRNA (Figure 3.1A, right). Neurexin TKD1 and TKD2 constructs were further evaluated by co-transfecting mGFP fusion-tagged constructs of Nrxn 1β, 2β, and 3β along with Ctrl, TKD1 or TKD2 plasmids into HEK293 cells and performing a western blot with an anti-GFP antibody (Fig. 3.1B).

In a second approach to disrupt the function of all Nrxns, we created a mutant Nrxn-1β construct in which the LNS domain essential for binding Neuroligins and LRRTMs was deleted (Nrxn-1βΔLNS, Figure 3.1C). To characterize the subcellular localization of Nrxn-1βΔLNS, we inserted the pH-sensitive fluorescent protein, superecliptic pHluorin (pHl) in place of the extracellular LNS domain to create pHl-Nrxn-1βΔLNS (pHl-ΔLNS, Figure 3.1C-E). pHl-ΔLNS co-localized with synaptophysin-mCherry (Syph-mCh) puncta at putative presynaptic specializations (Figure 3.1D). To test whether the pHl-ΔLNS construct was properly inserted into the plasma membrane, we imaged pHl-ΔLNS expressing axons before, during, and after perfusion with a pH 5.5 buffer. The average fluorescent intensity of pHl-ΔLNS puncta was significantly reduced during perfusion of the pH 5.5 buffer and increased upon reperfusion with pH 7.3 buffer (Figure 3.1E). Taken together, these findings suggest that the pHl-ΔLNS construct is correctly inserted into the plasma membrane at presynaptic specializations.

To confirm that knockdown and Nrxn-1βΔLNS constructs perturb the function of endogenous neurexins in neurons, we co-cultured neurons transfected with knockdown or Nrxn-1βΔLNS constructs with fibroblasts expressing the neurexin ligand LRRTM2. Non-neuronally expressed LRRTM2 induces the recruitment of presynaptic specializations, or hemisynapses, in contacting axons in a neurexin-dependent manner (Linhoff et al., 2009; de Wit et al., 2009). Functional perturbation of endogenous neurexins should therefore inhibit the formation of hemisynapses at contact sites with LRRTM2 expressing fibroblasts. We co-cultured COS7 cells with dissociated hippocampal neurons that were transfected with either an empty knockdown vector (pS), NrxnTKD1, NrxnTKD2 or Nrxn-1βΔLNS (Figure 3.2A). Synaptophysin-mCherry (Syph-mCh) was included in the neuronal transfection as a fluorescent marker of synaptic vesicles to detect hemisynapses. After 48 hours, co-cultures were fixed and neuronal dendrites were immunostained with

an antibody raised against MAP2 to exclude Syph-mCh puncta made onto dendrites from the analysis. LRRTM2-CFP expression in COS7 cells induced dramatic clustering of Syph-mCh puncta in control axons expressing an empty knockdown vector, in contrast to COS cells expressing a CFP control vector (Figure 3.2A). Compared to control axons, expression of NrxnTKD1, NrxnTKD2 or Nrxn-1βΔLNS in neurons significantly reduced both the average number of Syph-mCh puncta per COS7 cell (*$p < 0.05$, **$p < 0.01$, one-way ANOVA and post hoc Tukey test, Figure 3.2B left graph), as well as the average intensity of Syph-mCh puncta per COS7 cell (*$p < 0.01$, one-way ANOVA and post hoc Tukey test, Figure 3.2B, right graph). These data suggest that shRNA constructs diminish endogenous Nrxn expression and that our Nrxn-1βΔLNS acts in a dominant negative fashion to perturb Nrxn function, presumably by inhibiting the binding of endogenous α- and β-Nrxns to presynaptic scaffolding proteins such as the CASK/Mint1/Veli complex (Hata et al., 1996), (Butz et al., 1998).

3.3.2 Nrxn Disruption Reduces Synapse Density

As a first step in testing the role of Nrxn in synapse refinement, we analyzed the effect of pan-Nrxn perturbation on synapse density using immunocytochemistry. We transfected neurons in hippocampal cultures with NrxnTKD1, NrxnTKD2 or Nrxn-1βΔLNS along with a plasmid encoding Syph-EGFP to mark transfected axons. Since our transfection method results in sparse expression of the constructs in 5-10% of all neurons, we were unable to employ the conventional methodology of measuring the density of dendritic spines in postsynaptic neurons. We therefore developed a novel approach to quantify synapse density on transfected cultures immunostained for Bsn, the postsynaptic protein Homer1, and MAP2. We initially identified points at which axons of transfected neurons traversed MAP2-positive dendrites (Figure 3.3A-B). We then determined the fraction of contact points bearing co-localized Bsn and Homer1 puncta as a measure of the density of synaptic contacts made by transfected presynaptic neurons. Compared to control neurons, neurons expressing NrxnTKD1, NrxnTKD2 or Nrxn-1βΔLNS constructs displayed a significant reduction in the fraction of axodendritic contacts bearing synapses (Figure 3.3C). In NrxnTKD experiments, the average percentage of synapse-bearing

axodendritic contacts was 59.2 +/- 2.8% for Ctrl, 48.8 +/- 3.3% for NrxnTKD1, and 47.6 +/- 2.5% for NrxnTKD2 (*$p < 0.05$ as determined by 1-way ANOVA and post hoc Tukey test). In experiments assessing the effect of Nrxn-1βΔLNS on synaptic density, the average percentage of synapse-bearing axodendritic contacts per experiment was 59.4 +/- 3.7% for Ctrl and 38.2 +/- 4.1% for Nrxn-1βΔLNS (*$p < 0.05$ for as determined by Student's t-test). These experiments demonstrate that functional perturbation of all Nrxns leads to a reduction in the density of glutamatergic synapses.

3.3.3 Nrxn Disruption Reduces the Stability of Synaptic Contacts

The reduced density of glutamatergic synapses we observed at contacts between Nrxn-perturbed axons and dendrites may be either due to a reduced rate of synapse formation or, alternatively, an increased rate of synapse elimination. To discern between these two possibilities, we performed live time-lapse imaging of fluorescently labeled hippocampal neurons. We first co-transfected empty knockdown, NrxnTKD1or Nrxn-1βΔLNS plasmids along with Syph-mCh to label presynaptic specializations. We then subsequently transfected PSD95-EGFP to label postsynaptic densities in a separate population of neurons. Co-localizations of Syph-mCh and PSD95-EGFP were imaged over a period of 24 hours and the percentage of stable, eliminated, and newly formed synapses was recorded in NrxnTKD1 and Nrxn-1βΔLNS groups and compared with control cultures. In all groups, we found examples of co-localized Syph-mCh and PSD95-EGFP that were stable, eliminated or newly formed during the observation period (Figure 3.4A). Quantification of the percentage of stable, eliminated, and newly formed synaptic contacts showed that both NrxnTKD1and Nrxn-1βΔLNS overexpression resulted in synaptic contacts that were significantly less stable compared to control cultures (Figure 3.4B). In experiments employing NrxnTKD1 to perturb Nrxn function, the percentage of stable synapses per postsynaptic cell over 24 hours was 52.0 +/- 2.7% in Ctrl and 42.3 +/- 3.4% in NrxnTKD1 expressing axons (*$p < 0.05$, Student's t-test, Figure 3.4 left graph). In separate experiments using Nrxn-1βΔLNS, the percentage of stable synapses per postsynaptic cell was 46.7 +/- 4.9% in ctrl and 27.7 +/- 7.0% in Nrxn-1βΔLNS expressing neurons (*$p < 0.05$, Student's t-test, Figure 3.4 right graph). Interestingly, in both

NrxnKD1 and Nrxn-1βΔLNS groups, rates of synapse formation were not significantly different from those in control cultures. In summary, these experiments provide evidence for the notion that Nrxns have an important role in the stabilization of synapses but are not essential for the initial formation of synaptic contacts.

3.4 Discussion

In this study, we show that the Nrxn family of presynaptic cell adhesion molecules play an important role in the refinement of synaptic contacts. Disruption of Nrxn function in hippocampal neurons, either by shRNA-mediated knockdown of all Nrxn isoforms or by overexpression of a mutant Nrxn unable to bind postsynaptic ligands, led to a reduction in the density of glutamatergic synaptic connections. Importantly, using time-lapse imaging of synaptically connected neurons, we show that disruption of Nrxn function increases the rate of synapse elimination but does not affect the rate of synaptogenesis. Our data therefore suggest a prominent function of these presynaptic cell adhesion proteins in the stabilization of glutamatergic synapses.

Previous studies using co-culture experiments have shown that Nrxns and Nrxn ligands are able to recruit components of pre- and postsynaptic specializations to synapses, respectively, suggesting a synaptogenic function of these proteins. However, isoform-specific knockouts of either all α- or all β-Nrxn did not lead to reductions in synaptic density, suggesting that these cell adhesion proteins are potentially dispensable for synaptogenesis (Missler et al., 2003; Anderson et al., 2015). To examine the role of Nrxns in synaptic development, we interfered with the function of all Nrxn isoforms and assessed the effect of this manipulation on synapse density as well as on synaptic turnover. Immunocytochemical analysis of pre- and postsynaptic protein content showed that pan-Nrxn KD or overexpression of Nrxn-1βΔLNS results in a significant reduction in the density of glutamatergic synapses. This result is consistent with previous studies demonstrating that overexpression of neuroligins increases the density of glutamatergic synapses, while the attenuation of neuroligin and LRRTM2 expression decreases their density (Ko et al., 2011; Chubykin et al., 2007). To address whether this reduction is the

result of a decreased rate of synapse formation or due to increased synapse elimination, we carried out time-lapse imaging of synaptically connected hippocampal neurons. Surprisingly, we found that Nrxn perturbation did not affect the rate of synapse formation but instead increased the elimination of preexisting synaptic contacts.

Since the publication of our results, neuron subset-specific pan-Nrxn triple knockout (TKO) mice have been generated (Chen et al., 2017). In this study, pan-Nrxn TKO in inferior olivary (IO) neurons supplying climbing fiber afferents to cerebellar Purkinje neurons led to a decrease in climbing fiber synapses. Interestingly, the degree of the reduction in synapse density was dependent on the fraction of IO neurons lacking Nrxns: Nrxn knockout in only a small subset of IO neurons led to a *far larger* reduction of synapses from Nrxn TKO neurons onto Purkinje cells than a knockout in the overwhelming majority of these afferent neurons. This finding indicates that Nrxns may not be required for the formation of synaptic contacts between IO neurons and Purkinje cells, but rather play a role in the competitive process that ensures climbing fiber synapse refinement during a critical phase in development (Kano and Hashimoto, 2009). This observation is in agreement with our data showing that, albeit in a different synaptic preparation, attenuation of neurexin expression leads to enhanced synapse elimination rather than to a reduction in synapse formation.

In summary, our results indicate that Nrxns function in the stabilization of already formed synaptic contacts and are consistent with two alternative models (Figure 3.5). In the first model, the initial formation of synaptic contacts between cortical neurons is mediated by synaptic cell adhesion proteins other than Nrxns. Nrxns and/or postsynaptic Nrxn ligands may be incorporated into synapses only during their maturation, and may prevent elimination of nascent synapses at this stage. In an alternative scenario, Nrxns are co-expressed with other families of cell adhesion proteins, such as protein tyrosine phosphatases, before the formation of synaptic contacts and induce synapse formation in a highly redundant manner. In this model, which is also consistent with the findings of studies showing formation of presynaptic specializations in axons contacting non-neuronal cells expressing Nrxn ligands (Linhoff et al., 2009), (Uemura et al., 2010),

(Pettem et al., 2013), (Scheiffele et al., 2000), elimination of one class of cell adhesion proteins has little effect on the rate of synapse formation, because other cell adhesion proteins are able to fully compensate. However, the attenuation of transsynaptic cell adhesion during synaptic maturation may place synapses deficient in any individual cell adhesion protein at a disadvantage and favor their elimination. To conclusively distinguish between these alternative models, better insight into the role of other families of synaptic cell adhesion proteins in synapse stabilization is required.

Figure 3.1. Molecular tools for disrupting Nrxn function. (A) For each of the three Nrxn gene transcripts, shRNA knockdown constructs were designed to target sequences present in both α and β Nrxn mRNA. Two different shRNA sequences were validated for each of the three Nrxn genes (pink and red arrows). shRNA sequences were combined into two unique Nrxn triple knockdown vectors (TKD1, TKD2). shRNA sequences for each TKD were driven by a combination of U6 and H1 promoters. (B) Knockdown efficiency was assessed by co-transfecting mGFP tagged versions of Nrxn 1β, 2β, and 3β along with Ctrl, TKD1 or TKD2 plasmids into HEK293 cells and performing a western blot with and an anti-GFP antibody. (C) A dominant negative Nrxn-1β construct was created by excising the extracellular LNS 6 domain of Nrxn-1β. The LNS 6 domain is essential for the binding of Nrxn with postsynaptic Neuroligins and LRRTMs. Nrxn-1βΔLNS reduces Nrxn-mediated transsynaptic cell adhesion by competing with endogenous α- and β-Nrxns for binding presynaptic scaffolding proteins such as CASK and Mint1. We analyzed the cellular properties of Nrxn-1βΔLNS by tagging it to a pH sensitive fluorescent molecule called pHluorin to create pHl- Nrxn-1βΔLNS. (D) Representative image of pHl-Nrxn-1βΔLNS (pHl-ΔLNS) construct co-transfected with Synaptophysin-mCherry (Syph-mCh). Co-localization of pHl-ΔLNS with Syph-mCh suggests that pHl-ΔLNS localizes to synapses. pHl-ΔLNS fluorescence reversibly quenches when imaged in a pH 5.5 buffer suggesting that pHl-ΔLNS is properly inserted into the plasma membrane. (E) The average fluorescent intensity of pHl-ΔLNS puncta was significantly reduced by a pH 5.5 buffer and increased upon perfusion of original pH 7.3 imaging buffer. $^{**}p < 0.01$, and $^{***}p < 0.001$ as determined by 1-way ANOVA and post hoc Tukey test. n = 34 pHl-ΔLNS puncta. Scale bar = 1 μm. (This figure was included in our published paper: Quinn et al., 2017; Scientific Reports, 7, Article number: 42920.)

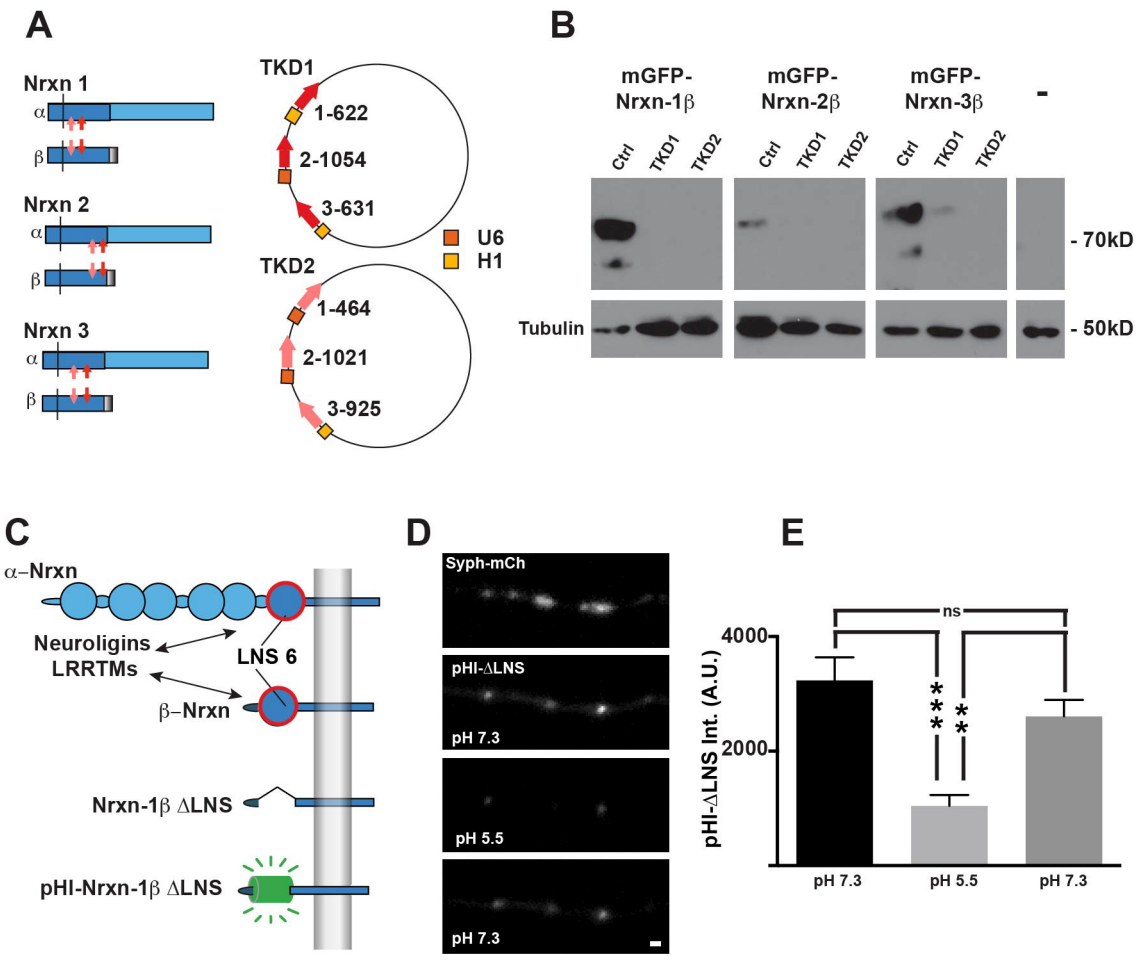
A
Nrxn 1
α
β
Nrxn 2
α
β
Nrxn 3
α
β
TKD1
1-622
2-1054
3-631
TKD2
1-464
2-1021
3-925
U6
H1
B
mGFP-
Nrxn-1β
mGFP-
Nrxn-2β
mGFP-
Nrxn-3β
-
Ctrl
TKD1
TKD2
Ctrl
TKD1
TKD2
Ctrl
TKD1
TKD2
- 70kD
Tubulin
- 50kD
C
α–Nrxn
Neuroligins
LRRTMs
LNS 6
β–Nrxn
Nrxn-1β ΔLNS
pHl-Nrxn-1β ΔLNS
D
Syph-mCh
pHl-ΔLNS
pH 7.3
pH 5.5
pH 7.3
E
ns
***
***
4000
2000
pHl-ΔLNS Int. (A.U.)
pH 7.3
pH 5.5
pH 7.3

Figure 3.2. Perturbation of Nrxn function blocks the synaptogenic effect of LRRTM2 in co-culture synapse formation assay. (A) COS7 cells expressing CFP or LRRTM2-CFP cultured with hippocampal neurons expressing either an empty knockdown vector (pS), NrxnTKD1, NrxnTKD2, or Nrxn-1βΔLNS along with Synaptophysin-mCherry (Syph-mCh, red). CFP in COS7 cells is pseudo-colored green to allow for better detection of anti-MAP2 stained dendrites, shown in blue. (B) Quantification of Syph-mCh puncta density and intensity. LRRTM2-induced clustering of Syph-mCh puncta in NrxnTKD1, NrxnTKD2, or Nrxn-1βΔLNS expressing axons was significantly reduced compared to axons expressing an empty knockdown vector when quantified as average number of Syph-mCh puncta per COS7 cell or as average Syph-mCh cluster intensity per COS7 cell (*$p < 0.05$, **$p < 0.01$, as determined by one-way ANOVA and post hoc Tukey test). Numbers of COS7 cells analyzed are indicated in the graphs. Data are shown as mean +/- SEM. Scale bar indicates 10 μm. (This figure was included in our published paper: Quinn et al., 2017; Scientific Reports, 7, Article number: 42920.)

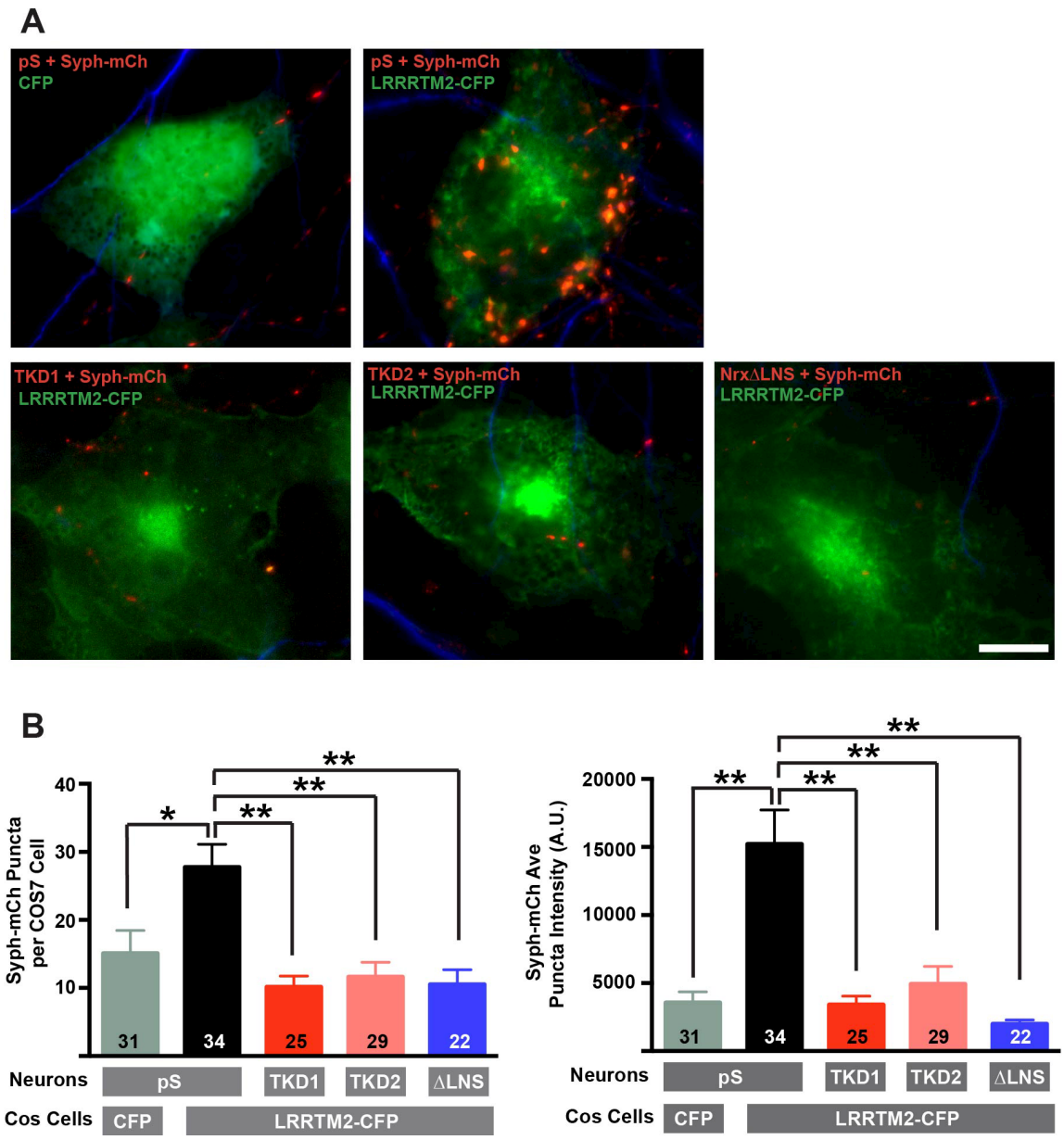
A
pS + Syph-mCh
CFP
pS + Syph-mCh
LRRRTM2-CFP
TKD1 + Syph-mCh
LRRRTM2-CFP
TKD2 + Syph-mCh
LRRRTM2-CFP
NrxΔLNS + Syph-mCh
LRRRTM2-CFP
B
Syph-mCh Puncta per COS7 Cell
40
30
20
10
*
**
**
**
31
34
25
29
22
Neurons
pS
TKD1
TKD2
ΔLNS
Cos Cells
CFP
LRRTM2-CFP
Syph-mCh Ave Puncta Intensity (A.U.)
20000
15000
10000
5000
**
**
**
**
31
34
25
29
22
Neurons
pS
TKD1
TKD2
ΔLNS
Cos Cells
CFP
LRRTM2-CFP

Figure 3.3. Nrxn disruption reduces synaptic density. (A) Overview image of synaptic contacts between MAP2 positive dendrites (blue) and axons co-transfected with synaptophysin-EGFP (Syph-EGFP, green) + experimental treatment (Ctrl plasmid, NrxnTKD1 or Nrxn-1βΔLNS). Bassoon immunofluorescence is shown in red. (B) Contacts between transfected axons and dendrites were classified as synaptic if both Homer (Hmr, upper panel) and Bassoon (Bsn, middle panel) puncta were present. Contacts missing Hmr, Bsn, or both were classified as non-synaptic. Bottom panel: Merged image of Bsn (red), Syph-EGFP (green) and MAP2 (blue) fluorescence. Circled puncta show Bsn and Hmr clusters that correspond to the transfected axon. (C) Percentage of axodendritic contacts with both Bsn and Homer clusters per experiment for NrxnTKD (upper graph) and Nrxn-1βΔLNS overexpression (lower graph). The number of analyzed postsynaptic neurons is indicated in the respective graphs. *$p < 0.05$ as determined by 1-way ANOVA and post hoc Tukey test (For TKD experiments) and Student's t-test (For Nrxn-1βΔLNS experiments). Data are shown as mean +/- SEM. Scale bars = 10 μm (A), 1 μm (B). Number of analyzed axodendritic contacts was 759, 520 and 767 for Ctrl, NrxnTKD1 and NrxnTKD2, respectively, in NrxnTKD experiments and 636 and 708 for Ctrl and Nrxn-1βΔLNS, respectively, in Nrxn-1βΔLNS experiments. Scale bars = 10 μm (A), 1 μm (B-C). (This figure was included in our published paper: Quinn et al., 2017; Scientific Reports, 7, Article number: 42920.)

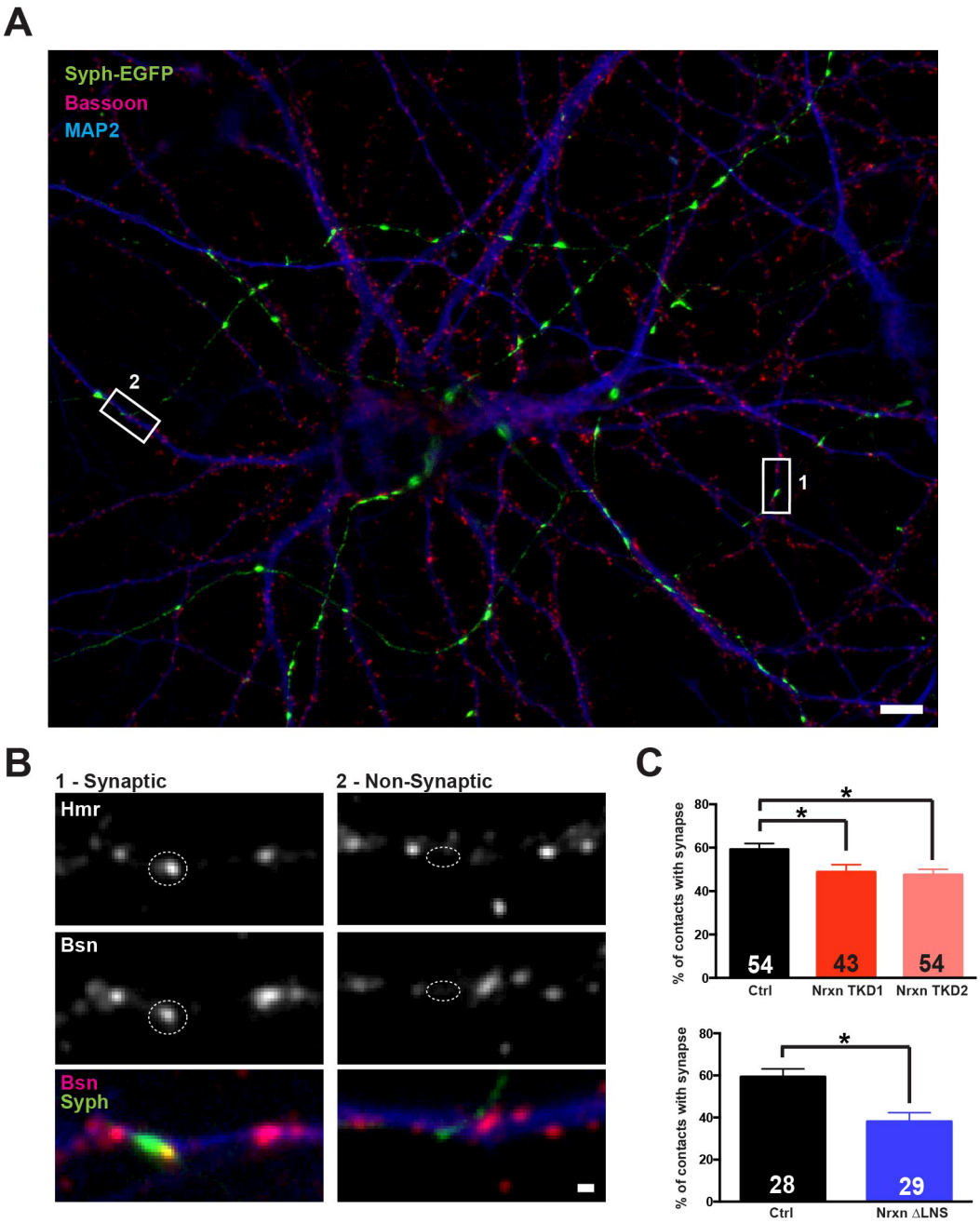
A
Syph-EGFP
Bassoon
MAP2
2
1
B
1 - Synaptic
2 - Non-Synaptic
Hmr
Bsn
Bsn
Syph
C
% of contacts with synapse
80
60
40
20
0
*
*
54
43
54
Ctrl
Nrxn TKD1
Nrxn TKD2
% of contacts with synapse
80
60
40
20
0
*
28
29
Ctrl
Nrxn ΔLNS

Figure 3.4. Nrxn perturbation reduces the stability of synaptic contacts. (A) Example images of contacts between Syph-mCherry expressing axons and PSD95-EGFP expressing dendrites imaged on Day 0 and 24 hrs later (Day1). Examples of stable (filled arrowheads), eliminated (open arrowheads), and formed synapses (asterisks) are shown for control, NrxnTKD1, and Nrxn-1βΔLNS groups. (B) Average percentage of stable, eliminated and formed synapses, grouped by postsynaptic cell for NrxnTKD1 (left graph) and Nrxn-1βΔLNS (right graph) experiments. *$p < 0.05$, **$p < 0.01$ as determined by Student's t-test. In NrxnTKD1 experiments, n = 41 (Ctrl) and 39 (NrxnTKD1) postsynaptic neurons and 566 (Ctrl) and 614 (NrxnTKD1) analyzed synapses. In Nrxn-1βΔLNS experiments, n = 14 (Ctrl) and 11 (Nrxn-1βΔLNS) postsynaptic neurons and 345 (Ctrl) and 185 (Nrxn-1βΔLNS) analyzed synapses. Data are shown as mean +/- SEM. Scale bar = 1μm. (This figure was included in our published paper: Quinn et al., 2017; Scientific Reports, 7, Article number: 42920.)

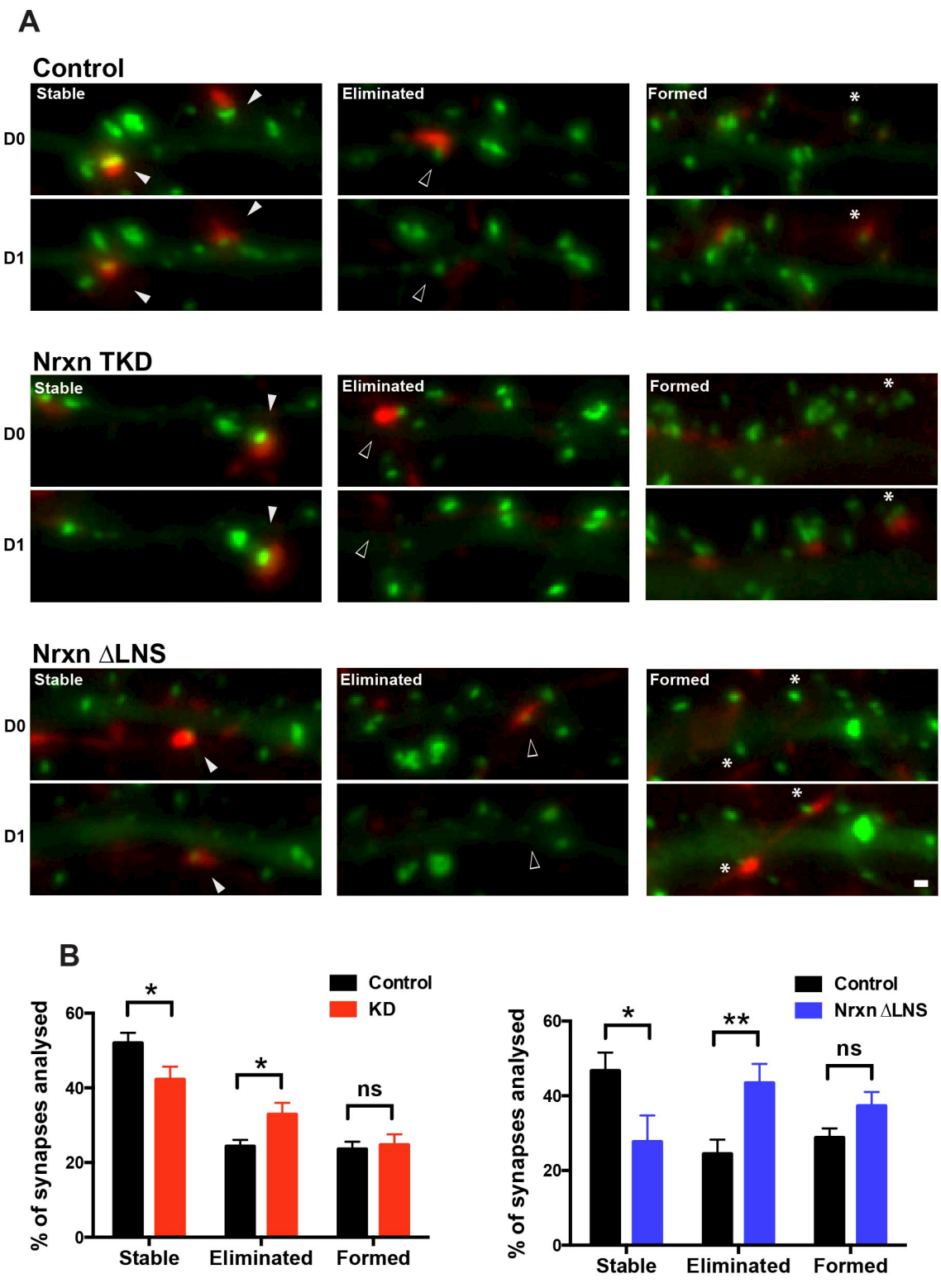
A
Control
Stable
Eliminated
Formed
D0
D1
Nrxn TKD
Stable
Eliminated
Formed
D0
D1
Nrxn ΔLNS
Stable
Eliminated
Formed
D0
D1
B
Control
KD
% of synapses analysed
60
40
20
0
*
*
ns
Stable
Eliminated
Formed
Control
Nrxn ΔLNS
% of synapses analysed
60
40
20
0
*
**
ns
Stable
Eliminated
Formed

Figure 3.5. Models for the role of Neurexin in synapse formation and maturation. Model 1 (upper panel) The initial formation of synaptic contacts is mediated by synaptic cell adhesion proteins other than Nrxns. Nrxns and postsynaptic Nrxn ligands may be incorporated into synapses only during their maturation, and may prevent elimination of nascent synapses at this stage. Model 2 (lower panel) Nrxns are co-expressed with other cell adhesion proteins and function redundantly to induce synapse formation. Elimination of one class of adhesion molecules has little effect on the rate of synapse formation, because other cell adhesion proteins are able to fully compensate. However, the attenuation of transsynaptic cell adhesion during synaptic maturation may place synapses deficient in any individual cell adhesion protein at a disadvantage and favor their elimination. (This figure was included in our published paper: Quinn et al., 2017; Scientific Reports, 7, Article number: 42920.)

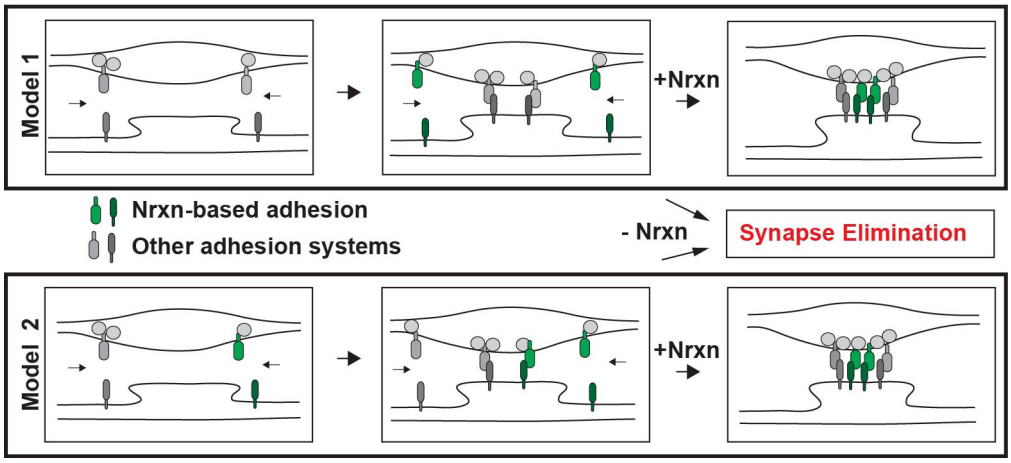
Model 1
+Nrxn
Nrxn-based adhesion
Other adhesion systems
- Nrxn
Synapse Elimination
Model 2
+Nrxn

CHAPTER 4

NEUREXIN PERTURBATION RESULTS IN A REDUCTION IN READILY RELEASABLE SYNAPTIC VESICLE POOL SIZE

Co-Authorship Statement

Portions of this chapter have been published in Quinn et al., 2017; Scientific Reports, 7, Article number: 42920.

DPQ performed the majority of data acquisition and analysis. DPQ and SRK designed the experiments and wrote the manuscript. SRK was the principal investigator and supervised the work.

4.1 Introduction

Numerous lines of evidence suggest that Nrxn ligands facilitate the recruitment and surface expression of AMPA and NMDA receptors (Chubykin et al., 2007; Barrow et al., 2009; Mondin et al., 2011; Aoto et al., 2013; Aoto et al., 2015; Jiang et al., 2016; Chanda et al., 2017) suggesting that Nrxns may transsynaptically modulate neurotransmission by controlling the nucleation of adhesion molecules and neurotransmitter receptors at postsynaptic sites. Nrxns have also been suggested to play a direct role in modulating neurotransmission. For example, loss of Nrxn function enhances paired-pulse ratio (Chen et al., 2017) and neurotransmission failure rates (Missler et al., 2003), indicating that Nrxns are important for maintaining efficient neurotransmitter release probability. These effects have chiefly been ascribed to reduced calcium channel function or localization, as whole cell calcium currents and presynaptic calcium transients are also reduced in neurons with impaired Nrxn function (Missler et al., 2003; Anderson et al., 2015; Chen et al., 2017). In addition to presynaptic calcium influx, efficient neurotransmitter release also depends on the number of docked and primed synaptic vesicles at the presynaptic active zone; the so-called readily releasable pool (RRP) of synaptic vesicles. The role of Nrxn in establishing or maintaining the size of the RRP is less well understood. Mice devoid of all α-Nrxns show less neurotransmitter release in response to hypertonic shock compared to control neurons, indicating that RRP sizes are reduced by Nrxn perturbation (Missler et al., 2003). Conversely, mice devoid of all β-Nrxns show no such effect (Anderson et al., 2015). To gain additional insight into the role of Nrxns in neurotransmitter release, we disrupt the function of both α- and β-Nrxns using shRNA-mediated knockdowns or overexpression of a Nrxn mutant that is unable to bind postsynaptic ligands. We then measure synaptic vesicle exocytosis using a presynaptic sensor for synaptic vesicle exocytosis, called synaptophysin-pHluorin. In comparison to the electrophysiological techniques used in the aforementioned studies, this optical method has the advantage of probing presynaptic function directly, in isolation from any effects of Nrxn perturbation on synaptic density and the recruitment of postsynaptic neurotransmitter receptors. Using these techniques, as well as calcium

imaging and quantitative immunocytochemistry, we find that Nrxns play an essential role in the organization and function of the presynaptic release machinery.

4.2 Methods

4.2.1 Additional cDNA Constructs

GCaMP6m was a gift from Loren Looger.

4.2.2 Immunocytochemistry

An antibody towards RIM1/2 (Rabbit polyclonal Ab, Synaptic Systems, Lot # 140203, 1:1000) was used in this chapter.

4.2.3 Assessment of Active Zone Size

To assess the effect of Nrxn disruption on active zone size, we performed immunocytochemistry on cultures of transfected hippocampal neurons. Neurons were transfected with three cDNA plasmids: 1) 80 μg of either TKD1, TKD2, Nrxn-1βΔLNS, or control plasmid, 2) 25 μg of Syph-EGFP, a fusion protein that labels clusters of synaptic vesicles and 3) 10 mg of cytosolic EGFP, as an axonal fill stain. Three days after transfection, neurons were immunostained for Bsn, RIM1/2 and MAP2 to assess active zone size. Experimenters were blinded to the experimental conditions during image acquisition and analysis. Fluorescence images were taken on a Nikon TE2000 epifluorescence microscope equipped with a 60 X (N.A. 1.40) objective and Hamamatsu camera (Model C4742-80-12AG). To quantify the effect of Nrxn disruption on the size of active zone cytomatrices, we measured the fluorescence intensity of Bsn and RIM1/2 puncta (segment size = 0.5 μm^2) that co-localized with Syph-EGFP + EGFP expressing axons and MAP2 positive dendrites. Bsn and RIM1/2 fluorescence intensities, averaged for individual neurons, were compared using either a one-way analysis of variance

(ANOVA, for Ctrl, TKD1, TKD2 experiments) or a two-tailed Student's t-test for independent samples (for Ctrl and Nrxn-1βΔLNS experiments).

4.2.4 Synaptophysin-pHluorin Experiments

Cultures of hippocampal neurons were transfected with SypHl to quantify synaptic vesicle exocytosis. 80 µg of either a control plasmid, NrxnTKD1, NrxnTKD2 or Nrxn-1βΔLNS were transfected along with 80 µg of SypHl. 20 µg of the presynaptic marker Syph-mCh was also included in the transfection to identify axons and presynaptic varicosities of transfected neurons. Fluorescence microscopy was carried out on a Nikon TE2000 epifuorescence microscope equipped with a 60x (N.A. 1.40) objective, Smart shutter (Sutter Instruments) and Lumencor solid-state illumination. Images were acquired at 10 Hz with a Hamamatsu ORCA CCD camera and IPLab software. Experiments were performed at 36 ± 2 °C in HBS solution containing (in mM) 110 NaCl, 5.3 KCl, 2 $CaCl_2$, 1 $MgCl_2$, 20 4-(2-hydroxyethyl)-1-piperazineethanesulfonic acid (HEPES), and 25 D-glucose adjusted to pH 7.30, supplemented with 10 µM 6,7-dinitroquinoxaline-2,3-dione (DNQX) and 50 µM (2R)-amino-5-phosphonovaleric acid (APV) to prevent recurrent excitation. Axons were selected based on Syph-mCh fluorescence, and SypHl fluorescence changes were measured in response to field stimulation employing 1 ms square current pulses yielding electrical fields of approximately 10 V/cm through platinum electrodes placed 0.5 cm apart. Image acquisition and extracellular stimulation were synchronized using a Master-8 stimulator (AMPI). Stimulus trains of 80 stimuli at 80 Hz were given to measure the readily releasable pool of synaptic vesicles. In this study, we chose a higher stimulus number and stimulation frequency to deplete the RRP than in earlier studies by us and others (Matz et al., 2010; Pyle et al., 2000; Murthy et al., 2001) to maximize mobilization of readily releasable vesicles while minimizing contributions of RRP refilling to the signal. Fluorescence increases in response to isolated stimuli (100 trials at 0.2 Hz) provided a relative measure of release probability (Pr) at individual presynaptic specializations. Subsequent image analysis was performed using IPLab software. Image stacks were background-subtracted and aligned. Synaptic regions for measurement were identified

according to an RRP threshold. ROIs had a size between 0.32 and 0.64 μm^2. Multi-trial fluorescent responses at each synapse were averaged and an average synaptic response for each experiment was calculated. Data were expressed as change in fluorescence (ΔF). The statistical significance of differences in ΔF values for Ctrl, NrxnTKD1, and Nrxn-1$\beta\Delta$LNS groups was tested with a one-way ANOVA and post hoc Tukey test.

4.2.5 GCaMP6m Experiments

To measure presynaptic calcium transients, cultures of hippocampal neurons were transfected with 80 µg GCaMP6m and 80 µg of either a control plasmid, NrxnTKD1 or Nrxn-1$\beta\Delta$LNS. 20 µg of the presynaptic marker Syph-mCh was also included in the transfection to identify transfected axons. Images were acquired using the same microscope setup and solutions as describe for SypHl experiments (above, section 4.2.3). Fields were selected based on Syph-mCh fluorescence and GCaMP6m fluorescence changes were measured in response to field stimulation. Isolated stimuli as well as pairs and bursts of four stimuli at 80 Hz were acquired over 5, 10, and 20 trials, respectively, with an inter-trial period of 5 s. Image stacks were background-subtracted and aligned using IPLab software. For GCaMP6m experiments, synaptic regions for measurement, 0.32 - 0.64 μm^2 in size, were identified on Syph-mCh images according to an intensity threshold. The baseline fluorescence (F0) was calculated by averaging the three frames taken before stimulation. Data were expressed as the ratio of change in fluorescence and baseline fluorescence ($\Delta F/F0$). Multi-trial fluorescence responses at each synapse were averaged and a field average synaptic responses were calculated. The statistical significance of $\Delta F/F0$ values for Ctrl, NrxnTKD1, and Nrxn-1$\beta\Delta$LNS groups were tested with a one-way ANOVA and post hoc Tukey tests.

4.3 Results

4.3.1 Nrxn Disruption Reduces Active Zone Protein Content

Evoked neurotransmitter release relies on the proper docking and priming of synaptic vesicles at the presynaptic active zone. Docked and primed synaptic vesicles make up the readily releasable pool of synaptic vesicles (RRP), which are capable of immediate fusion with the presynaptic membrane upon action potential-evoked calcium influx. Previous work has shown that the size of the active zone cytomatrix correlates with the size of the RRP (Matz et al., 2010; Holderith et al., 2012), suggesting that active zone size may determine the number of docking sites available for synaptic vesicles. Considering that Nrxns are known to bind to presynaptic scaffolding proteins such as CASK and Mint1 (Hata et al., 1996; Butz et al., 1998), it is possible that Nrxns modulate RRP size by controlling the size of the presynaptic active zone. We therefore tested if perturbation of Nrxn function alters the recruitment of active zone cytomatrix proteins to presynaptic specializations. We transfected hippocampal cultures at 12-14 DIV with either empty KD vector, NrxnTKD1, NrxnTKD2 or Nrxn-1βΔLNS along with a plasmid encoding synaptophysin-EGFP (Syph-EGFP) to mark transfected axons and presynaptic specializations. Three days following the transfection, we performed immunocytochemistry to quantify the amount of the active zone cytomatrix proteins Bassoon (Bsn) and, in a separate set of experiments, Rab3-associated molecule 1/2 (RIM1/2). We also immunolabeled microtubule associated protein 2 (MAP2) to restrict our analysis to points of contact between transfected axons and MAP2-positive dendrites (Figure 4.1A-B). We observed that NrxnTKD or overexpression of Nrxn-1βΔLNS significantly attenuated the intensity of Bsn and RIM puncta at axodendritic contacts (Figure 4.1C). Average Bsn intensity was reduced by 29.8% with NrxnTKD1, 28.5% with NrxnTKD2, and 39.4% with Nrxn-1βΔLNS (**$p < 0.01$ as determined by 1-way ANOVA and post hoc Tukey test, Figure 4.1C, left graph). Average RIM intensity per experiment was reduced by 33.3% with NrxnTKD1 and 44% with Nrxn-1βΔLNS (**$p < 0.01$ as determined by 1-way ANOVA and post hoc Tukey test, Figure 4.1C, right graph). Histograms for Bsn and RIM puncta intensity suggest that Nrxn perturbation results in a proportional reduction of Bsn and RIM at all synapses rather than a selective reduction at a subset of synapses (Figure 4.1C). These results show that Nrxn perturbation reduces the accumulation of the active zone cytomatrix proteins Bsn and RIM at axodendritic

contacts. These effects may limit the number of docking sites for synaptic vesicles and thus impact RRP size.

4.3.2 Nrxn Perturbation Reduces Readily Releasable Pool Size and Attenuates Neurotransmitter Release Probability

Electrophysiological studies of Nrxn gene knockouts have indicated isoform-specific roles of Nrxns in the modulation of neurotransmitter release (Missler et al., 2003), (Anderson et al., 2015). In contrast, several studies that have disrupted the function of one or several postsynaptic Nrxn ligands have failed to find evidence for changes in presynaptic function (Soler-Llavina et al., 2011; Blundell et al., 2010; Zhang et al., 2015), questioning the notion of a transsynaptic modulation of neurotransmitter release through postsynaptic Nrxn ligands (Futai et al., 2007). To test the role of Nrxns in the modulation of neurotransmitter release, we used a genetically encoded sensor, synaptophysin-pHluorin (SypHl), to quantify synaptic vesicle exocytosis at synapses from neurons with attenuated Nrxn function. Cultures of dissociated hippocampal cells were transfected at 12-14 DIV with either Nrxn knockdown or Nrxn-1βΔLNS plasmids or a knockdown vector devoid of shRNA sequences, along with SypHl. Syph-mCh was included in the transfection mixes and was used to identify transfected axons (Figure 4.2A, top panel). A high-frequency stimulus train (80 Hz for 1 s) was used to compare the size of the readily releasable pool (RRP) of synaptic vesicles at synapses from neurons expressing NrxnTKD1, Nrxn-1βΔLNS or empty knockdown vector (Figure 4.2A, middle panel; Figure 4.2B, upper graph). The SypHl fluorescence increase in response to high-frequency train stimulation, ΔF(80Hz, 1s), was reduced by 34% and 32% in NrxnTKD1 and Nrxn-1βΔLNS groups, respectively, compared to control cultures (Figure 4.2C, left graph), indicating a reduction of RRP size in both groups (**$p < 0.01$, one-way ANOVA and post hoc Tukey test). To ensure that the effects of NrxnTKD1 shRNA on RRP size are not due to off-target effects of the shRNA, we performed a separate set of experiments using NrxnTKD2; a KD plasmid with 3 different shRNA sequences targeted towards Nrxn mRNA. Perturbation of Nrxn function with NrxnTKD2 resulted in a comparable reduction in peak SypHl fluorescence during high frequency stimulation

(41% reduction, ***p < 0.001, Student's t-test, independent samples, Figure 4.2C. right graph). At synapses that responded to high frequency stimulation, we measured the SypHl fluorescence increases in response to single action potentials, ΔF(1AP), a measure of the probability of neurotransmitter release at individual presynaptic specializations (Pr; Matz et al., 2010). Average SypHl fluorescence increases in response to isolated action potentials were strongly reduced in NrxnTKD1 and Nrxn-1βΔLNS groups (Figure 4.2D). Compared to control synapses, ΔF(1AP) was reduced by 81% at NrxnTKD1 synapses and 66% at Nrxn-1βΔLNS synapses (**p < 0.01, ***p < 0.001, one-way ANOVA and post hoc Tukey test).

While the amplitude of SypHl fluorescence increases to high-frequency train stimulation allows an assessment of RRP size, the density of axonal varicosities with increases in SypHl fluorescence can serve as a measure of the density of synapses that release neurotransmitter. We therefore also analyzed the effect of Nrxn perturbation on the density of axonal sites with SypHl fluorescence increases in response to high frequency stimulation. In accordance with our immunocytochemistry-based assessment of synaptic density, neurons expressing NrxnTKD1 and Nrxn-1βΔLNS groups showed a 73% and 56% reduction, respectively, in the density of axonal sites displaying a SypHl fluorescence increase in response to high-frequency stimulation as compared to control neurons (p** < 0.01, one-way ANOVA and post hoc Tukey test, Figure 4.2, left graph). Similarly, neurons expressing NrxnTKD2 displayed 49% reduction in the density of axonal sites with SypHl increases (***p < 0.001, Student's t-test for independent samples, Figure 4.2E, right graph). Taken together, these results suggest that the disruption of Nrxn function causes a decrease in release probability that is partly due to a reduction in RRP size, as well as a reduction in the density of functional synapses.

4.3.3 Overexpression of a Dominant-Negative Nrxn construct Reduces Presynaptic Calcium Influx

While our SypHl data suggest that the reduction in release probability we observe in Nrxn-disrupted neurons is at least partly a consequence of smaller pools of readily

releasable synaptic vesicles, previous studies have suggested that dysfunctional presynaptic calcium influx may underlie neurotransmitter release phenotypes at Nrxn-deficient synapses (Missler et al., 2003; Anderson et al., 2015). To test if presynaptic calcium handling is disrupted in parallel with RRP size in Nrxn-perturbed neurons, we measured presynaptic calcium influx with a genetically encoded calcium sensor, GCamP6m (Chen et al., 2013). Cultures of hippocampal neurons at 12-14 DIV were transfected with GCamP6m, along with empty knockdown vector, NrxnTKD1, or Nrxn-1βΔLNS plasmids and Syph-mCh, to mark presynaptic specializations (Figure 4.3A). Action potentials were elicited with electrical field stimulation and presynaptic calcium influx was measured by quantifying the increase in GCamP6m fluorescence at Syph-mCh-labelled synapses normalized to basal fluorescence for each synapse (ΔF/F0). Nrxn disruption by overexpression of Nrxn-1βΔLNS significantly decreased presynaptic calcium influx compared to control synapses (Figure 4.3C). In contrast, we found that knockdown of all Nrxn isoforms did not significantly reduce presynaptic calcium influx in response to 4, 2, or single action potentials compared to control fields (Figure 4.3C). On average, overexpression of Nrxn-1βΔLNS causes a 32% reduction in GCamP6m ΔF/F during 4 AP (*$p < 0.05$), a 45% reduction during 2 AP (**$p < 0.01$) and a 48% reduction during a single AP (*$p < 0.05$) compared to control synapses. Because Nrxn-1βΔLNS over-expression and Neurexin shRNA knockdown yielded conflicting results, we were unable to confirm previous studies suggesting that perturbation of Neurexin function leads to attenuated presynaptic calcium transients.

4.4 Discussion

In this study, we show that the Nrxn family of presynaptic cell adhesion molecules are essential for the organization and function of the presynaptic neurotransmitter release machinery. By using an optical method to directly measure synaptic vesicle exocytosis in cultured hippocampal neurons, we demonstrate that release probability is strongly reduced at synapses with attenuated Nrxn function. This finding is consistent with electrophysiological evidence from previous studies indicating that neurotransmitter release probability at glutamatergic synapses is reduced in mice

deficient in either all α- or all β-Nrxns (Missler et al., 2003; Anderson et al., 2015). Our results further suggest that the attenuation of neurotransmitter release probability in Nrxn-depleted neurons is in part due to a strong reduction in the size of the readily releasable pool of synaptic vesicles. The reduction in RRP size we observed with pan-Nrxn knockdown was more pronounced than the decrease in α-Nrxn specific knockout neurons (Missler et al., 2003) and is in contrast to unchanged pools of readily releasable synaptic vesicles in β-Nrxn deficient neurons (Anderson et al., 2015). To enter the RRP, synaptic vesicles have to dock to the plasma membrane and undergo SNARE complex formation, or priming. These processes crucially depend on the availability of active zone cytomatrix components that provide synaptic vesicle docking sites and facilitate priming. Interestingly, we show here that two components of active zone cytomatrices, Bsn and RIM, are reduced at synapses made by neurons with perturbed Nrxn function. This finding suggests that the decrease of RRP size observed with disruption of Nrxn function may be secondary to diminished recruitment of active zone cytomatrix components, which then causes a reduction in synaptic vesicle docking and priming.

In addition to reductions in RRP size, a decrease in presynaptic calcium transients (Anderson et al., 2015) or changes in the spatial coupling of presynaptic voltage-gated calcium channels and readily releasable synaptic vesicles (Missler et al., 2003) may also contribute to the reduction in neurotransmitter release probability observed in α- and β-isoform specific Nrxn knockouts. Our results in this respect were equivocal. Overexpression of a mutant Nrxn construct deficient in the extracellular binding domain reduced calcium influx. In contrast, knockdown of all Nrxn isoforms did not significantly affect presynaptic calcium transients. This apparent discrepancy could be due to a more efficient disruption of Nrxn function by Nrxn-1βΔLNS overexpression than by knockdown of Nrxn isoforms. However, we cannot exclude the possibility that overexpression of Nrxn-1βΔLNS has Nrxn-independent effects on presynaptic calcium transients.

Since the publication of our findings, pan-Nrxn knockout mice have been generated (Chen et al., 2017). By analyzing the effect of pan-Nrxn knockout on 3

different types of synapses, Chen et al., confirm a complex role of Nrxns in organizing presynaptic function. They find that Nrxn deletion reduces release probability at climbing fiber-Purkinje cell synapses in the cerebellum and synapses made by SST^+ interneurons in the prefrontal cortex, an effect that is at least in part due to reduced presynaptic calcium influx. Conversely, at synapses made by PV^+ interneurons, release probability and presynaptic calcium influx were unaffected by Nrxn deletion. Such synapse-specific effects of Nrxn perturbation may also be present in our dissociated hippocampal cultures and could contribute to the fact that pan-Nrxn KD failed to significantly reduce presynaptic calcium influx.

Collectively, our data show that Nrxns are important for organizing the presynaptic active zone for functional neurotransmitter release. When Nrxn function is perturbed, active zones are smaller and synaptic vesicles fail to populate the RRP. These effects cause a large reduction in neurotransmitter release probability that may be compounded by an attenuation of presynaptic calcium influx.

Figure 4.1. Nrxn perturbation reduces active zone cytomatrix protein content. (A-B) The intensity of Bsn and Rim1/2 puncta immunofluorescence was measured at contacts between transfected axons and dendrites. Shown are representative images for Ctrl, NrxnTKD1 and Nrxn-1βΔLNS groups. Circles show synaptic puncta that correspond to the transfected axon. Bottom panels show merged images of Syph-EGFP (green) and MAP2 (blue) fluorescence and Bsn (A) or RIM1/2 (B). (C) Cumulative histogram of immunofluorescence for Bsn (left graph) and RIM1/2 (right graph). Inset graphs show average puncta immunofluorescence per postsynaptic cell, normalized to control. For Bsn immunofluorescence experiments, n = 89 (Ctrl), 57 (TKD1), 38 (TKD2) and 30 (Nrxn-1βΔLNS) postsynaptic neurons and 894 (Ctrl), 612 (TKD1), 181 (TKD2), and 85 (Nrxn-1βΔLNS) analyzed synapses. For RIM immunofluorescence experiments, n = 25 (Ctrl), 23 (TKD1), and 21 (Nrxn-1βΔLNS) postsynaptic neurons and 226 (Ctrl), 190 (TKD1) and 138 (Nrxn-1βΔLNS) analyzed synapses. **$p < 0.01$ as determined by 1-way ANOVA and post hoc Tukey test. Data are shown as mean +/- SEM. Scale bars = 1 μm. (This figure was included in our published paper: Quinn et al., 2017; Scientific Reports, 7, Article number: 42920.)

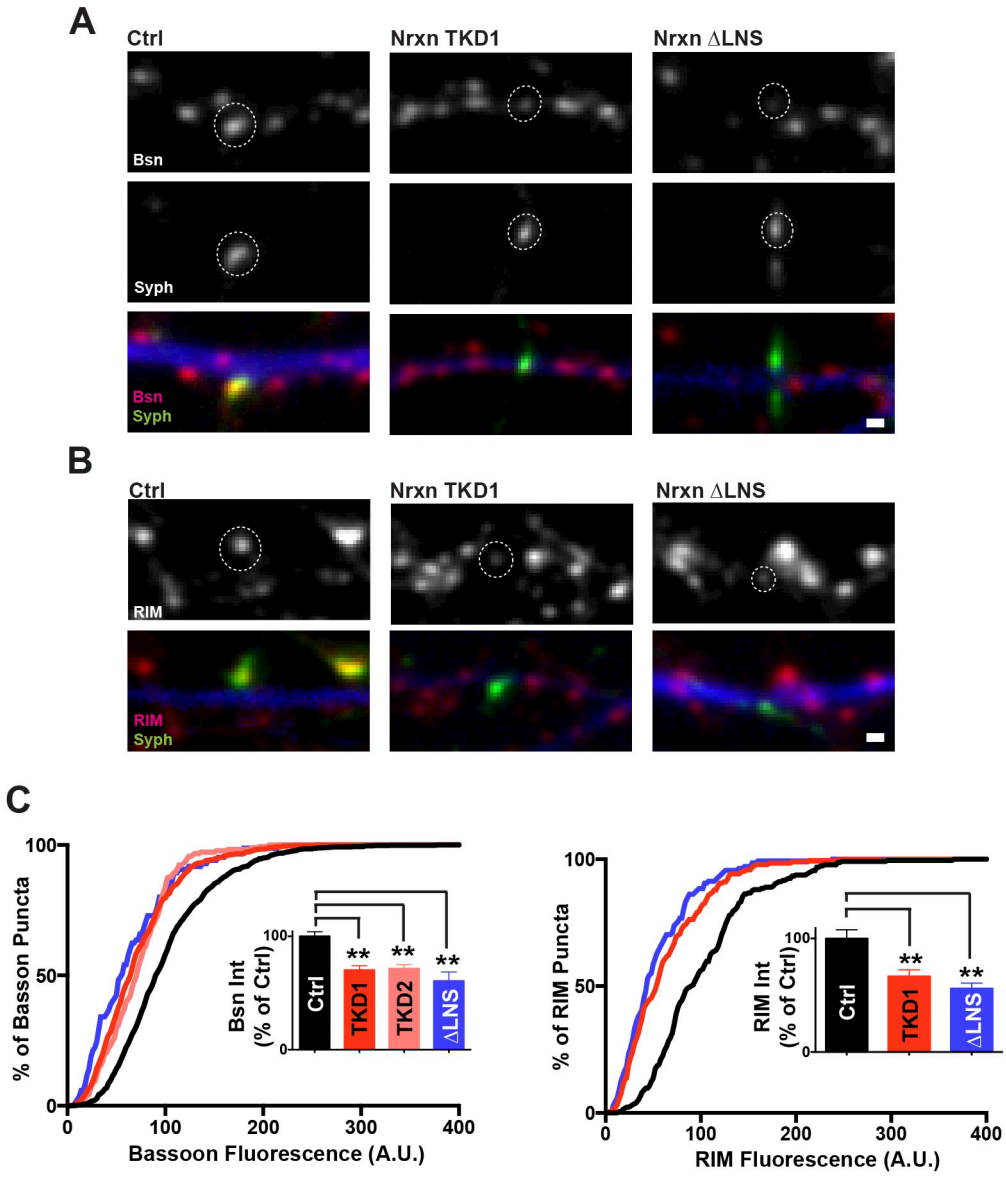
A
Ctrl
Nrxn TKD1
Nrxn ΔLNS
Bsn
Syph
Bsn
Syph
B
Ctrl
Nrxn TKD1
Nrxn ΔLNS
RIM
RIM
Syph
C
% of Basson Puncta
Bassoon Fluorescence (A.U.)
Bsn Int (% of Ctrl)
Ctrl
TKD1
TKD2
ΔLNS
% of RIM Puncta
RIM Fluorescence (A.U.)
RIM Int (% of Ctrl)
Ctrl
TKD1
ΔLNS

Figure 4.2. Nrxn perturbation attenuates neurotransmitter release. (A) Upper panel: synaptophysin-mCherry (Syph-mCh) expressing axons for control, NrxnTKD1 and Nrxn-1βΔLNS groups. Syph-mCh puncta were used to identify transfected axons. Middle Panel: SypHl fluorescence change (ΔF) that occurs during high frequency stimulation, ΔF(80Hz, 1s), which exhausts the readily releasable pool of synaptic vesicles. Lower panel SypHl fluorescence change that occurs during single stimulation (ΔF(Single). (B) SypHl fluorescent traces for micrographs presented above. Upper panel: SypHl fluorescence traces during high frequency stimulation (ΔF(80Hz, 1s) for control, NrxnTKD1 and Nrxn-1βΔLNS groups. Lower panel: SypHl fluorescence traces during single stimulation (ΔF(Single) for control, NrxnTKD1 and Nrxn-1βΔLNS groups. Gray traces show SypHl ΔF at individual synapses (high frequency stimulation averaged over 4 trials; single stimulation averaged over 180 trials). Black traces show the average synaptic SypHl response. (C) Average SypHl fluorescence changes per experiment in response to high frequency stimulation for NrxnTKD1/Nrxn-1βΔLNS experiments (left graph) and for NrxnTKD2 experiments (right graph). (D) Average SypHl fluorescence changes per experiment in response to single stimulation for NrxnTKD1/Nrxn-1βΔLNS experiments. (E) Density of high frequency SypHl fluorescent responses for NrxnTKD1/Nrxn-1βΔLNS experiments (left graph) and for NrxnTKD2 experiments (right graph). $^{**}p < 0.01$ and $^{***}p < 0.001$ as determined by 1-way ANOVA and post hoc Tukey test. Number of independent experiments are indicated in the respective graphs. Number of analyzed puncta = 1919, 697, and 1086 for Ctrl, NrxnTKD1, and Nrxn-1βΔLNS respectively in the left panels of Figure 4.2C and 4.2E. Number of analyzed puncta = 1727 and 887 for Ctrl and NrxnTKD2 respectively in the right panels of Figure 4.2C and 4.2E. Number of analyzed puncta = 1116, 297, and 502 for Ctrl, NrxnTKD1, and Nrxn-1βΔLNS respectively in Figure 4.2D. Data are shown as mean +/- SEM. Scale bar = 1 μm. (This figure was included in our published paper: Quinn et al., 2017; Scientific Reports, 7, Article number: 42920.)

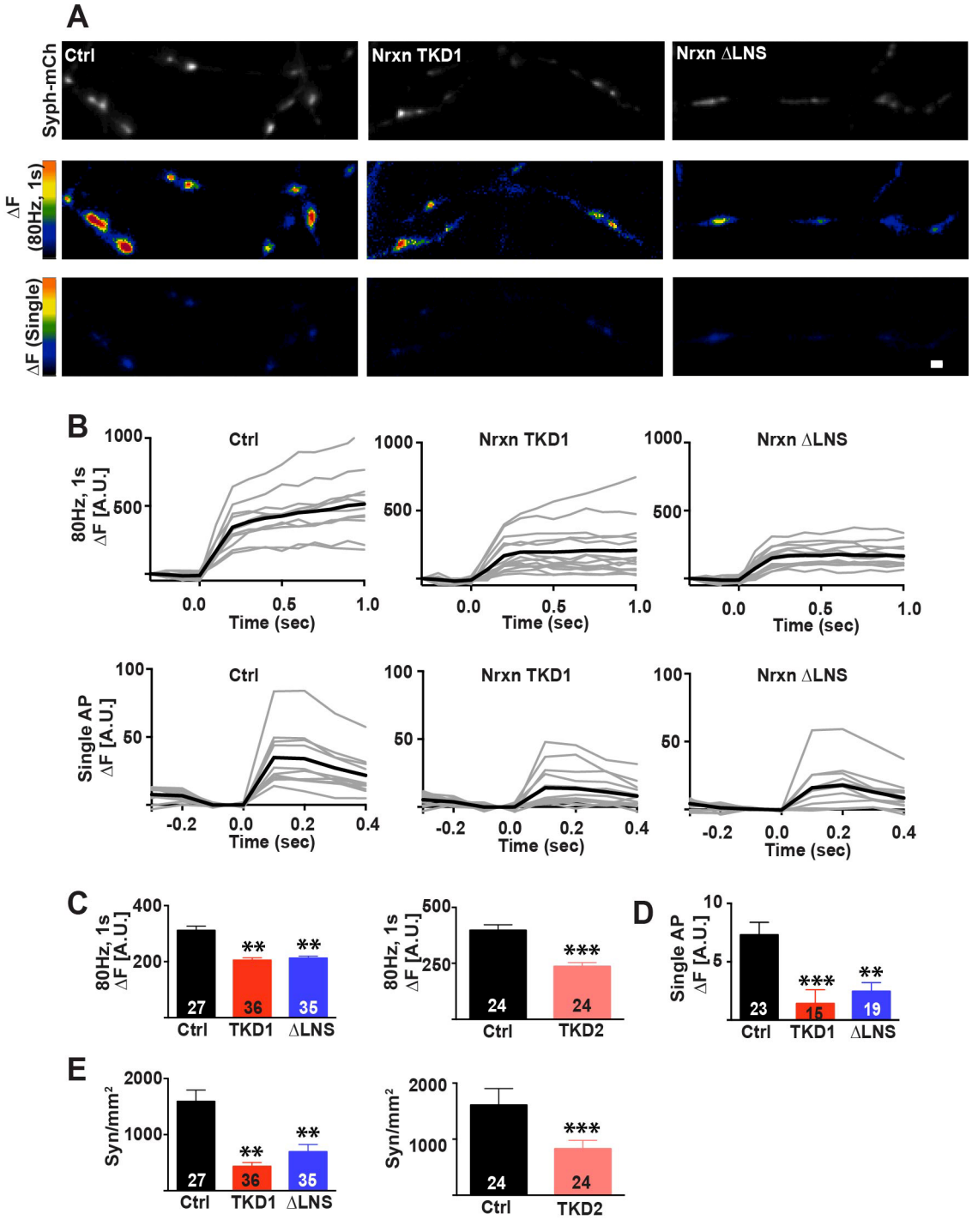
A
Ctrl
Nrxn TKD1
Nrxn ΔLNS
Syph-mCh
ΔF (80Hz, 1s)
ΔF (Single)
B
Ctrl
Nrxn TKD1
Nrxn ΔLNS
80Hz, 1s ΔF [A.U.]
Single AP ΔF [A.U.]
Time (sec)
C
80Hz, 1s ΔF [A.U.]
27
36
35
Ctrl
TKD1
ΔLNS
24
24
Ctrl
TKD2
D
Single AP ΔF [A.U.]
23
15
19
E
Syn/mm²
27
36
35
24
24

Figure 4.3. Overexpression of a dominant-negative Nrxn construct decreases presynaptic calcium influx. (A) Synaptophysin-mCherry labeled presynaptic specializations (upper panel) and GCamP6m fluorescence chance that occurs during single action potentials (lower panel). (B) Representative single field traces of the average GCamP6m response during single action potentials. (C) Average GCamP6m fluorescence changes per field in response to 1, 2 and 4 stimuli. $^{**}p < 0.01$, and $^{*}p < 0.05$ as determined by 1-way ANOVA and post hoc Tukey test. Data are shown as mean +/- SEM. n = 19, 23, and 15 fields for Ctrl, NrxnTKD1 and Nrxn-1βΔLNS groups respectively. Scale bar = 1 μm.

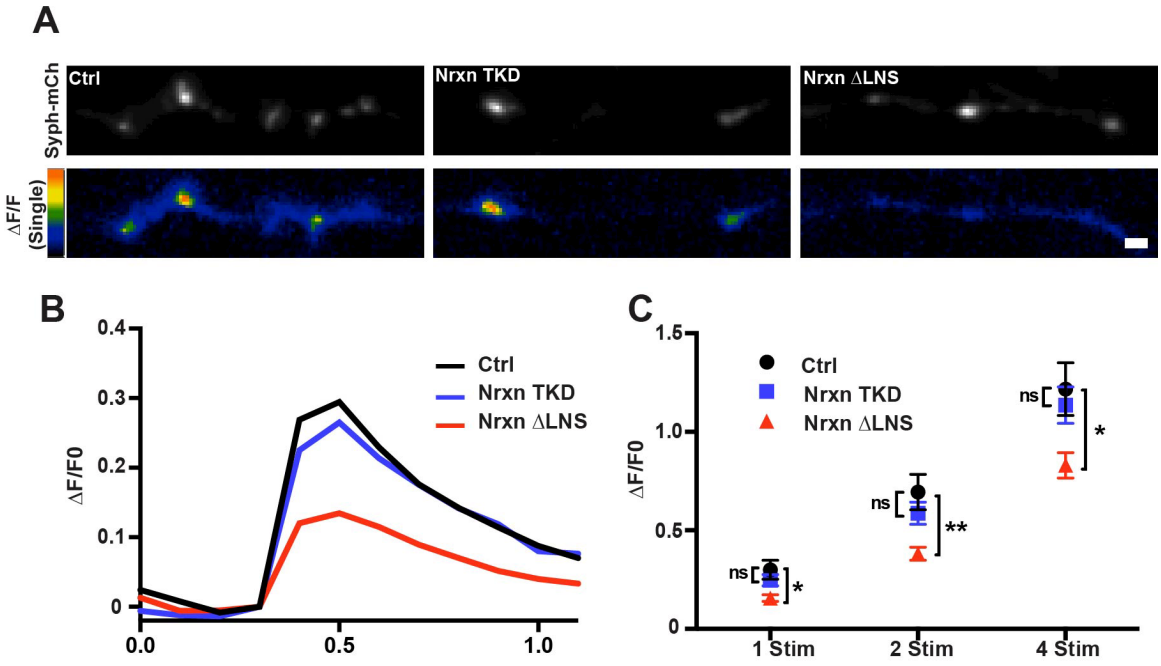
A
Ctrl
Nrxn TKD
Nrxn ΔLNS
Syph-mCh
ΔF/F (Single)
B
ΔF/F0
0.4
0.3
0.2
0.1
0
0.0
0.5
1.0
Ctrl
Nrxn TKD
Nrxn ΔLNS
C
ΔF/F0
1.5
1.0
0.5
0
ns
*
ns
**
ns
*
1 Stim
2 Stim
4 Stim

CHAPTER 5

NEUREXINS STABILIZE SYNAPSES INDEPENDENT OF NEURONAL ACTIVITY

5.1 Introduction

Previous research, and results from our lab show that synapse refinement can proceed in the absence of neurotransmission, suggesting that additional, activity-independent factors may modulate synapse stability and synapse elimination during this time. In chapter 3, we demonstrate that Nrxn perturbation leads to the enhanced elimination of glutamatergic synapses, indicating that Nrxns modulate synapse refine during circuit development. However, we (chapter 4) and others (Missler et al., 2003; Anderson et al., 2015; Chen et al., 2017) find that Nrxns also have an important role in synaptic transmission, raising the possibility that synapse destabilization in response to Nrxn perturbation may be a consequence of aberrant synaptic transmission at the affected synapses. To address this question, we block activity in both control and NrxnTKD neurons, and re-assess the effect of Nrxn-perturbation on synapse stability under these conditions.

5.2 Methods

No additional methods were used in this chapter.

5.3 Results

5.3.1 Nrxns Stabilize Synapses Independent of Global Activity Blockade

In chapter 3, we show that Nrxn perturbation effects synapse refinement by decreasing the stability of synaptic contacts. Considering that we and others have shown that Nrxn-TKD reduces neurotransmitter release, it is possible that activity plays a modulatory role in this effect. To test if Nrxn-based synaptic cell adhesion can modulate synapse refinement independent of neurotransmission, we performed synapse stability experiments in the presence of iGluR antagonists. Empty knockdown or NrxnTKD1 plasmids were transfected along with Syph-mCh to label presynaptic specializations. The next day EGFP-Hmr was transfected to label postsynaptic densities in a separate

population of neurons. Following the second transfection, pharmacological blockers of NMDA receptors (APV, 50 μM) and AMPA receptors (DNQX, 20 μM) were applied to both control cultures and NrxnTKD cultures for the remainder of the experiment. Putative synaptic contacts of co-localized Syph-mCh and EGFP-Hmr were imaged on 2 consecutive days and the percentage of stable, eliminated, and newly formed synapses was tallied (Figure 5.1). We found that global activity blockade with iGluR antagonist did not alter the effect of NrxnTKD on destabilizing synapses; synapse elimination was significantly higher at NrxnTKD synapses compared to control synapses (% synapses eliminated: Ctrl = 35.4 +/- 1.4%, NrxnTKD = 40.4 +/- 1.7%, Figure 5.1B). In agreement with chapter 3 results, synapse formation rates were unaffected by NrxnTKD when tested during iGluR blockade. These results show that the synapse destabilizing effect of NrxnTKD persists during iGluR blockade and suggest that Nrxns have an activity independent role in modulating synapse stability during circuit refinement.

5.3.2 Nrxns Stabilize Synapses Independent of Sparse Neuronal Activity

As shown in Chapter 2, iGluR blockade may cause homeostatic plasticity, which may complicate our measures of stability at silenced control and NrxnTKD synapses. To remove additional effects due to homeostatic plasticity, we silenced isolated afferents in control and TKD cultures with sparse transfection of TeNT-LC and tested if NrxnTKD synapses remained less stable than controls. Empty knockdown or NrxnTKD1/NrxnTKD2 plasmids were transfected along with TeNT-LC-Syph-mCh to label presynaptic specializations and block neurotransmitter release in all groups. The following day Hmr-EGFP was transfected to label postsynaptic densities in a separate population of neurons. Synapse turnover assays were performed and the percentage of stable, eliminated, and newly formed synapses was recorded (Figure 5.2). Synapse elimination was significantly enhanced in TeNT-LC-silenced neurons expressing NrxnTKDs compared to TeNT-LC-silenced neurons expressing a control plasmid (% synapses eliminated: Ctrl = 29.1 +/- 1.9%, NrxnTKD1 = 36.5 +/- 2.1%, NrxnTKD2 = 36.5 +/- 1.7%, Figure 5.2B). These results indicate that Nrxns have an activity-

independent function in circuit refinement, and suggest that Nrxns play a structural role in stabilizing synapses.

5.4 Discussion

In this chapter, we sought to examine whether the role played by Nrxn in synapse refinement is independent from its role in sustaining synaptic transmission. To this end, we blocked neurotransmission at both control and NrxnKD synapses and assessed the ability of NrxnTKD to destabilize synapses under these conditions. We find that the synapse destabilizing effect of NrxnTKD persisted with activity blockade, showing that Nrxn-based synaptic cell adhesion can modulate synapse refinement in an entirely activity-independent manner.

Our results build on previous studies showing that synapse refinement can occur in the absence of neuronal activity (Kerschensteiner et al., 2009; Lu et al., 2013; Sigler et al., 2017). These studies indicate that additional, activity-independent mechanisms likely modulate synapse refinement in addition to the much more thoroughly studied activity-dependent processes. Our data show that Nrxn-based adhesion can modulate synapse refinement independent of activity and suggest that the quantity and/or identity of presynaptic and postsynaptic synaptic cell adhesion molecules at synapses may be an important determinant in synapse elimination or retention during circuit refinement. In this chapter, we also address the direction of causality that exists between two consequences of Nrxn perturbation, altered neurotransmission and reduced synapse stability. Attenuated neurotransmission can conceivably lead to synapse weakening and enhanced synapse elimination similar to LTD-inducing stimuli (Wiegert and Oertner, 2013). If altered neurotransmission at NrxnTKD synapses was the causative factor for synapse instability, the effect NrxnTKD on synapse stability should have been rescued by normalizing neurotransmission in control and NrxnTKD neurons with iGluR blockade or TeNT-LC expression. Instead, we find that NrxnTKD destabilizes synapses in the absence of activity, showing that Nrxns play a structural, activity-independent role in modulating synapse stability and circuit refinement.

Figure 5.1. Neurexins stabilize synapses independent of global activity blockade. (A) Example images of axons expressing Syph-mCherry and either control or NrxnTKD plasmids in contact with EGFP-Hmr expressing dendrites imaged during iGluR blockade. Examples of stable (filled arrowheads), eliminated (open arrowheads), and formed synapses (asterisks) are shown for control and NrxnTKD groups. (B) Average percentage of eliminated (left graph) and formed synapses (right graph), grouped by postsynaptic cell. *$p < 0.05$ as determined by Student's t-test. n = 81 (Ctrl) and 69 (NrxnTKD) postsynaptic neurons. Data are shown as mean +/- SEM. Scale bar = 1μm.

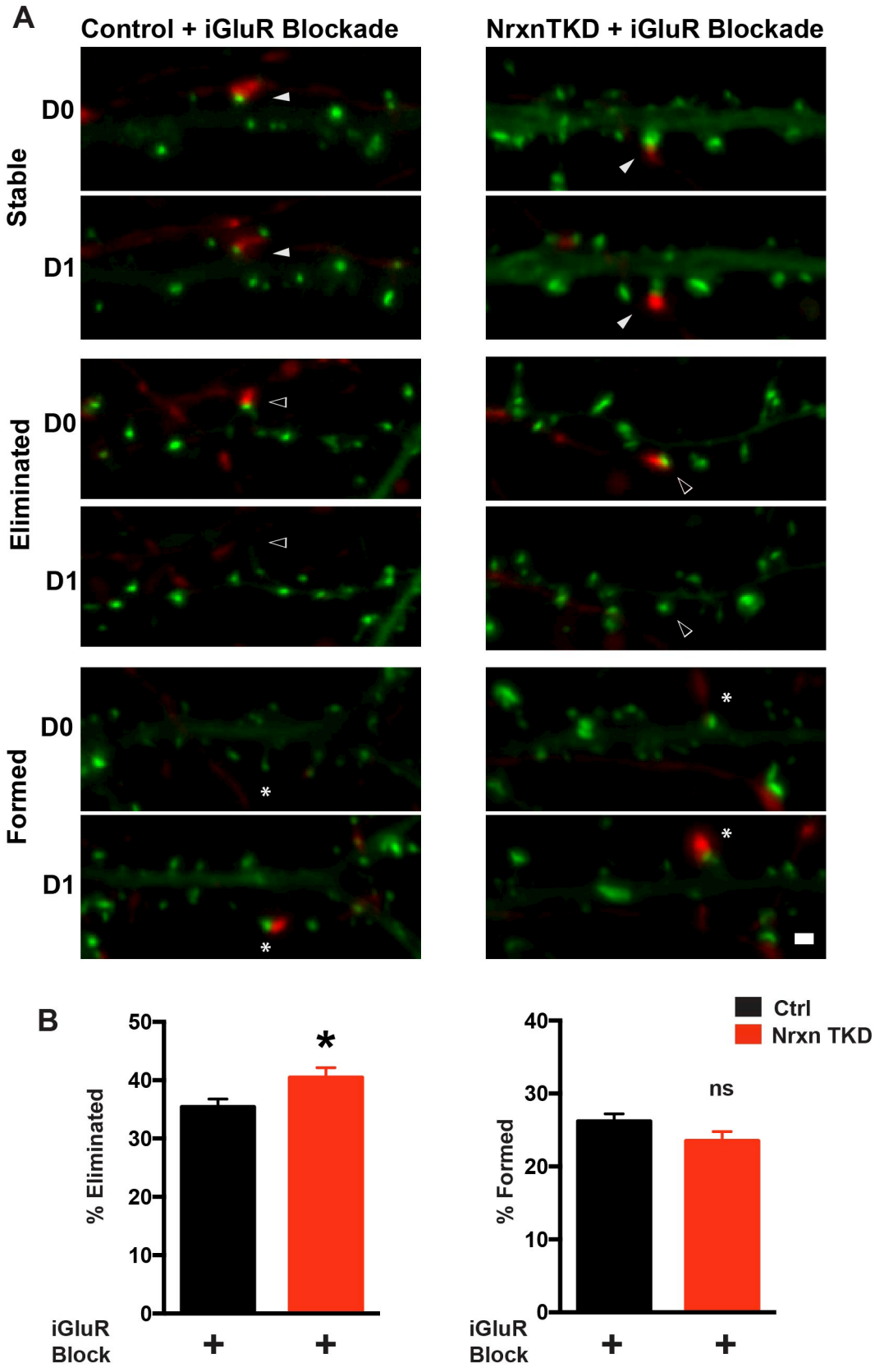
A
Control + iGluR Blockade
NrxnTKD + iGluR Blockade
Stable
D0
D1
Eliminated
D0
D1
Formed
D0
D1
B
% Eliminated
50
40
30
20
10
0
*
iGluR Block
+
+
Ctrl
Nrxn TKD
% Formed
40
30
20
10
0
ns
iGluR Block
+
+

Figure 5.2. Neurexins stabilize synapses independent of sparse neuronal activity. (A) Example images of axons expressing TeNT-LC-Syph-mCh and either control or NrxnTKD plasmids in contact with EGFP-Hmr expressing dendrites. Examples of stable (filled arrowheads), eliminated (open arrowheads), and formed synapses (asterisks) are shown for control and NrxnTKD groups. (B) Average percentage of eliminated (left graph) and formed synapses (right graph), grouped by postsynaptic cell. *$p < 0.05$ as determined by 1-way ANOVA and post hoc Tukey test. n = 41 (Ctrl), 34 (NrxnTKD1), and 52 (NrxnTKD2) postsynaptic neurons. Data are shown as mean +/- SEM. Scale bar = 1μm.

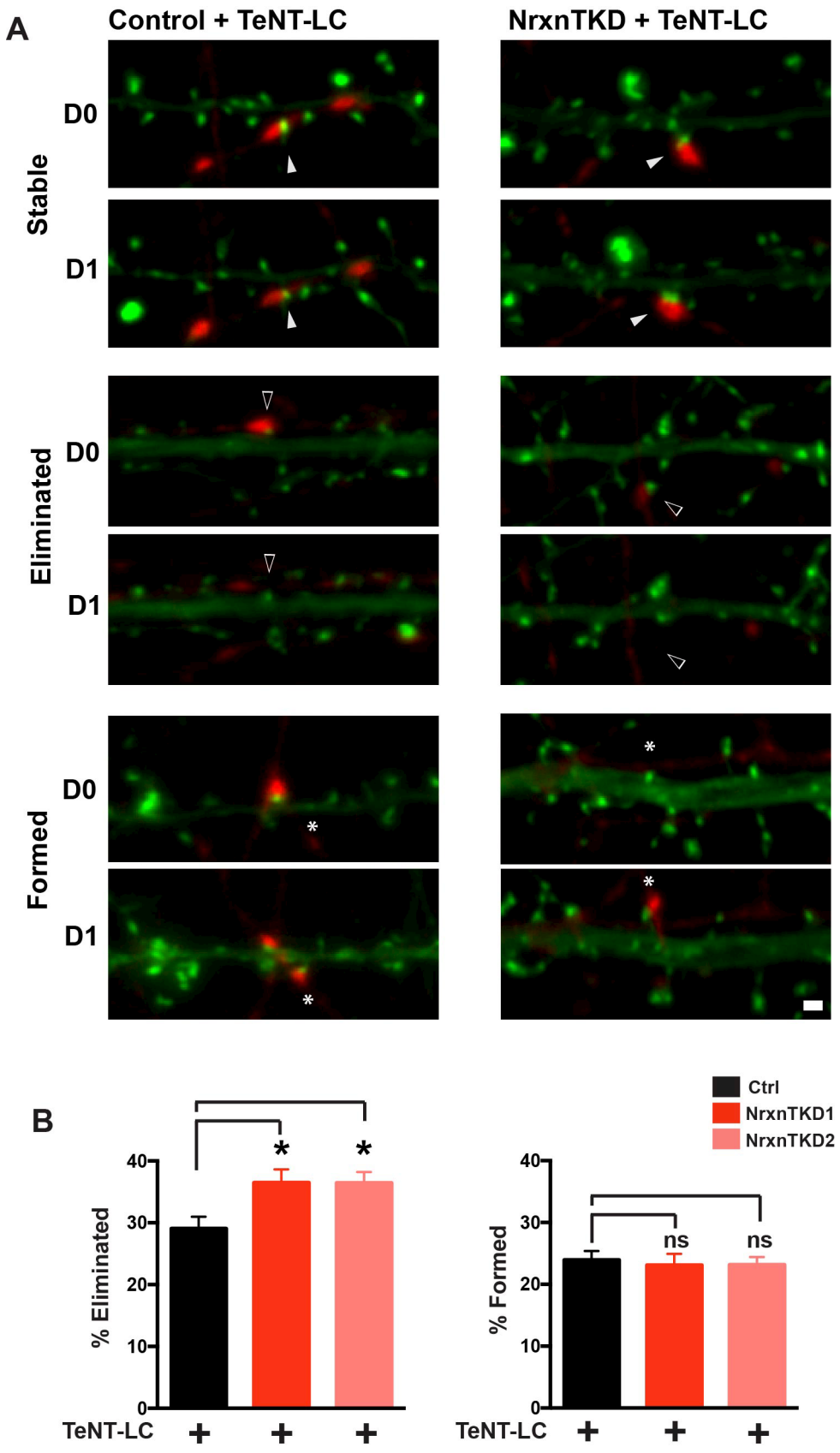
A
Control + TeNT-LC
NrxnTKD + TeNT-LC
Stable
Eliminated
Formed
D0
D1
B
Ctrl
NrxnTKD1
NrxnTKD2
% Eliminated
% Formed
TeNT-LC
ns
*

CHAPTER 6

DISCUSSION

6.1 The Role Neuronal Activity in Synapse Refinement

During development, neuronal circuits are populated with an overabundance of synapses. The role of synapse refinement is to eliminate synapses that are unnecessary for circuit function and behaviour. Neuronal activity has been shown to play a complex role in mediating synapse refinement. At neuromuscular junction synapses and at climbing fiber synapses onto cerebellar purkinje cells, multiple presynaptic inputs compete with one another in an activity-dependent manner for contact with the postsynaptic specialization (Darabid et al., 2014; Piochon et al., 2016). Here, we tested if synapse competition, or heterosynaptic plasticity, exists in dissociated hippocampal culture by silencing neurotransmission in a subset of axons with sparse expression of TeNT-LC. If activity-dependent synapse competition exists in our culture system, silenced synapses should be put at a competitive disadvantage compared to neighboring wildtype synapses and be eliminated at a higher rate. Interestingly, we find that synapse elimination was not elevated in TeNT-LC-expressing axons, suggesting that synapse competition does not play a dominant role in refining synapses between hippocampal neurons in dissociated cultures. A possible limitation that may prevent us from detecting effects of heterosynaptic plasticity is that neuronal activity levels in our preparation, primary cultures of hippocampal neurons, may not reflect those observed *in vivo*. It is conceivable that heterosynaptic plasticity may require a certain threshold activity. In fact, recent work in hippocampal slices has shown that mechanisms that cause the heterosynaptic weakening of spines require the simultaneous activation of several neighbouring spines (Oh et al., 2015), a circumstance that, under physiological conditions, may require threshold levels of neuronal activity and/or coordinated activation of afferent input. While we are unable to completely dispel this concern, we note that hippocampal cultures used for these experiments displayed spontaneous synaptic currents, spiking activity including transient, coordinated bursting activity, and an ability to homeostatically respond to pharmacological manipulation of afferent input, similar to hippocampal and cortical circuits *in vivo*.

The processes of LTP and LTD have also been suggested to play important roles in synapse refinement and structural plasticity (Bosch and Hayashi, 2012; Piochon et al., 2016). During circuit refinement, synapses that are important to overall circuit function likely undergo LTP due to correlated activity in pre- and postsynaptic neurons. Synapses that are not essential to circuit function likely experience non-correlated activity and LTD processes. Numerous lines of evidence suggest that LTD can decrease synapse size and lead to the eventual destabilization and elimination of synaptic connections (Oh et al., 2013; Wiegert and Oertner, 2013; Piochon et al., 2016). We find that TeNT-LC expression, which likely blocks both LTP and LTD at synapses, has no effect on synapse stability. To reconcile our finding that silenced synapses are eliminated to the same degree as active input with the observation that LTD facilitates synapse elimination, one would have to postulate the co-existence of activity-dependent mechanisms that increase synapse stability. Such a candidate mechanism is LTP occurring at synapses receiving input coincident with postsynaptic firing or activation of neighboring synapse clusters. The notion that LTP stabilizes synapses is indirectly supported by studies showing that synaptic potentiation can lead to enhanced synapse size (Matsuzaki et al., 2004; Hill and Zito, 2013), which we and others find is correlated with enhanced synapse stability (Hill and Zito, 2013). Clearly, further studies will be required to directly test the role of LTP in synapse refinement.

6.2 The Role of Synaptic Cell Adhesion in Synapse Refinement

Our finding that synapse elimination persists at silenced TeNT-LC suggests that neurotransmission is not essential for driving synapse elimination and circuit refinement. Instead, it suggests that synaptic activity plays a modulatory role in circuit refinement and invites the possibility that additional activity-independent processes may regulate the retention or elimination of synapses in developing circuits. We find that the Nrxn family of synaptic cell adhesion molecules (SAMs) plays such a role. Perturbation of Nrxn function with either shRNA mediated knockdown or overexpression of a mutant Nrxn construct led to synapse instability and the enhanced elimination of synaptic contacts. This effect persisted when neuronal activity was blocked, showing that Nrxns can

regulate synapse refinement in an activity-independent manner. This suggests that in addition to LTP/LTD-based modulation of synapse refinement, a second system based on synaptic cell adhesion may determine whether a synapse is preferentially retained or eliminated during circuit refinement. What purpose could a SAM-based mechanism for synapse refinement serve in circuit refinement? In the mammalian CNS, SAMs are expressed in a highly redundant, albeit cell type-specific manner in individual neurons (Varoqueaux et al., 2006; Pettem et al., 2013; de Wit and Ghosh, 2014; Fuccillo et al., 2015; de Wit and Ghosh, 2016; Paul et al., 2017). Therefore, synapse stability may be strongly influenced by the identity and/or quantity of SAMs at developing synapses. For example, the selective expression of compatible synaptic cell adhesion systems such as Nrxns presynaptically and Neuroligins/LRRTMs postsynaptically likely promotes the stabilization of developing synapses. Conversely, synapses that principally express less compatible SAMs, would be more prone to synapse elimination.

6.3 SAMs and Activity-Dependent Mechanisms in Synapse Refinement: Cooperative Function or Independent Roles?

SAM-dependent processes and activity-dependent mechanisms may cooperate to establish input in appropriate ratios from divergent afferent neurons according to functional criteria. The stability of individual synapses in developing circuits may be determined by the parallel actions of LTP/LTD-based activity patterns and SAM compatibility in pre- and postsynaptic neurons. Synapses with highly compatible SAMs will be resistant to LTD-induced synapse elimination and will be retained even if they experience very little LTP. Synapses with low SAM compatibility will be prone to LTD-induced eliminated and will require high amounts of LTP to persist in developing circuits. In this way, SAM compatibility could represent an activity-independent ‘stabilization factor’ at each synapse which is then further modulated towards or away from synapse elimination by LTD and LTP.

However, SAM-mediated and activity-dependent refinement could also operate independently and serve different functions in circuit refinement. This possibility is best

illustrated in a sensory cortical circuit like the barrel cortex. During the first postnatal week, thalamocortical (TC) afferents carrying whisker information segregate into anatomically defined columns in layer 4 (L4) of the somatosensory cortex called barrels. Numerous lines of evidence suggest that homosynaptic LTP and LTD processes at TC-L4 synapses play an essential role in barrel formation (Feldman and Brecht, 2005; Daw et al., 2007). Blockade of cortical NMDA receptor activity or TC neurotransmitter release impairs barrel development and the refinement of whisker receptive fields (Fox et al., 1996; Li et al., 2013). Although silenced TC afferents no longer organize into barrels, they continue to innervate layer 4 in a similar manner to active axons (Li et al., 2013). Therefore, it is possible that neuronal activity does not control the density of TC synapses, but instead controls the proper segregation of sensory afferents into topographic maps. Synaptic cell adhesion molecules may serve an entirely different role in the development of sensory cortical circuits. As in many other regions in the CNS, neurons in the barrel cortex receive afferent input from different classes of presynaptic neurons in specific ratios. For example, spiny stellate neurons in the barrel cortex only receive about 10% of input from TC afferents and the rest from intracortical (IC) afferents (Schoonover et al., 2014). We propose that the expression of compatible SAMs in pre- and postsynaptic neurons is essential for establishing this innervation ratio during development. Changes in expression of Nrxns and other SAMs in TC afferents would alter afferent input ratios by rendering TC synapses onto spiny stellate neurons more or less stable, and thus more or less prone to elimination. This manipulation may not affect the segregation of TC afferents into barrels, as activity dependent process could still eliminate inappropriate TC synapses. Instead, spiny stellate neurons would now receive a lower or higher fraction of input from TC afferents compared to IC afferents, which may alter the way sensory information is integrated in this sensory circuit. In this way, the cell-type specific expression of SAMs may play an essential role in circuit refinement by ensuring that each neuron receives the proper proportion of input from distinct sources.

6.4 Conclusion

The elimination of inappropriate synapses is an essential step in the development of neuronal circuits. Insufficient or excessive synaptic pruning may contribute to the etiology of several neurodevelopmental disorders such as autism, schizophrenia, and epilepsy (Neniskyte and Gross, 2017). Neuronal activity and genetic factors play essential and interrelated roles in the process of circuit refinement. In this thesis, I show that synapse refinement can proceed in the absence of neuronal activity. Using genetic tools, I show that the Nrxn family of synaptic cell adhesion molecules can regulate synapse refinement in an entirely activity-independent manner. Loss of presynaptic Nrxns made synapses functionally immature, and prone to synapse elimination. Considering that different cell types express different suites of SAMs (Paul et al., 2017), our results indicate that SAMs may be important for establishing the correct ratio of distinct afferent inputs onto postsynaptic cells. Disruption of SAM expression may therefore create an imbalance in circuit activity and disrupt circuit development; a notion supported by the implication of many families of SAMs in neurodevelopmental disorders such as autism.

REFERENCES

Allen, C.B., T. Celikel, and D.E. Feldman. 2003. Long-term depression induced by sensory deprivation during cortical map plasticity in vivo. *Nat. Neurosci*. 6:291–299.

Anderson, G.R., J. Aoto, K. Tabuchi, C. Földy, J. Covy, A.X. Yee, D. Wu, S.-J. Lee, L. Chen, R.C. Malenka, and T.C. Südhof. 2015. B-neurexins control neural circuits by regulating synaptic endocannabinoid signaling. *Cell*. 1–15.

Aoto, J., C. Foldy, S.M.C. Ilcus, K. Tabuchi, and T.C. Sudhof. 2015. Distinct circuit-dependent functions of presynaptic neurexins-3 at GABAergic and glutamatergic synapses. *Nat. Neurosci*. 1–13.

Aoto, J., D.C. Martinelli, R.C. Malenka, K. Tabuchi, and T.C. Südhof. 2013. Presynaptic neurexin-3 alternative splicing trans-synaptically controls postsynaptic AMPA receptor trafficking. *Cell*. 154:75–88.

Arellano, J.I., R. Benavides-Piccione, J. DeFelipe, and R. Yuste. 2007. Ultrastructure of dendritic spines: correlation between synaptic and spine morphologies. *Front. Neurosci*. 1:131–143.

Attardo, A., J.E. Fitzgerald, and M.J. Schnitzer. 2015. Impermanence of dendritic spines in live adult CA1 hippocampus. *Nature*. 523:592–596.

Banovic, D., O. Khorramshahi, D. Owald, C. Wichmann, T. Riedt, W. Fouquet, R. Tian, SJ. Sigrist, and H. Aberle. 2010. Drosophila neuroligin 1 promotes growth and postsynaptic differentiation at glutamatergic neuromuscular junctions. *Neuron.* 66: 724-738.

Barrow, S.L., J.R. Constable, E. Clark, F. El-Sabeawy, A.K. McAllister, and P. Washbourne. 2009. Neuroligin1: a cell adhesion molecule that recruits PSD-95 and NMDA receptors by distinct mechanisms during synaptogenesis. *Neural Dev*. 4:17.

Bastrikova, N., G.A. Gardner, J.M. Reece, A. Jeromin, and S.M. Dudek. 2008. Synapse elimination accompanies functional plasticity in hippocampal neurons. *Proc. Natl. Acad. Sci.* 105:3123–3127.

Biederer, T., Y. Sara, M. Mozhayeva, D. Atasoy, X. Liu, E.T. Kavalali, and T.C. Südhof. 2002. SynCAM, a synaptic adhesion molecule that drives synapse assembly. *Science*. 297:1525–1531.

Blankenship, A.G., and M.B. Feller. 2009. Mechanisms underlying spontaneous patterned activity in developing neural circuits. *Nat. Rev. Neurosci*. 11:18–29.

Blundell, J., C.A. Blaiss, M.R. Etherton, F. Espinosa, K. Tabuchi, C. Walz, M.F. Bolliger, T.C. Sudhof, and C.M. Powell. 2010. Neuroligin-1 deletion results in impaired spatial memory and increased repetitive behavior. *J. Neurosci*. 30:2115–2129.

Bosch, M., and Y. Hayashi. 2012. Structural plasticity of dendritic spines. *Curr Opin Neurobio*. 22:383–388.

Budreck, E.C., and P. Scheiffele. 2007. Neuroligin-3 is a neuronal adhesion protein at GABAergic and glutamatergic synapses. *Eur. J. Neurosci.* 26:1738–1748.

Buffelli, M., R.W. Burgess, G. Feng, C.G. Lobe, J.W. Lichtman, and J.R. Sanes. 2003. Genetic evidence that relative synaptic efficacy biases the outcome of synaptic competition. *Nature*. 424:430–434.

Butz, S., M. Okamoto, and T.C. Südhof. 1998. A tripartite protein complex with the potential to couple synaptic vesicle exocytosis to cell adhesion in brain. *Cell*. 94:773–782.

Chanda, S., W.D. Hale, B. Zhang, M. Wernig, and T.C. Südhof. 2017. Unique versus Redundant Functions of Neuroligin Genes in Shaping Excitatory and Inhibitory Synapse Properties. *J. Neurosci*. 37:6816–6836.

Chen, L.Y., M. Jiang, B. Zhang, O. Gokce, and T.C. Südhof. 2017. Conditional deletion of all neurexins defines diversity of essential synaptic organizer functions for neurexins. *Neuron*. 94:611–625.e4.

Chen, T.-W., T.J. Wardill, Y. Sun, S.R. Pulver, S.L. Renninger, A. Baohan, E.R. Schreiter, R.A. Kerr, M.B. Orger, V. Jayaraman, L.L. Looger, K. Svoboda, and D.S. Kim. 2013. Ultrasensitive fluorescent proteins for imaging neuronal activity. *Nature*. 499:295–300.

Chih, B., H. Engelman, and P. Scheiffele. 2005. Control of excitatory and inhibitory synapse formation by neuroligins. *Science*. 307:1321–1324.

Chubykin, A.A., D. Atasoy, M.R. Etherton, N. Brose, E.T. Kavalali, J.R. Gibson, and T.C. Südhof. 2007. Activity-dependent validation of excitatory versus inhibitory synapses by neuroligin-1 versus neuroligin-2. *Neuron*. 54:919–931.

Clem, R.L., and A. Barth. 2006. Pathway-specific trafficking of native AMPARs by in vivo experience. *Neuron*. 49:663–670.

Connor, S.A., I. Ammendrup-Johnsen, A.W. Chan, Y. Kishimoto, C. Murayama, N. Kurihara, A. Tada, Y. Ge, H. Lu, R. Yan, J.M. LeDue, H. Matsumoto, H. Kiyonari, Y. Kirino, F. Matsuzaki, T. Suzuki, T.H. Murphy, Y.T. Wang, T. Yamamoto, and A.M. Craig. 2016. Altered cortical dynamics and cognitive function upon haploinsufficiency of the autism-linked excitatory synaptic suppressor MDGA2. *Neuron*. 91:1052–1068.

Courchesne, E., R. Carper, and N. Akshoomoff. 2003. Evidence of brain overgrowth in the first year of life in autism. *JAMA*. 290:337–344.

Craig, A.M., and Y. Kang. 2007. Neurexin–neuroligin signaling in synapse development. *Curr. Opin. Neurobio.* 17:43–52.

Craig, A.M., E.R. Graf, and M.W. Linhoff. 2006. How to build a central synapse: clues from cell culture. *Trends in Neurosciences*. 29:8–20.

Darabid, H., A.P. Perez-Gonzalez, and R. Robitaille. 2014. Neuromuscular synaptogenesis: coordinating partners with multiple functions. *Nat. Rev. Neurosci.* 15:703-718.

Darabid, H., D. Arbour, and R. Robitaille. 2013. Glial cells decipher synaptic competition at the mammalian neuromuscular junction. *Journal of Neuroscience*. 33:1297–1313.

Daw, M.I., H.L. Scott, and J.T.R. Isaac. 2007. Developmental synaptic plasticity at the thalamocortical input to barrel cortex: Mechanisms and roles. *Mol. Cell. Neurosci*. 34:493–502.

de Wit, J., and A. Ghosh. 2014. Control of neural circuit formation by leucine-rich repeat proteins. *Trends Neurosci*. 37:539–550.

de Wit, J., and A. Ghosh. 2016. Specification of synaptic connectivity by cell surface interactions. *Nat. Rev. Neurosci*. 17:22–35.

de Wit, J., E. Sylwestrak, M.L. O'Sullivan, S. Otto, K. Tiglio, J.N. Savas, J.R. Yates III, D. Comoletti, P. Taylor, and A. Ghosh. 2009. LRRTM2 interacts with neurexin1 and regulates excitatory synapse formation. *Neuron*. 64:799–806.

Diamond, M.E., M. Armstrong-James, and F.F. Ebner. 1993. Experience-dependent plasticity in adult rat barrel cortex. *Proc. Natl. Acad. Sci. U.S.A.* 90:2082–2086.

Engert, F., and T. Bonhoeffer. 1999. Dendritic spine changes associated with hippocampal long-term synaptic plasticity. *Nature*. 399:66–70.

Favero, M., G. Busetto, and A. Cangiano. 2012. Spike timing plays a key role in synapse elimination at the neuromuscular junction. *Proc. Natl. Acad. Sci.* 109:E1667–75.

Feldman, D.E. 2009. Synaptic mechanisms for plasticity in neocortex. *Annu. Rev. Neurosci.* 32:33–55.

Feldman, D.E., and M. Brecht. 2005. Map plasticity in somatosensory cortex. *Science*. 310:810–815.

Fox, K. 1992. A critical period for experience-dependent synaptic plasticity in rat barrel cortex. *J. Neurosci*. 12:1826–1838.

Fox, K., B.L. Schlaggar, S. Glazewski, and D.D. O'Leary. 1996. Glutamate receptor blockade at cortical synapses disrupts development of thalamocortical and columnar organization in somatosensory cortex. *Proc. Natl. Acad. Sci.* 93:5584–5589.

Fuccillo, M.V., C. Földy, O. Gokce, P.E. Rothwell, G.L. Sun, R.C. Malenka, and T.C. Südhof. 2015. Single-cell mRNA profiling reveals cell-type-specific expression of neurexin isoforms. *Neuron*. 87:326–340.

Futai, K., M.J. Kim, T. Hashikawa, P. Scheiffele, M. Sheng, and Y. Hayashi. 2007. Retrograde modulation of presynaptic release probability through signaling mediated by PSD-95–neuroligin. *Nat. Neurosci.* 10:186–195.

Glazewski, S., and K. Fox. 1996. Time course of experience-dependent synaptic potentiation and depression in barrel cortex of adolescent rats. *J. Neurophys*. 75:1714–1729.

Graf, E.R., X. Zhang, S.-X. Jin, M.W. Linhoff, and A.M. Craig. 2004. Neurexins induce differentiation of GABA and glutamate postsynaptic specializations via neuroligins. *Cell*. 119:1013–1026.

Hata, Y., S. Butz, and T.C. Sudhof. 1996. CASK: A novel dlg/PSD95 homolog with an N-terminal calmodulin-dependent protein kinase domain identified by interaction with neurexins. *J. Neurosci.* 2488–2494.

Hayama, T., J. Noguchi, S. Watanabe, N. Takahashi, A. Hayashi-Takagi, G.C.R. Ellis-Davies, M. Matsuzaki, and H. Kasai. 2013. GABA promotes the competitive selection of dendritic spines by controlling local Ca2+ signaling. *Nat*. *Neurosci.* 16:1409–1416.

Heine, M., O. Thoumine, M. Mondin, B. Tessier, G. Giannone, and D. Choquet. 2008. Activity-independent and subunit-specific recruitment of functional AMPA receptors at neurexin/neuroligin contacts. *Proc. Natl. Acad. Sci.* 105:20947–20952.

Hill, T.C., and K. Zito. 2013. LTP-induced long-term stabilization of individual nascent dendritic spines. *J. Neurosci*. 33:678–686.

Holderith, N., A. Lorincz, G. Katona, B. Rózsa, A. Kulik, M. Watanabe, and Z. Nusser. 2012. Release probability of hippocampal glutamatergic terminals scales with the size of the active zone. *Nat. Neurosci.* 15:988–997.

Holtmaat, A., L. Wilbrecht, G.W. Knott, E. Welker, and K. Svoboda. 2006. Experience-dependent and cell-type-specific spine growth in the neocortex. *Nature*. 441:979–983.

Holtmaat, A.J.G.D., J.T. Trachtenberg, L. Wilbrecht, G.M. Shepherd, X. Zhang, G.W. Knott, and K. Svoboda. 2005. Transient and persistent dendritic spines in the neocortex in vivo. *Neuron*. 45:279–291.

Huttenlocher, P.R. 1990. Morphometric study of human cerebral cortex development. *Neuropsychologia*. 28:517–527.

Ibata, K., Q. Sun, and G.G. Turrigiano. 2008. Rapid synaptic scaling induced by changes in postsynaptic firing. *Neuron*. 57:819–826.

Ichtchenko, K., Y. Hata, T. Nguyen, B. Ullrich, M. Missler, C. Moomaw, and T.C. Sudhof. 1995. Neuroligin 1: a splice site-specific ligand for β-neurexins. *Cell*. 81:435–443.

Irie, M., Y. Hata, M. Takeuchi, K. Ichtchenko, A. Toyoda, K. Hirao, Y. Takai, T.W. Rosahl, and T.C. Sudhof. 1997. Binding of neuroligins to PSD-95. *Science*. 277:1511–1515.

Jiang, M., J. Polepalli, L.Y. Chen, B. Zhang, T.C. Sudhof, and R.C. Malenka. 2016. Conditional ablation of neuroligin-1 in CA1 pyramidal neurons blocks LTP by a cell-autonomous NMDA receptor-independent mechanism. 22:375–383.

Kano, M., and K. Hashimoto. 2009. Synapse elimination in the central nervous system. *Curr. Opin. Neurobio.* 19:154–161.

Keck, T., G.B. Keller, R.I. Jacobsen, U.T. Eysel, T. Bonhoeffer, and M. Hübener. 2013. Synaptic scaling and homeostatic plasticity in the mouse visual cortex in vivo. *Neuron*. 80:327–334.

Keck, T., M. Hübener, and T. Bonhoeffer. 2017. Interactions between synaptic homeostatic mechanisms: an attempt to reconcile BCM theory, synaptic scaling, and changing excitation/inhibition balance. *Curr. Opin. Neurobio.* 43:87–93.

Kerschensteiner, D., J.L. Morgan, E.D. Parker, R.M. Lewis, and R.O.L. Wong. 2009. Neurotransmission selectively regulates synapse formation in parallel circuits in vivo. *Nature*. 460:1016–1020.

Knott, G.W., A. Holtmaat, L. Wilbrecht, E. Welker, and K. Svoboda. 2006. Spine growth precedes synapse formation in the adult neocortex in vivo. *Nat. Neurosci*. 9:1117–1124.

Ko, J., G.J. Soler-Llavina, M.V. Fuccillo, R.C. Malenka, and T.C. Sudhof. 2011. Neuroligins/LRRTMs prevent activity- and Ca2+/calmodulin-dependent synapse elimination in cultured neurons. *J. Cell Bio.* 194:323–334.

Kopp, D.M., D.J. Perkel, and R.J. Balice-Gordon. 2000. Disparity in neurotransmitter release probability among competing inputs during neuromuscular synapse elimination. *J. Neurosci*. 20:8771–8779.

Kornau, H.C., L.T. Schenker, M.B. Kennedy, and P.H. Seeburg. 1995. Domain interaction between NMDA receptor subunits and the postsynaptic density protein PSD-95. *Science*. 269:1737–1740.

Kwon, H.-B., and B.L. Sabatini. 2011. Glutamate induces ne novo of functional spines in developing cortex. *Nature*. 474:100–104.

Lee, M.-C., R. Yasuda, and M.D. Ehlers. 2010. Metaplasticity at single glutamatergic synapses. *Neuron*. 66:859–870.

Li, H., S. Fertuzinhos, E. Mohns, T.S. Hnasko, M. Verhage, R. Edwards, N. Sestan, and M.C. Crair. 2013. Laminar and columnar development of barrel cortex relies on thalamocortical neurotransmission. *Neuron*. 79:970–986.

Li, J., J. Ashely, V. Budnik, M.A. Bhat. 2007. Crucial role of drosophila neurexin in proper active zone apposition to postsynaptic densities, synaptic growth and synaptic transmission. *Neuron.* 55:741-755.

Li, Y., P. Zhang, T.-Y. Choi, S.K. Park, H. Park, E.-J. Lee, D. Lee, J.D. Roh, W. Mah, R. Kim, Y. Kim, H. Kwon, Y.C. Bae, S.-Y. Choi, A.M. Craig, and E. Kim. 2015. Splicing-dependent trans-synaptic SALM3–LAR-RPTP interactions regulate excitatory synapse development and locomotion. *Cell Rep*. 12:1618–1630.

Linhoff, M.W., J. Laurén, R.M. Cassidy, F.A. Dobie, H. Takahashi, H.B. Nygaard, M.S. Airaksinen, S.M. Strittmatter, and A.M. Craig. 2009. An unbiased expression screen for synaptogenic proteins identifies the LRRTM protein family as synaptic organizers. *Neuron*. 61:734–749.

Lu, W., E.A. Bushong, T.P. Shih, M.H. Ellisman, and R.A. Nicoll. 2013. The cell-autonomous role of excitatory synaptic transmission in the regulation of neuronal structure and function. *Neuron*. 78:433–439.

Maletic-Savatic, M., R. Malinow, and K. Svoboda. 1999. Rapid dendritic morphogenesis in CA1 hippocampal dendrites induced by synaptic activity. *Science*. 283:1923–1927.

Matsuzaki, M., N. Honkura, G.C.R. Ellis-Davies, and H. Kasai. 2004. Structural basis of long-term potentiation in single dendritic spines. *Nature*. 429:761–766.

Matz, J., A. Gilyan, A. Kolar, T. McCarvill, and S.R. Krueger. 2010. Rapid structural alterations of the active zone lead to sustained changes in neurotransmitter release. *Proc. Natl. Acad. Sci.* 107:8836–8841.

Meyer, D., T. Bonhoeffer, and V. Scheuss. 2014. Balance and stability of synaptic structures during synaptic plasticity. *Neuron*. 82:430–443.

Missler, M., W. Zhang, A. Rohlmann, G. Kattenstroth, R.E. Hammer, K. Gottmann, and T.C. Südhof. 2003. A-neurexins couple Ca2+ channels to synaptic vesicle exocytosis. *Nature*. 423:939–948.

Molnár, Z., G. López-Bendito, J. Small, L.D. Partridge, C. Blakemore, and M.C. Wilson. 2002. Normal development of embryonic thalamocortical connectivity in the absence of evoked synaptic activity. *J. Neurosci*. 22:10313–10323.

Mondin, M., V. Labrousse, E. Hosy, M. Heine, B. Tessier, F. Levet, C. Poujol, C. Blanchet, D. Choquet, and O. Thoumine. 2011. Neurexin-neuroligin adhesions capture surface-diffusing AMPA receptors through PSD-95 scaffolds. *J. Neurosci*. 31:13500–13515.

Murthy, V.N., T. Schikorski, C.F. Stevens, and Y. Zhu. 2001. Inactivity produces increases in neurotransmitter release and synapse size. *Neuron*. 32:673–682.

Nägerl, U.V., G. Köstinger, J.C. Anderson, K.A.C. Martin, and T. Bonhoeffer. 2007. Protracted synaptogenesis after activity-dependent spinogenesis in hippocampal neurons. *J. Neurosci*. 27:8149–8156.

Nägerl, U.V., N. Eberhorn, S.B. Cambridge, and T. Bonhoeffer. 2004. Bidirectional activity-dependent morphological plasticity in hippocampal neurons. *Neuron*. 44:759–767.

Neniskyte, U., and C.T. Gross. 2017. Errant gardeners: glial-cell- dependent synaptic pruning and neurodevelopmental disorders. *Nat. Rev. Neurosci*. 18:658–670.

O'Brien, R.J., S. Kamboj, M.D. Ehlers, K.R. Rosen, G.D. Fischbach, and R.L. Huganir. 1998. Activity-dependent modulation of synaptic AMPA receptor accumulation. *Neuron*. 21:1067–1078.

Oh, W.C., L.K. Parajuli, and K. Zito. 2015. Heterosynaptic structural plasticity on local dendritic segments of hippocampal CA1 neurons. *Cell Rep*. 10:162–169.

Oh, W.C., T.C. Hill, and K. Zito. 2013. Synapse-specific and size-dependent mechanisms of spine structural plasticity accompanying synaptic weakening. *Proc. Natl. Acad. Sci.* 110:E305–12.

Okabe, S., H.D. Kim, A. Miwa, T. Kuriu, and H. Okado. 1999. Continual remodeling of postsynaptic density and its regulation by synaptic activity. *Nat. Neurosci*. 2:804–811.

Owald, D., O. Khorramshahi, V.K. Gupta, D. Banovic, H. Depner, Q. Fouquet, C. Wichmann, S. Mertel, S. Eimer, E. Reynolds, M. Holt, H. Aberle, and S.J. Sigrist. 2012. Cooperation of syd-1 with neurexin synchronizes pre- with postsynaptic assembly. *Nat. Neurosci.* 15: 1219-1226.

Paul, A., M. Crow, R. Raudales, M. He, J. Gillis, and Z.J. Huang. 2017. Transcriptional architecture of synaptic communication delineates GABAergic neuron identity. *Cell*. 1–39.

Pettem, K.L., D. Yokomaku, L. Luo, M.W. Linhoff, T. Prasad, S.A. Connor, T.J. Siddiqui, H. Kawabe, F. Chen, L. Zhang, G. Rudenko, Y.T. Wang, N. Brose, and A.M. Craig. 2013. The specific α-neurexin interactor calsyntenin promotes excitatory and inhibitory synapse development. *Neuron*. 80:113–128.

Piochon, C., A.D. Kloth, G. Grasselli, H.K. Titley, H. Nakayama, K. Hashimoto, V. Wan, D.H. Simmons, T. Eissa, J. Nakatani, A. Cherskov, T. Miyazaki, M. Watanabe, T. Takumi, M. Kano, S.S.-H. Wang, and C. Hansel. 2014. Cerebellar plasticity and motor learning deficits in a copy-number variation mouse model of autism. *Nat. Commun*. 5:5586.

Piochon, C., M. Kano, and C. Hansel. 2016. LTD-like molecular pathways in developmental synaptic pruning. *Nat*. *Neurosci.* 19:1299–1310.

Poulopoulos, A., G. Aramuni, G. Meyer, T. Soykan, M. Hoon, T. Papadopoulos, M. Zhang, I. Paarmann, C. Fuchs, K. Harvey, P. Jedlicka, S.W. Schwarzacher, H. Betz, R.J. Harvey, N. Brose, W. Zhang, and F. Varoqueaux. 2009. Neuroligin 2 drives postsynaptic assembly at perisomatic inhibitory synapses through gephyrin and collybistin. *Neuron*. 63:628–642.

Pyle, J.L., E.T. Kavalali, E.S. Piedras-Rentería, and R.W. Tsien. 2000. Rapid reuse of readily releasable pool vesicles at hippocampal synapses. *Neuron*. 28:221–231.

Rawson, R.L., E.A. Martin, and M.E. Williams. 2017. Mechanisms of input and output synaptic specificity: finding partners, building synapses, and fine-tuning communication. *Curr. Opin. Neurobio.* 45:39–44.

Ribchester, R.R., and J.A. Barry. 1994. Spatial versus consumptive competition at polyneuronally innervated neuromuscular junctions. *Exp. Physiol*. 79:465–494.

Riccomagno, M.M., and A.L. Kolodkin. 2015. Sculpting neural circuits by axon and dendrite pruning. *Annu. Rev. Cell Dev. Biol.* 31:779–805.

Richards, D.A., J.M. Mateos, S. Hugel, V. De Paola, P. Caroni, B.H. Gähwiler, and R.A. McKinney. 2005. Glutamate induces the rapid formation of spine head protrusions in hippocampal slice cultures. *Proc. Natl. Acad. Sci. U.S.A.* 102:6166–6171.

Robbins, E.M., A.J. Krupp, K.P. de Arce, A.K. Ghosh, A.I. Fogel, A. Boucard, T.C. Südhof, V. Stein, and T. Biederer. 2010. SynCAM 1 adhesion dynamically regulates synapse number and impacts plasticity and learning. *Neuron*. 68:894–906.

Rui, M., J. Qian, L. Liu, Y. Cai, H. Lv, J. Han, Z. Jia, and W. Xie. 2017. The neuronal protein neurexin directly interacts with the scribble-pix complex to stimulate F-actin assembly for synaptic vesicle clustering. *J. Biol. Chem.* 292: 14334-14348.

Sankaranarayanan, S., D. De Angelis, J.E. Rothman, and T.A. Ryan. 2000. The use of pHluorins for optical measurements of presynaptic activity. *Biophys*. *J.* 79:2199–2208.

Scheiffele, P., J. Fan, J. Choih, R. Fetter, and T. Serafini. 2000. Neuroligin expressed in nonneuronal cells triggers presynaptic development in contacting axons. *Cell*. 101:657–669.

Schiavo, G., F. Benfenati, B. Poulain, O. Rossetto, P. Polverino de Laureto, B.R. DasGupta, and C. Montecucco. 1992. Tetanus and botulinum-B neurotoxins block neurotransmitter release by proteolytic cleavage of synaptobrevin. *Nature*. 359:832–835.

Schoonover, C.E., J.C. Tapia, V.C. Schilling, V. Wimmer, R. Blazeski, W. Zhang, C.A. Mason, and R.M. Bruno. 2014. Comparative strength and dendritic organization of thalamocortical and corticocortical synapses onto excitatory layer 4 neurons. *J. Neurosci*. 34:6746–6758.

Siddiqui, T.J., and A.M. Craig. 2011. Synaptic organizing complexes. *Curr. Opin. Neurobio.* 21:132–143.

Sigler, A., W.C. Oh, C. Imig, B. Altas, H. Kawabe, B.H. Cooper, H.-B. Kwon, J.-S. Rhee, and N. Brose. 2017. Formation and maintenance of functional spines in the absence of presynaptic glutamate release. *Neuron*. 94:304–311.

Soler-Llavina, G.J., M.V. Fuccillo, J. Ko, T.C. Sudhof, and R.C. Malenka. 2011. The neurexin ligands, neuroligins and leucine-rich repeat transmembrane proteins, perform convergent and divergent synaptic functions in vivo. *Proc. Natl. Acad. Sci. U.S.A.* 108:16502–16509.

Song, J.Y., K. Ichtchenko, T.C. Sudhof, and N. Brose. 1999. Neuroligin 1 is a postsynaptic cell-adhesion molecule of excitatory synapses. *Proc. Natl. Acad. Sci. U.S.A.* 96:1100–1105.

Spruston, N. 2008. Pyramidal neurons: dendritic structure and synaptic integration. *Nat. Rev. Neurosci*. 9:206–221.

Supekar, K., L.Q. Uddin, A. Khouzam, J. Phillips, W.D. Gaillard, L.E. Kenworthy, B.E. Yerys, C.J. Vaidya, and V. Menon. 2013. Brain hyperconnectivity in children with autism and its links to social deficits. *Cell Reports*. 5:738–747.

Südhof, T.C. 2008. Neuroligins and neurexins link synaptic function to cognitive disease. *Nature*. 455:903–911.

Tabuchi, K., and T.C. Südhof. 2002. Structure and evolution of neurexin genes: Insight into the mechanism of alternative splicing. *Genomics*. 79:849–859.

Tapia, J.C., J.D. Wylie, N. Kasthuri, K.J. Hayworth, R. Schalek, D.R. Berger, C. Guatimosim, H.S. Seung, and J.W. Lichtman. 2012. Pervasive synaptic branch removal in the mammalian neuromuscular system at birth. *Neuron*. 74:816–829.

Tomàs, J., N. Garcia, M.A. Lanuza, M.M. Santafé, M. Tomàs, L. Nadal, E. Hurtado, A. Simó, and V. Cilleros. 2017. Presynaptic membrane receptors modulate ACh release, axonal competition and synapse elimination during neuromuscular junction development. *Front. Mol. Neurosci*. 10:132.

Trachtenberg, J.T., B.E. Chen, G.W. Knott, G. Feng, J.R. Sanes, E. Welker, and K. Svoboda. 2002. Long-term in vivo imaging of experience-dependent synaptic plasticity in adult cortex. *Nature*. 420:788–794.

Turrigiano, G.G., K.R. Leslie, N.S. Desai, L.C. Rutherford, and S.B. Nelson. 1998. Activity-dependent scaling of quantal amplitude in neocortical neurons. *Nature*. 391:892–896.

Uemura, T., S.-J. Lee, M. Yasumura, T. Takeuchi, T. Yoshida, M. Ra, R. Taguchi, K. Sakimura, and M. Mishina. 2010. Trans-synaptic interaction of GluRdelta2 and neurexin through Cbln1 mediates synapse formation in the cerebellum. *Cell*. 141:1068–1079.

Ushkaryov, Y.A., A.G. Petrenko, M. Geppert, and T.C. Sudhof. 1992. Neurexins: synaptic cell surface proteins related to the α-latrotoxin receptor and laminin. *Science*. 257:50–56.

Van der Loos, H., and T.A. Woolsey. 1973. Somatosensory cortex: structural alterations following early injury to sense organs. *Science*. 179:395–398.

Varoqueaux, F., A. Sigler, J.-S. Rhee, N. Brose, C. Enk, K. Reim, and C. Rosenmund. 2002. Total arrest of spontaneous and evoked synaptic transmission but normal synaptogenesis in the absence of Munc13-mediated vesicle priming. *Proc. Natl. Acad. Sci. U.S.A.* 99:9037–9042.

Varoqueaux, F., G. Aramuni, R.L. Rawson, R. Mohrmann, M. Missler, K. Gottmann, W. Zhang, T.C. Südhof, and N. Brose. 2006. Neuroligins determine synapse maturation and function. *Neuron*. 51:741–754.

Vitureira, N., M. Letellier, and Y. Goda. 2012. Homeostatic synaptic plasticity: from single synapses to neural circuits. *Curr. Opin. Neurobio.* 22:516–521.

Walsh, M.K., and J.W. Lichtman. 2003. In vivo time-lapse imaging of synaptic takeover associated with naturally occurring synapse elimination. *Neuron*. 37:67–73.

Watt, A.J., M.C. van Rossum, K.M. MacLeod, S.B. Nelson, and G.G. Turrigiano. 2000. Activity coregulates quantal AMPA and NMDA currents at neocortical synapses. *Neuron*. 26:659–670.

Wiegert, J.S., and T.G. Oertner. 2013. Long-term depression triggers the selective elimination of weakly integrated synapses. *Proc. Natl. Acad. Sci.* 110:E4510–9.

Wierenga, C.J., K. Ibata, and G.G. Turrigiano. 2005. Postsynaptic expression of homeostatic plasticity at neocortical synapses. *J. Neurosci*. 25:2895–2905.

Williams, M.E., S.A. Wilke, A. Daggett, E. Davis, S. Otto, D. Ravi, B. Ripley, E.A. Bushong, M.H. Ellisman, G. Klein, and A. Ghosh. 2011. Cadherin-9 regulates synapse-specific differentiation in the developing hippocampus. *Neuron*. 71:640–655.

Woo, J., S.-K. Kwon, S. Choi, S. Kim, J.-R. Lee, A.W. Dunah, M. Sheng, and E. Kim. 2009. Trans-synaptic adhesion between NGL-3 and LAR regulates the formation of excitatory synapses. *Nat. Neurosci*. 12:428–437.

Yasuda, M., E.M. Johnson-Venkatesh, H. Zhang, J.M. Parent, M.A. Sutton, and H. Umemori. 2011. Multiple forms of activity-dependent competition refine hippocampal circuits in vivo. *Neuron*. 70:1128–1142.

Yasumatsu, N., M. Matsuzaki, T. Miyazaki, J. Noguchi, and H. Kasai. 2008. Principles of long-term dynamics of dendritic spines. *J. Neurosci*. 28:13592–13608.

Zhang, B., L.Y. Chen, X. Liu, S. Maxeiner, S.-J. Lee, O. Gokce, and T.C. Südhof. 2015. Neuroligins sculpt cerebellar purkinje-cell circuits by differential control of distinct classes of synapses. *Neuron*. 87:781–796.

Zhao, C., E. Dreosti, and L. Lagnado. 2011. Homeostatic synaptic plasticity through changes in presynaptic calcium influx. *J. Neurosci*. 31:7492–7496.

Zhou, Q., K.J. Homma, and M.-M. Poo. 2004. Shrinkage of dendritic spines associated with long-term depression of hippocampal synapses. *Neuron*. 44:749–757.

Zito, K., V. Scheuss, G. Knott, T. Hill, and K. Svoboda. 2009. Rapid functional maturation of nascent dendritic spines. *Neuron*. 61:247–258.

Zuo, Y., G. Yang, E. Kwon, and W.-B. Gan. 2005. Long-term sensory deprivation prevents dendritic spine loss in primary somatosensory cortex. *Nature*. 436:261–265.

APPENDIX A: NEURONAL KNOCKDOWN SCREEN

cDNA segments of Nrxn 1, 2, and 3 were used as shRNA target sequences in a fluorescence-based screen for shRNA knockdown efficiency. The full-length cDNA for rat Nrxn-1β was obtained from Addgene (Plasmid 20173). Large cDNA fragments for rat Nrxn2 and Nrxn3 mRNA were obtained via RT-PCR. For Nrxn2, PCR primers 5'-ACCACTTCCACAGCAAGCAC-3' (forward) and 5'-GCGTAGAGAAGGATAAGGATGC-3' (reverse) were used to isolate a 967 bp fragment. For Nrxn3 primers 5'-GCGTTGACCATGCACCTGAG-3' (forward) and 5'-GTAAACATCACACCACCAGTCGTATGC-3' (reverse) were used to isolate a 1742 bp fragment. Nrxn cDNA fragments were ligated into an EGFP expression vector 3' to the EGFP stop codon, but 5' to the polyadenylation signal that defines the end of the mRNA, resulting in translation of only EGFP encoding parts of an mRNA also containing the neurexin target sequences. Target vectors also encoded BFP, which was expressed from a separate Cytomegalovirus (CMV) promoter to allow for normalization of cDNA expression. Target constructs for either Nrxn1, 2, or 3 were co-transfected into 10-13 DIV hippocampal neurons along with a shRNA KD vector or control vector. shRNA KD constructs that effectively targeted and degraded the EGFP-Nrxn transcript were identified by quantifying the intensity of somatic EGFP/BFP fluorescence intensity in KD neurons compared to control neurons which expressed an empty KD vector.

Figure A1. Neuronal shRNA knockdown screen. (A) To test the KD efficiency of candidate shRNA sequences we created target constructs for Nrxn1β, Nrxn2β, and Nrxn3β. Target constructs were generated from a vector that allows for expression of EGFP from a CMV promoter. Nrxn target sequences were ligated 3' to the EGFP stop codon, but 5' to the polyadenylation signal that defines the end of the mRNA. EGFP and Nrxn sequences are transcribed onto a single mRNA, which is targeted by candidate shRNA constructs. Unsuccessful targeting of shRNA to the Nrxn portion of the target mRNA results in translation of cytosolic EGFP as normal. Successful targeting of shRNA to the Nrxn portion of the target mRNA results in the degradation of the EGFP-Nrxn transcript and a reduction in cytosolic EGFP fluorescence. Knockdown efficiency was assessed in cultured hippocampal neurons by co-expressing EGFP|Nrxn1, 2, or 3 target constructs along with candidate shRNA sequences for each Nrxn gene. The Nrxn-EGFP target constructs also encoded blue fluorescent protein (Tag-BFP), driven by a separate promoter, to allow for normalization of transfection efficiency. (B) Neurons from a test of Nrxn-3 KDs. Knockdown efficiency was quantified by comparing somatic EGFP/BFP fluorescence intensities in Nrxn knockdown cells to that of controls cells that were co-transfected with an empty knockdown vector. shRNAs that were effective at reducing Nrxn expression where combined into 2 triple knockdown vectors (TKD1 and TKD2), each with unique shRNA sequences target towards Nrxn 1, 2, and 3 mRNA. NrxnTKD1 and NrxnTKD2 were then retested in the fluorescent assay described above. (C) For NrxnTKD1, the residual fluorescent intensity of EGFP|Nrxn constructs was 34.4, 19.7, and 29.8% for EGFP|Nrxn 1, 2, and 3 respectively. In neurons expressing NrxnTKD2, the residual fluorescent intensity of EGFP|Nrxn constructs was 52.7, 40.5, and 17.1% for EGFP|Nrxn 1, 2, and 3 respectively. For Nrxn-1 experiments n's = 29, 15, and 12 cells for ctrl, sh-622, and sh-464 groups respectively. For Nrxn-2 experiments n's = 17, 18, and 14 cells for ctrl, sh-1054, and sh-1021 groups respectively. For Nrxn-3 experiments n's = 12, 10, and 10 cells for ctrl, sh-631, and sh-925 groups respectively. *$p < 0.05$, **$p < 0.01$ as determined by 1-way ANOVA and post hoc Tukey test. Data are shown as mean +/- SEM. Scale bar = 10 μm.

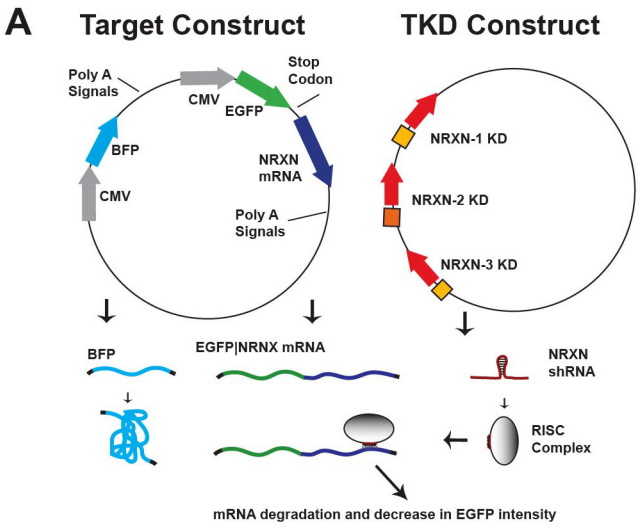
A
Target Construct
TKD Construct
Poly A Signals
CMV
Stop Codon
EGFP
BFP
CMV
NRXN mRNA
Poly A Signals
NRXN-1 KD
NRXN-2 KD
NRXN-3 KD
BFP
EGFP|NRNX mRNA
NRXN shRNA
RISC Complex
mRNA degradation and decrease in EGFP intensity

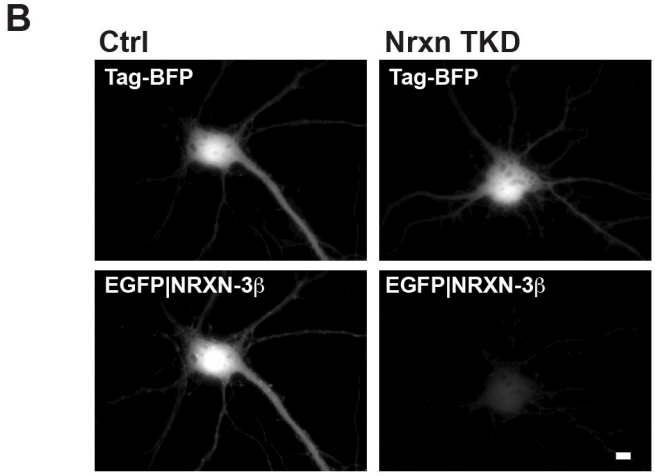
B
Ctrl
Nrxn TKD
Tag-BFP
Tag-BFP
EGFP|NRXN-3β
EGFP|NRXN-3β

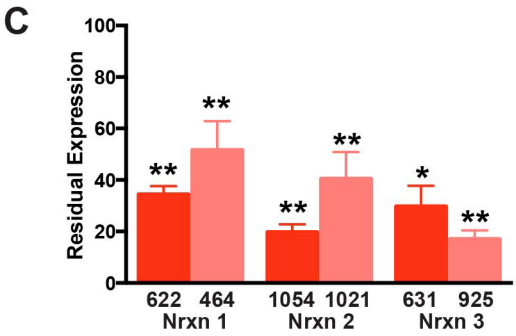
C
Residual Expression
100
80
60
40
20
0
622 464
Nrxn 1
1054 1021
Nrxn 2
631 925
Nrxn 3